NASA TECHNICAL NOTE

NASA TN D-7282

NASA TN D-7282

AERODYNAMIC AND FLOW-VISUALIZATION STUDIES OF TWO DELTA-WING ENTRY VEHICLES AT A MACH NUMBER OF 20.3

by James P. Arrington and David R. Stone

Langley Research Center
Hampton, Va. 23665

NATIONAL AERONAUTICS AND SPACE ADMINISTRATION • WASHINGTON, D. C. • AUGUST 1973

1. Report No.	2. Government Accession No.	3. Recipient's Catalog No.
NASA TN D-7282		

4. Title and Subtitle	5. Report Date
AERODYNAMIC AND FLOW-VISUALIZATION STUDIES OF TWO DELTA-WING ENTRY VEHICLES AT A MACH NUMBER OF 20.3	August 1973
	6. Performing Organization Code
7. Author(s)	8. Performing Organization Report No.
James P. Arrington and David R. Stone	L-8892
	10. Work Unit No.
9. Performing Organization Name and Address	502-37-01-04
NASA Langley Research Center Hampton, Va. 23665	11. Contract or Grant No.
	13. Type of Report and Period Covered
12. Sponsoring Agency Name and Address	Technical Note
National Aeronautics and Space Administration Washington, D.C. 20546	14. Sponsoring Agency Code

15. Supplementary Notes

Technical Film Supplement L-1137 available on request.

16. Abstract

The longitudinal, lateral, and directional aerodynamic characteristics of two space shuttle concepts have been obtained in helium for operational flight Reynolds numbers at angles of attack from -10° to 55°. Included are elevon control deflections, roll control due to ailerons, and the effects of a nose modification. Selected results were compared with those derived from tangent-cone and Newtonian theories. Also included are results of a flow-visualization study consisting of electron-beam-illuminated flow and surface oil-flow patterns.

17. Key Words (Suggested by Author(s))	18. Distribution Statement
Delta-wing shuttle orbiter Hypersonic aerodynamics Electron beam flow visualization	Unclassified – Unlimited

19. Security Classif. (of this report)	20. Security Classif. (of this page)	21. No. of Pages	22. Price*
Unclassified	Unclassified	70	$3.00

*For sale by the National Technical Information Service, Springfield, Virginia 22151

AERODYNAMIC AND FLOW-VISUALIZATION STUDIES OF TWO DELTA-WING ENTRY VEHICLES AT A MACH NUMBER OF 20.3

By James P. Arrington and David R. Stone
Langley Research Center

SUMMARY

The longitudinal, lateral, and directional aerodynamic characteristics of two space shuttle concepts, one designed by McDonnell Douglas Corp. and the other by North American Rockwell Corp., have been obtained over an angle-of-attack range of -10° to 55° in helium for operational flight Reynolds numbers at a Mach number of 20.3. Selected aerodynamic results for both concepts have been compared with characteristics derived from tangent-cone and Newtonian theories. Also included are results of a flow-visualization study consisting of electron-beam-illuminated flow and surface oil-flow patterns.

In general, the flow characteristics indicated by the flow-visualization studies were similar for both vehicles, with potential high-heating regions in areas of high shear and shock impingement. The bow-wing shock interactions were located inboard of the wing tips at 20° angle of attack, near the tips at 30° angle of attack, and beyond the tips at higher angles.

The experimental aerodynamic results showed that the hypersonic performance was relatively insensitive to the differences between the two configurations and that both would require stability augmentation for some portions of flight. For their design hypersonic angle-of-attack range, approximately 23° to 50°, both vehicles were longitudinally stable and could be trimmed with static stability, both had about the same lift-drag ratios, with a maximum value of about 2.2, both were directionally unstable and laterally stable, and both had a positive dynamic directional stability parameter. Although both concepts had adverse yaw due to roll control at angles of attack from 23° to 31°, the North American Rockwell configuration did not have this adverse cross coupling above 32° angle of attack. The vertical tail on this configuration became completely ineffective above 13° angle of attack and would be of no use over the operational hypersonic angle-of-attack range, as expected. A modified forebody with a smaller leading-edge radius and a slightly larger planform area increased the trim angle of attack from about 20° to 39° for undeflected elevon controls on this configuration. A comparison of the experimental

results with tangent-cone and Newtonian theories showed that both theories equally predicted the proper trends in the data, but the absolute values were not always predicted.

INTRODUCTION

Several studies in the past have resulted in the proposed use of delta-wing orbiters for reusable transportation systems capable of transferring large payloads to and from Earth orbit. (See, for example, refs. 1, 2, and 3.) Two of these studies, conducted by McDonnell Douglas Corp. (ref. 2) and North American Rockwell Corp. (ref. 3), were based on identical system requirements in the Phase B portion of the NASA space shuttle program. The different design approaches followed by the two studies resulted in significantly different vehicle concepts. One concept had a relatively high profile body with the cargo bay positioned above the internal propellant tanks, and the other had a low profile body with the cargo bay between the tanks. Both had delta wings with symmetrical airfoil sections, but each wing had a different leading-edge sweep angle, dihedral, incidence, and twist.

These two concepts have been evaluated hypersonically to determine the impact of the different design approaches on the performance, stability, and control. A portion of the evaluation, which was conducted in the Langley 22-inch helium tunnel at a Mach number of 20.3, is presented in this paper. The data were obtained at operational flight Reynolds numbers over an angle-of-attack range of -10° to 55° at sideslip angles of 0° and approximately 4.5°, and the experimental results have been compared with theoretical predictions. In addition to the aerodynamic data analysis, the results of a flow-visualization investigation consisting of surface oil-flow patterns and electron-beam-illuminated flow studies are also presented. Some of the results are recorded on a 16-mm, silent, color film (L-1137) which is available upon request from the Langley Research Center. A request card and a description of the film are included at the back of this document. Some of the aerodynamic results have been previously presented in reference 4.

SYMBOLS

The longitudinal data are referred to both the body- and stability-axis systems. Lateral and directional data are referred to the body system only.

b wing span

C_A axial-force coefficient, $\frac{\text{Axial force}}{qS}$

C_D drag coefficient, $C_A \cos \alpha + C_N \sin \alpha$

C_L lift coefficient, $C_N \cos \alpha - C_A \sin \alpha$

C_l rolling-moment coefficient, $\frac{\text{Rolling moment}}{qSb}$

C_{l_β} rate of change of rolling-moment coefficient with sideslip angle, $\frac{\Delta C_l}{\Delta \beta}$, per degree ($\beta = 0^\circ$ and 4.5°)

$C_{l_{\delta_a}}$ rate of change of rolling-moment coefficient with aileron deflection angle, $\frac{\Delta C_l}{\Delta \delta_a}$, per degree

C_m pitching-moment coefficient, $\frac{\text{Pitching moment}}{qS\bar{c}}$

C_N normal-force coefficient, $\frac{\text{Normal force}}{qS}$

C_n yawing-moment coefficient, $\frac{\text{Yawing moment}}{qSb}$

C_{n_β} rate of change of yawing-moment coefficient with sideslip angle, $\frac{\Delta C_n}{\Delta \beta}$, per degree ($\beta = 0^\circ$ and 4.5°)

$(C_{n_\beta})_{dyn}$ dynamic directional stability parameter, $C_{n_\beta} \cos \alpha - C_{l_\beta} \frac{I_z}{I_x} \sin \alpha$, per degree

$C_{n_{\delta_a}}$ rate of change of yawing-moment coefficient with aileron deflection angle, $\frac{\Delta C_n}{\Delta \delta_a}$, per degree

$C_{p,max}$ maximum Newtonian pressure coefficient

C_Y side-force coefficient, $\frac{\text{Side force}}{qS}$

C_{Y_β} rate of change of side-force coefficient with sideslip angle, $\frac{\Delta C_Y}{\Delta \beta}$, per degree ($\beta = 0^\circ$ and 4.5°)

$C_{Y_{\delta_a}}$ rate of change of side-force coefficient with aileron deflection angle, $\frac{\Delta C_Y}{\Delta \delta_a}$, per degree

$\bar{c}$	wing mean aerodynamic chord
$\frac{I_Z}{I_X}$	ratio of moments of inertia about yaw and roll axes
L/D	lift-drag ratio, $\frac{C_L}{C_D}$
l	body reference length
M	Mach number
q	dynamic pressure
r	radius
S	theoretical wing planform area
x	longitudinal coordinate measured from model nose
α	angle of attack, degrees
β	angle of sideslip, degrees
δ_a	aileron deflection angle, $\frac{\delta_{e,left} - \delta_{e,right}}{2}$, degrees
δ_e	elevon deflection angle (positive when deflected downward), $\frac{\delta_{e,left} + \delta_{e,right}}{2}$, degrees

Subscripts:

máx	maximum
trim	trimmed conditions

MODELS

The 0.0035-scale version of the North American Rockwell concept, designated the 134D (ref. 5), had a 60° swept delta wing with 5° negative twist, 7° dihedral, and a symmetrical airfoil section (baseline configuration in fig. 1(a)). The aerodynamic forces and moments of the vehicle were based on the values listed in figure 1(a). The moments

were referenced about a center of gravity located at 67 percent of the body length (ℓ = 18.85 cm) measured from the nose and at 47.3 percent of the body height measured from the bottom. For a portion of these studies, the 134D configuration was altered forward of the $x/\ell = 0.47$ station as indicated in figure 1(a). The modified forebody had a smaller leading-edge radius along the lower surface, a slight increase in planform area, and no change in the profile shape from the basic 134D configuration.

The 0.0033-scale version of the McDonnell Douglas concept (fig. 1(b)), designated the 050B (ref. 6), had a 55° delta wing with 10° dihedral, 2° incidence, no twist, and a symmetrical airfoil section. The aerodynamic forces and moments for the vehicle were based on the values listed in figure 1(b). The moments have been reduced about a center of gravity located at 67 percent of the body length (ℓ = 15.75 cm) measured from the nose and at 41.6 percent of the body height measured from the bottom. A detailed description of the geometric characteristics of both vehicles is listed in table I.

APPARATUS AND TESTS

Wind Tunnel

The experimental investigations were conducted in the Langley 22-inch helium tunnel at a Mach number of 20.3 for Reynolds numbers of 2.27×10^6 and 2.73×10^6 based on the 050B and the 134D body lengths, respectively. The stagnation pressure was 6.9 MPa, and the total temperature of the flow was within the range of 288 to 300 K. Operational characteristics of the facility and details of the contoured-nozzle flow calibrations are available in reference 7.

Tests

Flow-visualization tests.- Photographs of surface oil-flow patterns and electron-beam-illuminated flow were obtained for the two configurations. Small droplets of a mixture of lampblack and silicone oil were distributed onto the model surfaces, and photographs of the oil-flow patterns and the electron-beam-illuminated flow were obtained simultaneously during a test. Additional photographs of the oil-flow patterns were taken after the models were removed from the tunnel. Although the models were shielded from the tunnel flow at the beginning and end of each test by a retractable device, the oil-flow patterns were subjected to tunnel shutdown transients. The effect of these disturbances on the overall patterns has been observed to be small, but they can cause a slight splattering and rearward movement in heavy oil accumulation areas, such as along separation lines.

The electron beam is routinely used as a flow-visualization device in the 22-inch helium tunnel. The flow becomes illuminated when the gas molecules radiate light upon

returning from a momentarily excited state caused by a bombardment from a concentrated beam of electrons emitted from a gun device. More details of the equipment and a diagnosis of the illuminated flow can be obtained from reference 8.

Force and moment tests.- The models were mounted on sting-supported six-component strain-gage balances. Three stings were used to traverse the angle-of-attack range of -10° to 55°. (See fig. 1(c).) Data were obtained at predetermined angles of attack by using a prism mounted in the models to reflect light from a point (adjacent to the test-section window) onto electric eyes set at calibrated intervals. Additional features of this system can be found in reference 7. Sideslip angles were obtained with the stings yawed at fixed angles of 0° and approximately 4.5°.

The estimated maximum uncertainties in the measured basic data and in the test conditions are shown in the following table:

C_N	±0.0105
C_A	±0.0014
C_m	±0.0031
C_l	±0.0007
C_n	±0.0014
C_Y	±0.0035
α,β, deg	±0.1
M	±0.2

Uncertainties in the aerodynamic coefficients and the test parameters were determined from a static calibration of the balance, readout errors, and test-section Mach number calibrations. Base pressures were measured at one location, and the balance axial forces were adjusted to a condition in which free-stream pressure acted over the model base areas. The maximum value of the incremental axial-force coefficient due to the base-pressure correction was on the order of -0.0003.

THEORETICAL PREDICTION METHODS

The theoretical force and moment coefficients were computed by integrating the local surface pressures over representative models as determined by either tangent-cone theory or Newtonian theory $\left(C_{p,max} = 2\right)$ with Prandtl-Meyer expansion techniques for both. An indication of how the configurations were represented for these computations can be obtained from figure 2, where examples of typical computer drawings of the two concepts denote the number and size of surface elements considered. The theoretical increments due to laminar skin friction were included in the calculations according to the reference enthalpy method (ref. 9) by using the mode I option in the program described in reference 10.

RESULTS AND DISCUSSION

Operational Flight Regimes

Throughout the Phase B portion of the shuttle program, several entry trajectory schemes were proposed for the high-cross-range mission of 1150 n. mi. (See, for example, refs. 2 and 3.) In general, the entry modes can be grouped into two basic types: (1) high α entry (angles of attack on the order of 53° to 46°) with pitch modulation occurring during the hypersonic portion of the flight, beginning at Mach numbers of 22 to 15 and ending at $M \approx 18$ to 11, respectively, and (2) constant α entry ($\alpha \approx 30^{\circ}$) with a transition to lower angles of attack beginning at $M \approx 7$. In either case, the vehicles would be at angles of attack greater than approximately 23° and at altitudes on the order of 69 to 73 km for Mach numbers near 20. For these flight conditions, the Reynolds numbers, based on vehicle lengths, would range from 2.1×10^6 to 1.1×10^6 for the 050B orbiter and from 2.4×10^6 to 1.2×10^6 for the 134D orbiter. This range in Reynolds number has been shown in the past (ref. 11) to have little effect on the aerodynamic characteristics of this class of vehicles.

The proposed flight control during entry assumed an attitude control propulsion system (ACPS) to provide pitch, roll, and yaw control for the high-altitude portion of hypersonic flight where dynamic pressures are low. During hypersonic flight at the lower altitudes where the aerodynamic controls become more effective, a blended system using both aerodynamics and ACPS would be employed. Since the vertical tail was considered to be ineffective during the hypersonic portion of entry, reaction controls were designed for directional control.

Flow-Visualization Studies

The flow-visualization studies were conducted to observe the flow about the vehicles in order to identify flow phenomena that are generally difficult to predict. Photographs of electron-beam-illuminated flow with and without surface oil flow on the two orbiters during selected runs, and postrun photographs of oil patterns are presented in figures 3 to 11.

In general, the flow characteristics exhibited by both configurations were similar, with potential high-heating regions indicated in areas of high shear and in areas of shock impingement. The illuminated-flow results for both vehicles indicate that the interaction between the bow and wing shocks was located inboard of the wing tips at $\alpha = 20^{\circ}$ (evidence of interaction was dim on the original print of fig. 3(a) but brighter in fig. 7), near the wing tips for $\alpha = 30^{\circ}$ (figs. 3(c), 9(b), and 9(c)), and beyond the tips for higher angles (figs. 3(e), 11(b), and 11(c)). Under flight conditions, the shocks would be more inboard since shock detachment distances are generally smaller in air because of its lower ratio

of specific heats compared with the helium test medium. The oil patterns on both orbiters at $\alpha = 30^{\circ}$ (figs. 5, 6, and 10) show extensive attached flow along the sides of the forebody, vortex-type flow from the wing-body juncture that sweeps the sides of the bodies, and attached flow along the upper surfaces of the wings (substantial in fig. 5(b) for the 134D orbiter). There also appears to be attached flow on and behind the canopy, downstream of the separated flow along the top of the forebody. (See fig. 6(d), for example.) However, oil flow was limited in this region because of low shear and the tendency of the electron beam to dry the oil. On the bottom of both vehicles there was extensive outflow along the forebody and inflow near the wing-body juncture, but the flow over the bottom of the elevon controls was essentially two dimensional. Some of the flow-visualization results are recorded in a film supplement (L-1137) which is available upon request from the Langley Research Center.

Aerodynamic Characteristics

The 134D orbiter.- The 134D orbiter was tested with and without the wing to obtain general information about the effects of this component on the hypersonic aerodynamics; the results are presented in figure 12. The vehicle without the wing was longitudinally unstable over the test angle-of-attack range, and with the wing attached, it was stable above $\alpha \approx 14^{\circ}$ and trimmed at $\alpha = 20^{\circ}$. The L/D values were only slightly affected by the wing addition, with the $(L/D)_{max}$ being reduced from 2.45 to 2.32. Similar results were obtained in reference 12 for a delta-wing configuration with an $(L/D)_{max}$ of 2 at $M = 10$. The lateral and directional characteristics (fig. 12(c)) show, as expected, that the addition of the wing reduced the directional instability and increased the lateral stability.

The aerodynamic characteristics of the 134D orbiter with the baseline and modified forebodies are compared in figure 13 to indicate the effects of this type of modification at hypersonic speeds. The larger planform area and the smaller radius of the modified forebody caused the trim angle of attack to increase from 20° (baseline) to 39° and caused the $C_{L,max}$ to increase slightly. There was little effect of the modified forebody on the L/D values. In addition, the smaller forebody radius resulted in a small decrease in the directional instability (fig. 13(c)). The differences indicated in C_{n_β} above $\alpha = 20^{\circ}$ were apparently due to sting effects for the two stings shown in figure 1(c) for high angles of attack.

The 134D orbiter with the modified forebody was also tested with and without the vertical tail to indicate the extent of the influence of this component, and the results of these tests are presented in figure 14. The vertical tail did not affect the longitudinal characteristics above $\alpha = 4^{\circ}$, except for C_A, which was affected up to $\alpha = 10^{\circ}$. It also

had no influence on the lateral and directional stability parameters $\left(C_{l_\beta}\right.$ and $\left.C_{n_\beta}\right)$ above $\alpha \approx 13^\circ$. Since the vertical tail was ineffective at the operational angles of attack, rudder-control tests were not conducted.

The effect of elevon deflections on the longitudinal, lateral, and directional aerodynamic characteristics of the 134D orbiter is presented in figure 15. The vehicle was stable and trimmable from approximately 20° angle of attack up to about 46°, with $C_{L,max}$ occurring near $\alpha = 53^\circ$. It could also be trimmed with neutral stability near the angle of attack for $(L/D)_{max}$, $\alpha = 14^\circ$.

The lateral and directional results (fig. 15(c)) show that the 134D orbiter was directionally unstable $\left(\text{negative values of } C_{n_\beta}\right)$ and laterally stable $\left(\text{negative values of } C_{l_\beta}\right)$ for $\alpha = 4^\circ$ to 55°, and the values of $(C_{n_\beta})_{dyn}$ became positive above $\alpha = 21^\circ$. This dynamic directional stability parameter is often used as an indicator of directional stability at the higher angles of attack (ref. 13), with positive values being desirable. The elevon deflections had little effect on the directional stability (the small differences indicated in the C_{n_β} data above $\alpha = 20^\circ$ can be attributed to sting effects) and only a small effect on the lateral stability above $\alpha = 20^\circ$. These results indicate that longitudinal and lateral stability augmentation would be required in order to fly the vehicle at angles of attack where $(L/D)_{max}$ occurs.

Aileron tests were conducted to determine elevon roll control and the effect of the ailerons on yawing moment. The effect of roll control on the aerodynamic characteristics was obtained by differentially deflecting the elevons for three longitudinally trimmed conditions: $\delta_a = 10^\circ$ and $\delta_e = 0^\circ$ for trim near $\alpha = 22^\circ$, $\delta_a = 15^\circ$ and $\delta_e = -15^\circ$ for trim near $\alpha = 31^\circ$, and $\delta_a = 15^\circ$ and $\delta_e = -30^\circ$ for trim near $\alpha = 41^\circ$. The longitudinal data for these conditions are presented in figures 16(a) and (b), and the roll control and its effect on yawing moment are indicated in figure 16(c). Only the lower trim angle case studied $\left(\delta_e = 0^\circ\right)$ resulted in adverse yaw due to roll control $\left(-C_{n_{\delta_a}}\right.$ in fig. 16(c)$\left.\right)$. The dashed curve represents the longitudinal trimmed conditions and indicates that adverse yaw would occur below $\alpha \approx 32^\circ$ and that augmentation would be required to fly below this angle of attack. Apparently at the higher trim angles, the elevons that are deflected upward create a stable yawing moment as a result of the interaction with the flow over the upper surface of the wings. This flow is indicated by the oil-flow patterns on the wing upper surface in figure 5(b).

The 050B orbiter.- Most of the results for the 050B orbiter were obtained for an angle-of-attack range of 22° to 49° since this is the region of greatest interest for the test Mach number as indicated earlier, but the vehicle was tested down to $\alpha = 0^\circ$ for one elevon setting to obtain the value of $(L/D)_{max}$. The vehicle could be trimmed with longitudinal stability from approximately $\alpha = 25^\circ$ to near $\alpha = 50^\circ$ (fig. 17) for a relatively small change in elevon deflection (on the order of 10°). Compared with the elevon

control results of the 134D orbiter (fig. 15(a)), the 0.50B orbiter was more sensitive to elevon deflections. This difference can be attributed to the larger elevons on the 050B. The value of $(L/D)_{max}$ for this configuration was 2.2 at $\alpha = 14^{o}$, but it did not have a stable trim point at this angle of attack. Apparently the vehicle could be trimmed with neutral stability down to approximately $\alpha = 20^{o}$ where the L/D had a value of 2. The lateral and directional static stability characteristics (fig. 17(c)) show that the vehicle was directionally unstable and laterally stable with a positive value of $\left(C_{n_\beta}\right)_{dyn}$ for the angle-of-attack range of the tests ($\alpha = 22^{o}$ to 49^{o}).

The effect of roll control on the aerodynamic characteristics was studied by differentially deflecting the elevons for longitudinal trim at two angles of attack; $\delta_a = 5^{o}$ and $\delta_e = -5^{o}$ for trim near $\alpha = 26^{o}$, and $\delta_a = 10^{o}$ and $\delta_e = -10^{o}$ for trim near $\alpha = 32^{o}$. The longitudinal data for these two conditions are presented in figures 18(a) and (b), and the effect of roll control on the yawing moment is indicated in figure 18(c). Both trim cases resulted in adverse yaw due to roll control (fig. 18(c)). The magnitude of the cross coupling is indicated by the ratio of $C_{n_{\delta_a}}$ to $C_{l_{\delta_a}}$, which is approximately -0.37 for the two cases. This cross coupling could be reduced by sweeping the wing trailing edge and elevon hinge line forward as shown in reference 14 for a similar configuration, but it probably could not be completely eliminated because of realistic design constraints (limits on the forward sweep angle). The vehicle would therefore require some control augmentation to be flyable in this angle-of-attack range.

Theoretical predictions.- The experimental aerodynamic characteristics have been compared with tangent-cone and Newtonian theories (including skin-friction effects) for the following cases: the 134D orbiter with and without the wing (fig. 19), the 134D with elevon deflections (fig. 20), and the 050B for one elevon deflection (fig. 21). In general, the variations of the data with angle of attack were predicted but not the absolute values. The predictions for all the parameters (pitching-moment coefficient in particular) for the 134D orbiter without the wings were noticeably better than for the complete configuration in figure 19 and for the 050B orbiter in figure 21. For the complete configurations, both theories consistently overpredicted the pitching-moment coefficients, predicted the L/D values reasonably well above $\alpha = 25^{o}$, and predicted smaller effective dihedral $\left(-C_{l_\beta}\right)$ and less yaw instability $\left(-C_{n_\beta}\right)$ above $\alpha = 20^{o}$. For the elevon control results presented in figure 20, the trends in the data and the actual increments in the C_m values were predicted, but the effect of the elevon deflections on the longitudinal force characteristics was exaggerated. Similar experiences in predicting hypersonic aerodynamic characteristics for several delta-wing concepts were reported in reference 15.

CONCLUDING REMARKS

The longitudinal, lateral, and directional aerodynamic characteristics of two space shuttle concepts, one designed by McDonnell Douglas Corp. and the other by North American Rockwell Corp., have been obtained over an angle-of-attack range of -10° to 55° in helium for operational flight Reynolds numbers at a Mach number of 20.3. Selected aerodynamic results for both concepts have been compared with characteristics derived from tangent-cone and Newtonian theories. Also included are results of a flow-visualization study consisting of electron-beam-illuminated flow and surface oil-flow patterns.

In general, the flow characteristics indicated by the flow-visualization studies were similar for both vehicles with potential high-heating regions in areas of high shear and shock impingement. The bow-wing shock interactions were located inboard of the wing tips at 20° angle of attack, near the tips at 30° angle of attack, and beyond the tips at higher angles.

The experimental aerodynamic results showed that the hypersonic performance was relatively insensitive to the differences between the two configurations and that both would require stability augmentation for some portions of flight. For their operational hypersonic angle-of-attack range, approximately 23° to 50°, both vehicles were longitudinally stable and could be trimmed with static stability, both had about the same lift-drag ratios, with a maximum value of about 2.2, both were directionally unstable and laterally stable, and both had a positive dynamic directional stability parameter. Although both concepts had adverse yaw due to roll control at angles of attack from 23° to 31°, the North American Rockwell configuration did not have this adverse cross coupling above 32° angle of attack. The vertical tail on this configuration became completely ineffective above 13° angle of attack and would be of no use over the operational hypersonic angle-of-attack range, as expected. A modified forebody with a smaller leading-edge radius and a slightly larger planform area increased the trim angle of attack from about 20° to 39° for undeflected elevon controls on this configuration. A comparison of the experimental results with tangent-cone and Newtonian theories showed that both theories equally predicted the proper trends in the data, but the absolute values were not always predicted.

Langley Research Center,
National Aeronautics and Space Administration,
Hampton, Va., May 7, 1973.

REFERENCES

1. Anon.: Spacemaster – A Two-Stage Fully Reusable Space Transportation System, Phase A. MCR-69-36, Martin Marietta Corp., Dec. 1969.

2. Anon.: Space Shuttle System – Phase B Study Final Report. Pt. II-2(A). MDC E0308 (Contract NAS 8-26016), McDonnell Douglas Corp., June 30, 1971. (Available as NASA CR-119879.)

3. Anon.: Space Shuttle Phase B Final Report. Vol. II, Book 2. SD 71-114-2(2) (Contract NAS 9-10960), North American Rockwell Corp., June 25, 1971. (Available as NASA CR-119776.)

4. Love, E. S.: Advanced Technology and the Space Shuttle. AIAA Paper No. 73-31, Jan. 1973.

5. Allen, E. C.: Static Stability and Control Characteristics of the NR Delta Wing (134D) Space Shuttle Orbiter M=0.6-5.0. DMS-DR-1126 (Contract NAS 8-4016), Space Div., Chrysler Corp., Aug. 1971. (Available as NASA CR-119980.)

6. Seeny, P. J.; Field, D.; Heinemann, D.: Longitudinal and Lateral Directional Stability Characteristics of the MDAC High Cross Range Delta Wing Orbiter. DMS-DR-1067 (Contract NAS 8-4016), Space Div., Chrysler Corp., Feb. 1971. (Available as NASA CR-119857.)

7. Arrington, James P.; Joiner, Roy C., Jr.; and Henderson, Arthur, Jr.: Longitudinal Characteristics of Several Configurations at Hypersonic Mach Numbers in Conical and Contoured Nozzles. NASA TN D-2489, 1964.

8. Weinstein, Leonard M.; Wagner, Richard D., Jr.; Henderson, Arthur, Jr.; and Ocheltree, Stewart L.: Electron Beam Flow Visualization in Hypersonic Helium Flow. ICIASF '69 Record, IEEE Publ. 69-C-19 AES, pp. 72-78.

9. Monaghan, R. J.: An Approximate Solution of the Compressible Laminar Boundary Layer on a Flat Plate. R. & M. No. 2760, Brit. A.R.C., 1953.

10. Gentry, Arvel E.; and Smyth, Douglas N.: Hypersonic Arbitrary-Body Aerodynamic Computer Program (Mark III Version). Rep. DAC 61552 (Air Force Contract Nos. F33615 67 C 1008 and F33615 67 C 1602), Douglas Aircraft Co., Apr. 1968.
    Vol. I – User's Manual. (Available from DDC as AD 851 811.)
    Vol. II – Program Formulation and Listings. (Available from DDC as AD 851 812.)

11. Arrington, James P.; and Woods, William C.: Hypersonic Aerodynamics and Entry-Maneuver—Aerothermodynamic Interactions for Two Lifting Entry Vehicles. NASA TN D-6753, 1972.

12. Ellison, James C.; and Spencer, Bernard, Jr.: Hypersonic Aerodynamic Characteristics of a Variable-Dihedral Delta-Wing Spacecraft Configuration. NASA TM X-2391, 1971.

13. Moul, Martin T.; and Paulson, John W.: Dynamic Lateral Behavior of High-Performance Aircraft. NACA RM L58E16, 1958.

14. Arrington, James P.; and Ashby, George C., Jr.: Effect of Configuration Modifications on the Hypersonic Aerodynamic Characteristics of a Blended Delta Wing-Body Entry Vehicle. NASA TM X-2611, 1972.

15. Hamilton, Richard K.: Correlation of Space Shuttle Applicable Experimental Hypersonic Aerodynamic Characteristics With Theory. NASA Space Shuttle Technology Conference, Vol. I, NASA TM X-2272, 1971, pp. 455-492.

TABLE I.- FULL-SCALE GEOMETRIC CHARACTERISTIC OF CONFIGURATIONS

	134D	050B
Fuselage:		
Length, m	53.848	47.671
Maximum height, m	6.967	9.235
Maximum width, m	11.757	8.260
Wing:		
Root chord at fuselage center line, m	31.289	27.554
Mean aerodynamic chord, m	20.858	19.172
Span (total), m	36.141	29.718
Total planform area (theoretical), m^2	565.204	495.157
Leading-edge sweep, deg	60	55
Trailing-edge sweep, deg	0	0
Dihedral, deg	7	10
Incidence, deg	0	2
Aspect ratio	2.310	1.79
Taper ratio	0	----------
Aerodynamic twist, deg	-5.0	0
Airfoil section, root	NACA 0009-64	NACA 0010-64
Airfoil section, tip	NACA 0012-64	NACA 0012-64
Elevon:		
Area, m^2	36.519	49.757
Span (equivalent), m	10.892	12.754
Chord, m	3.353	3.901
Vertical tail stabilizer:		
Root chord, m	9.913	7.864
Tip chord (equivalent), m	3.115	4.999
Mean aerodynamic chord, m	7.105	6.532
Span (equivalent), m	9.464	8.382
Planform area, m^2	61.651	53.882
Leading-edge sweep, deg	45	30
Trailing-edge sweep, deg	15.7	13.4
Aspect ratio	1.453	1.3
Taper ratio	0.314	0.638
Airfoil section	5^o wedge	NACA 0009-64

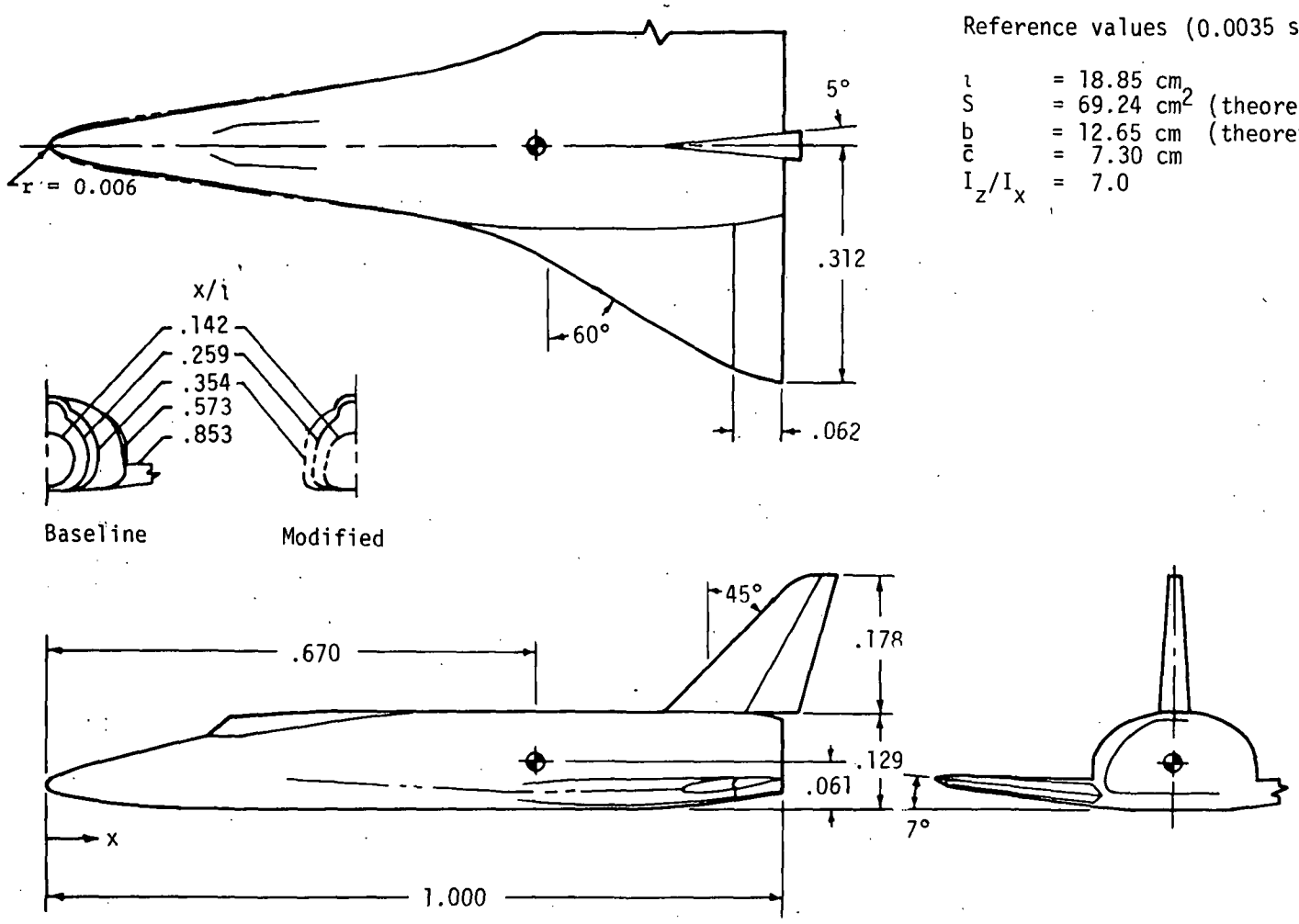

(a) 134D orbiter.

Figure 1.- Model drawings with dimensions normalized by body length l.

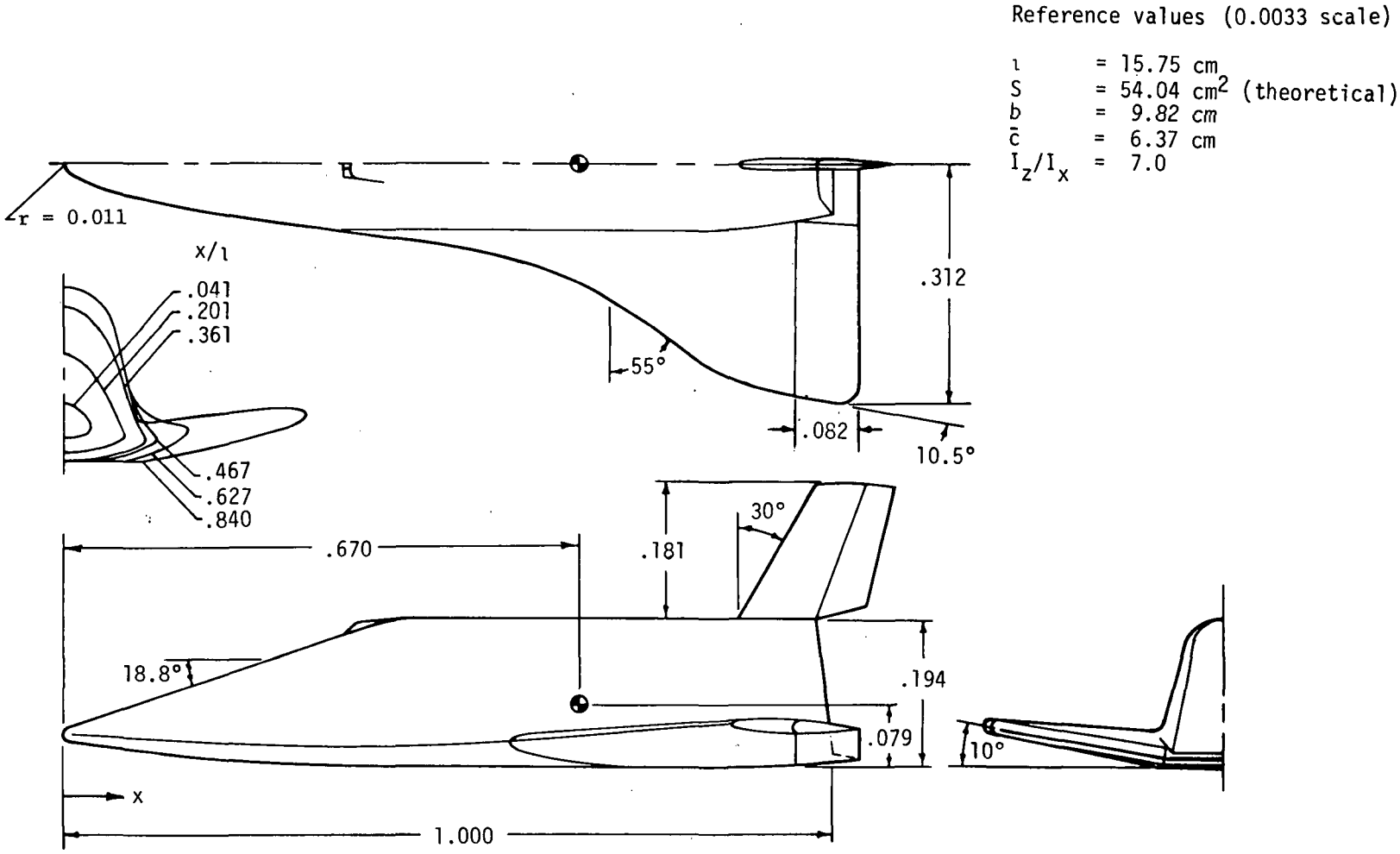

(b) 050B orbiter.

Figure 1.- Continued.

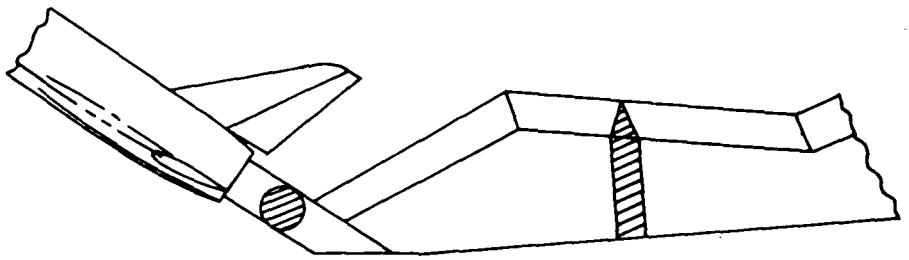

$19^{\circ} \leq \alpha \leq 55^{\circ}$

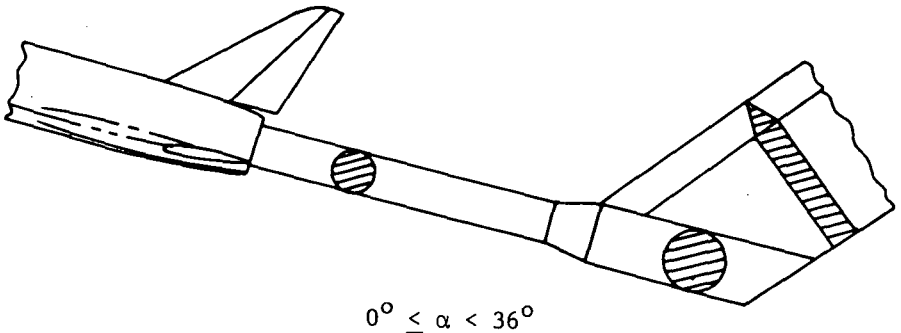

$0^{\circ} \leq \alpha \leq 36^{\circ}$

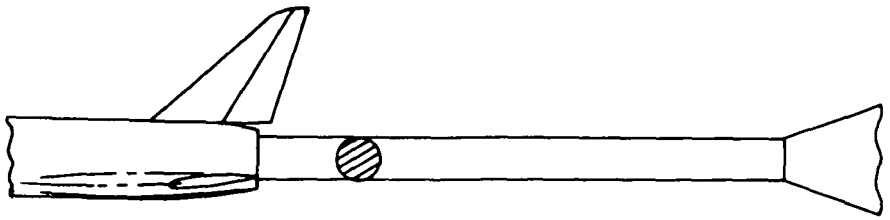

$-10^{\circ} \leq \alpha \leq 19^{\circ}$

(c) Typical model-sting arrangements for particular angle-of-attack ranges.

Figure 1.- Concluded.

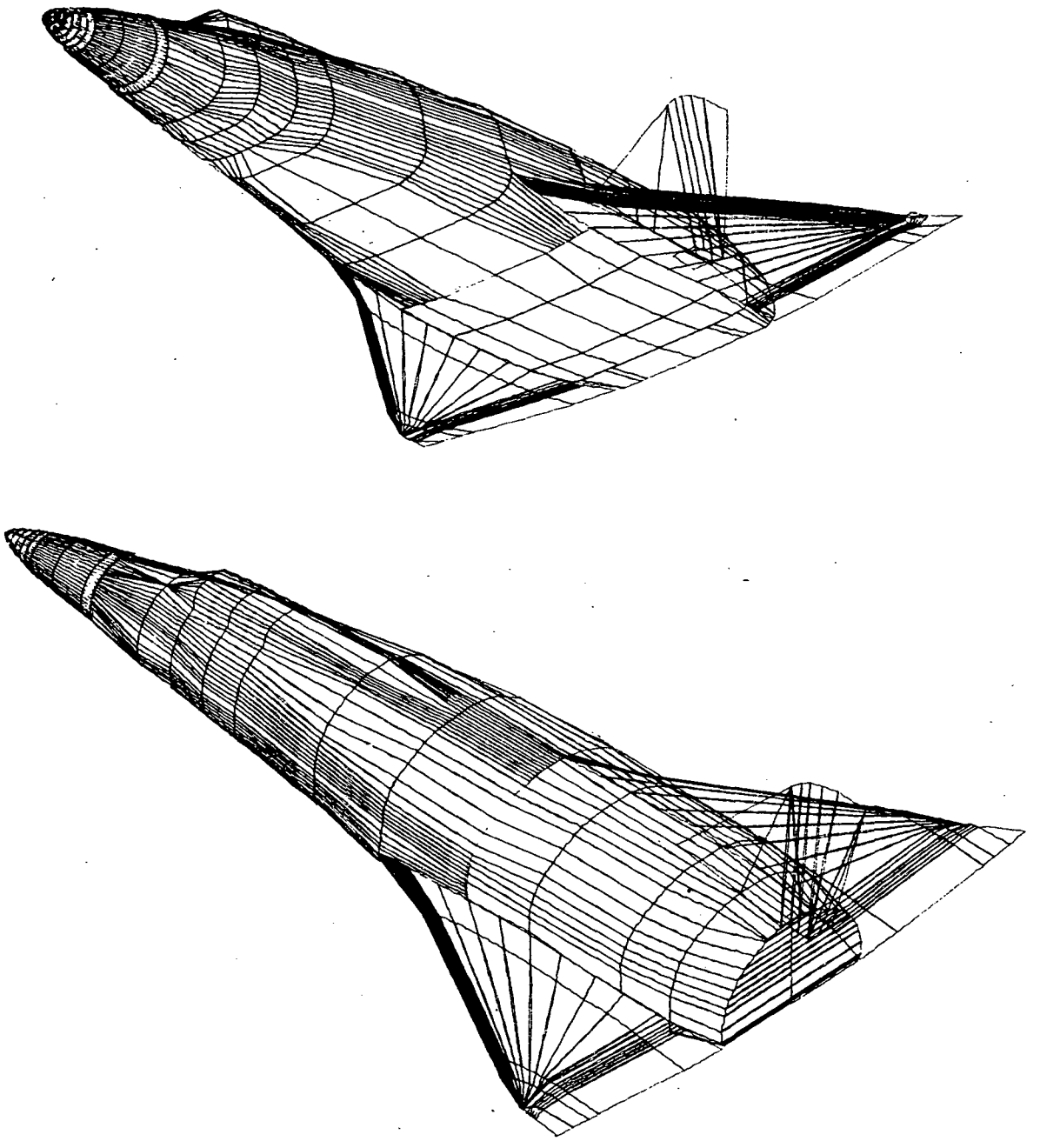

(a) Theoretical model of 134D orbiter.

Figure 2.- Configurations used in computer program for predicting aerodynamic forces and moments.

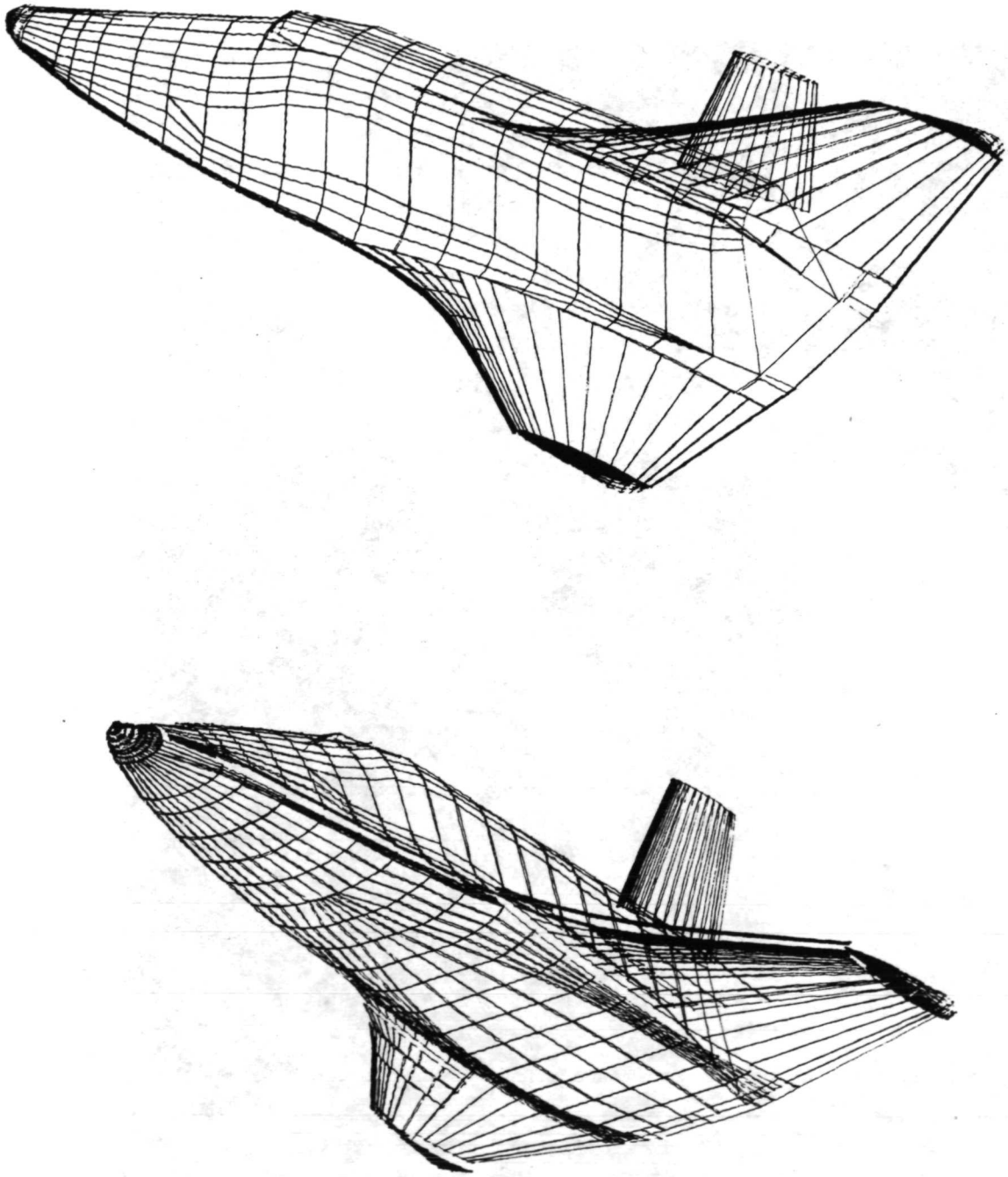

(b) Theoretical model of 050B orbiter.

Figure 2.- Concluded.

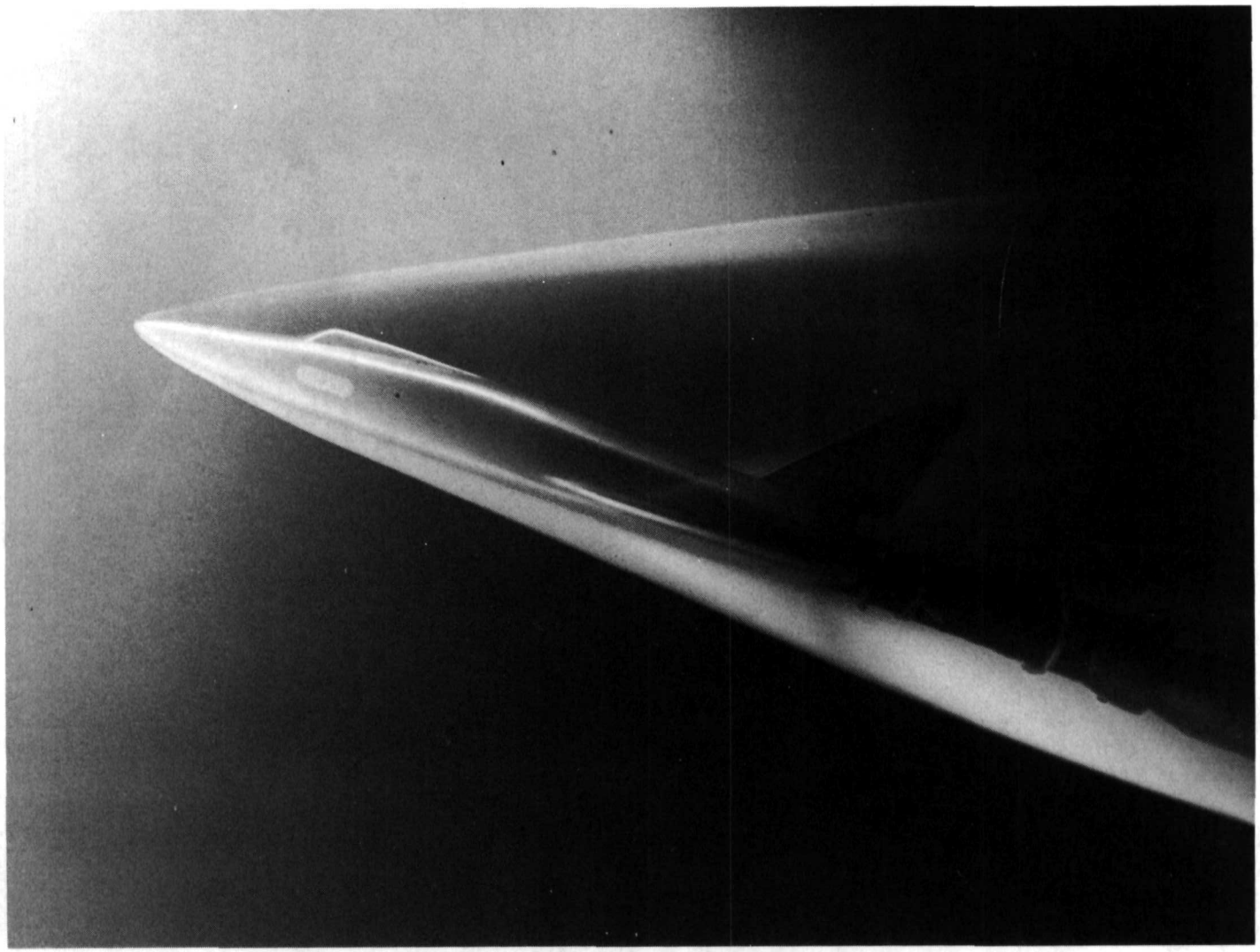

L-71-4621

(a) $\alpha = 20^{o}$; side view.

Figure 3.- Electron-beam-illuminated flow on 134D orbiter.

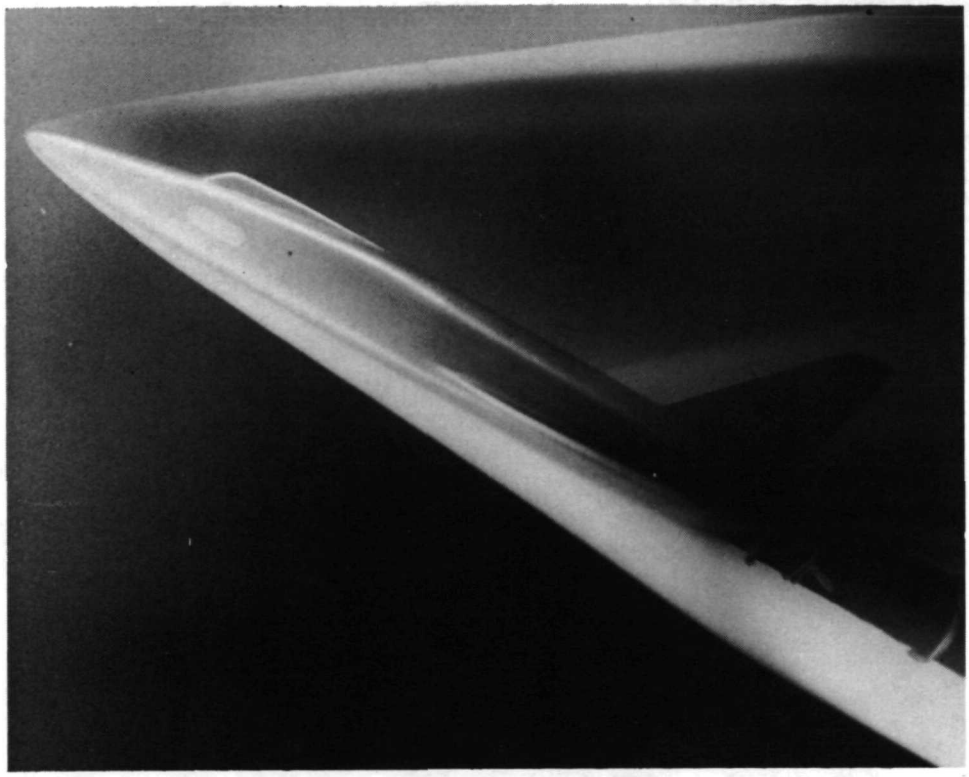

(b) $\alpha = 30^{o}$; side view.

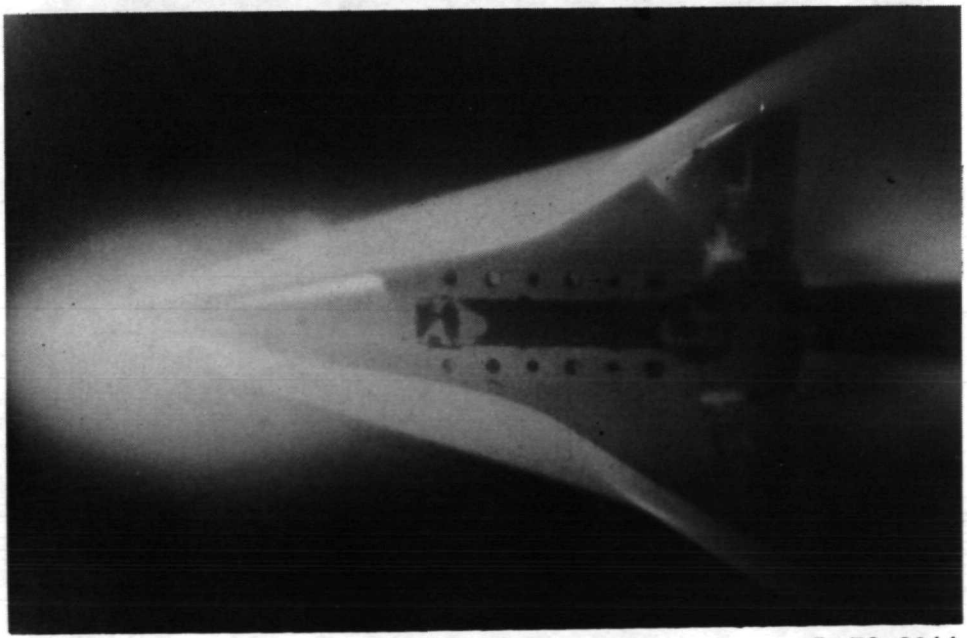

L-73-3044

(c) $\alpha = 30^{o}$; bottom view.

Figure 3.- Continued.

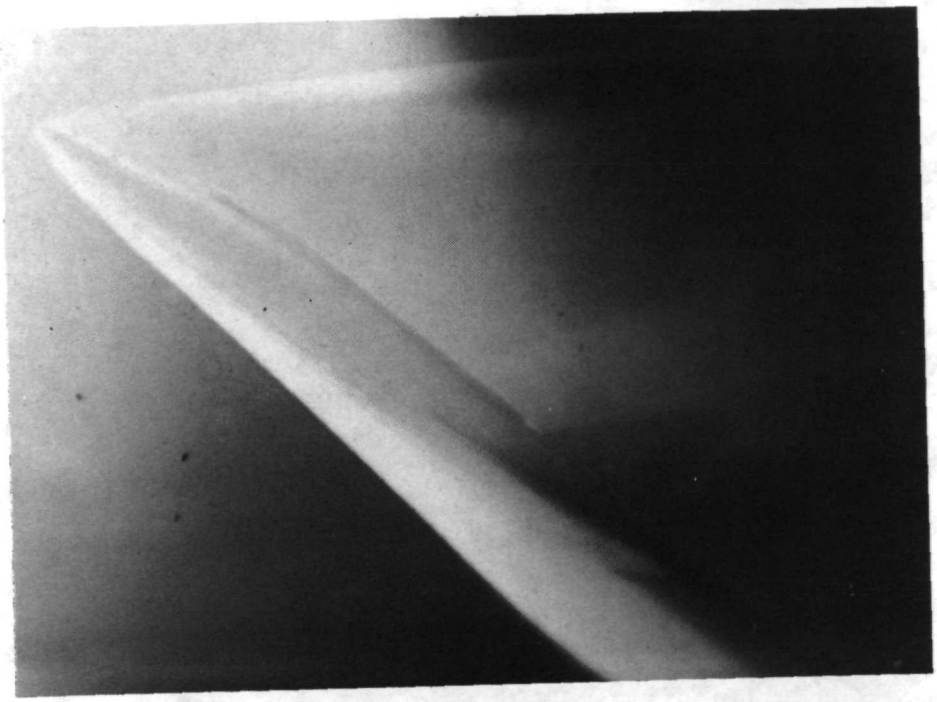

(d) $\alpha = 40^{o}$; side view.

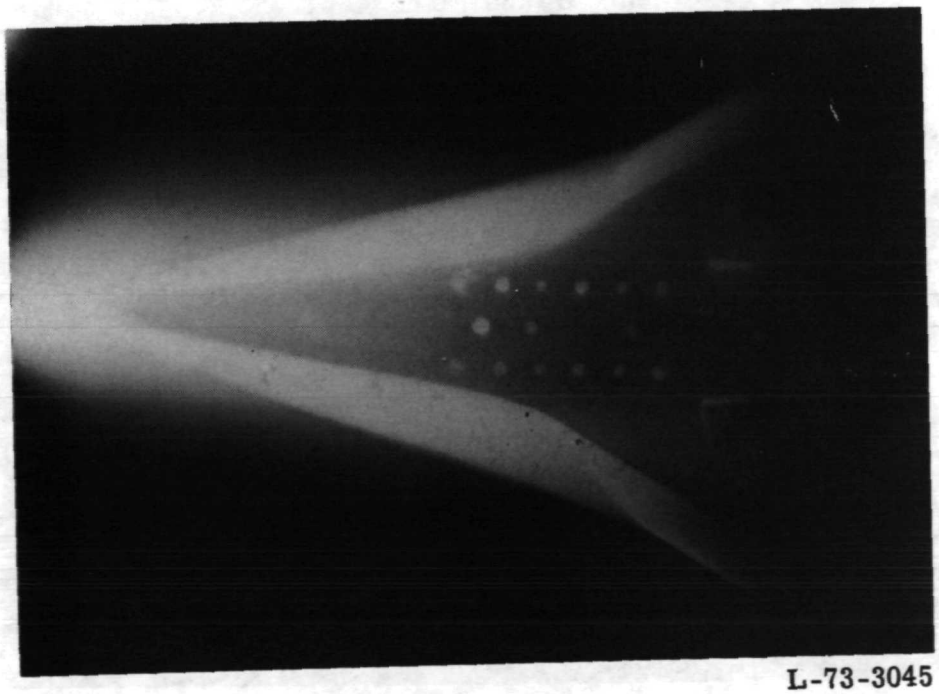

L-73-3045

(e) $\alpha = 40^{o}$; bottom view.

Figure 3.- Continued.

L-73-3046

(f) $\alpha = 55^{o}$; side view.

Figure 3.- Continued.

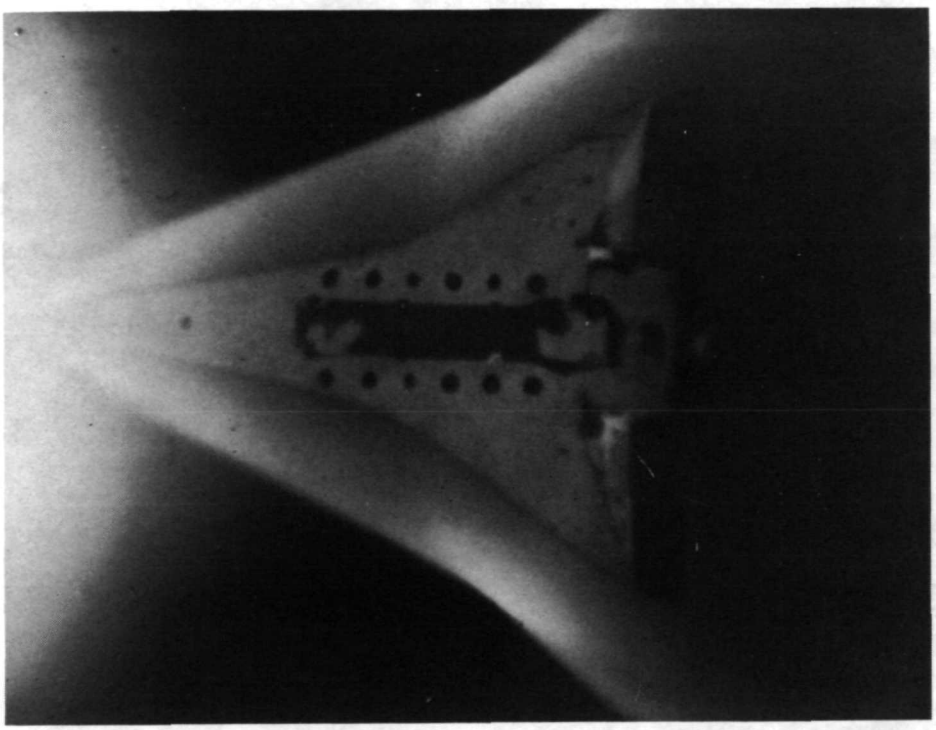

L-73-3047

(g) $\alpha = 55^{o}$; bottom view.

Figure 3.- Concluded.

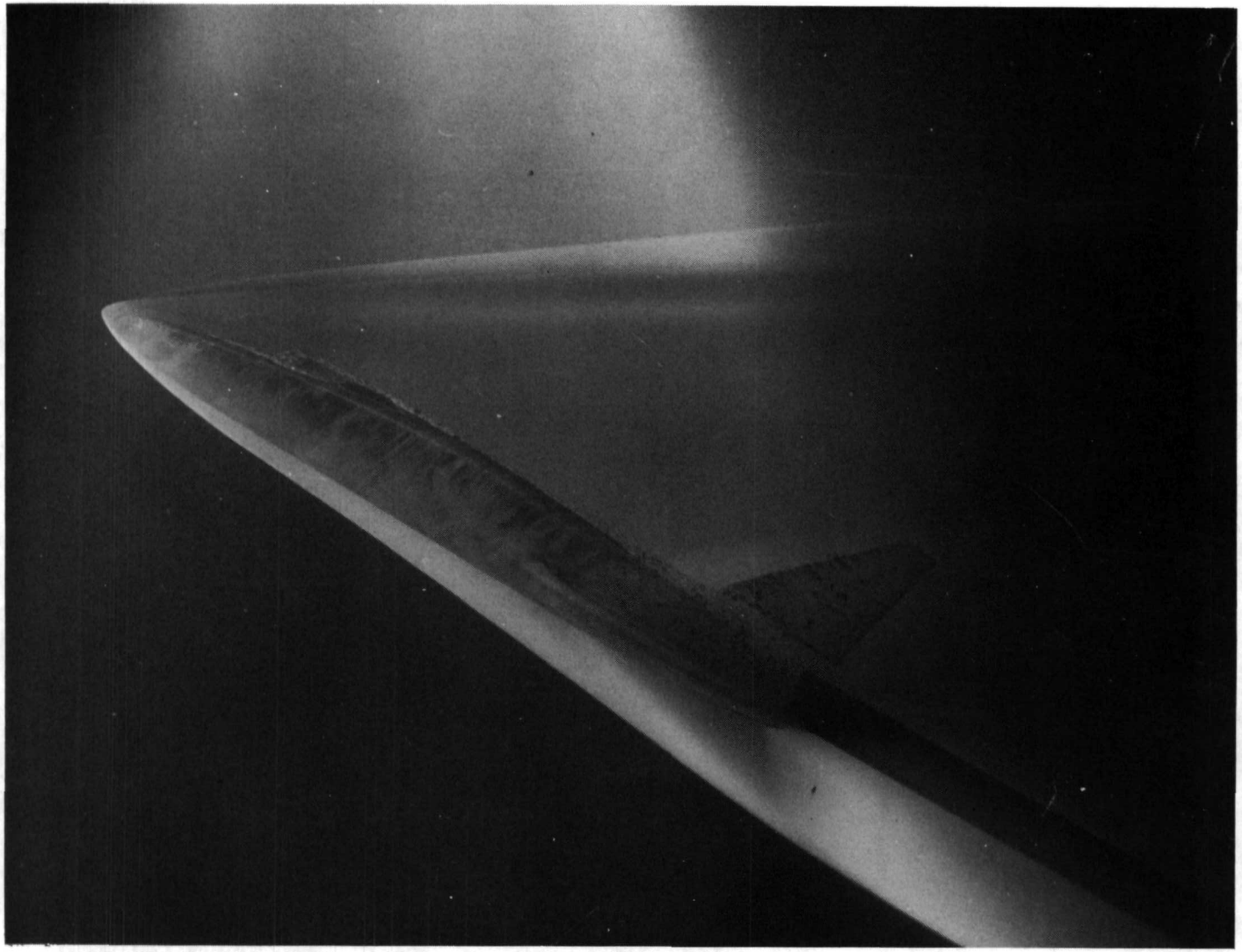

L-71-3751

Figure 4.- Electron-beam-illuminated surface oil flow on 134D orbiter $(\delta_e = 0^o)$ at $\alpha = 30^o$.

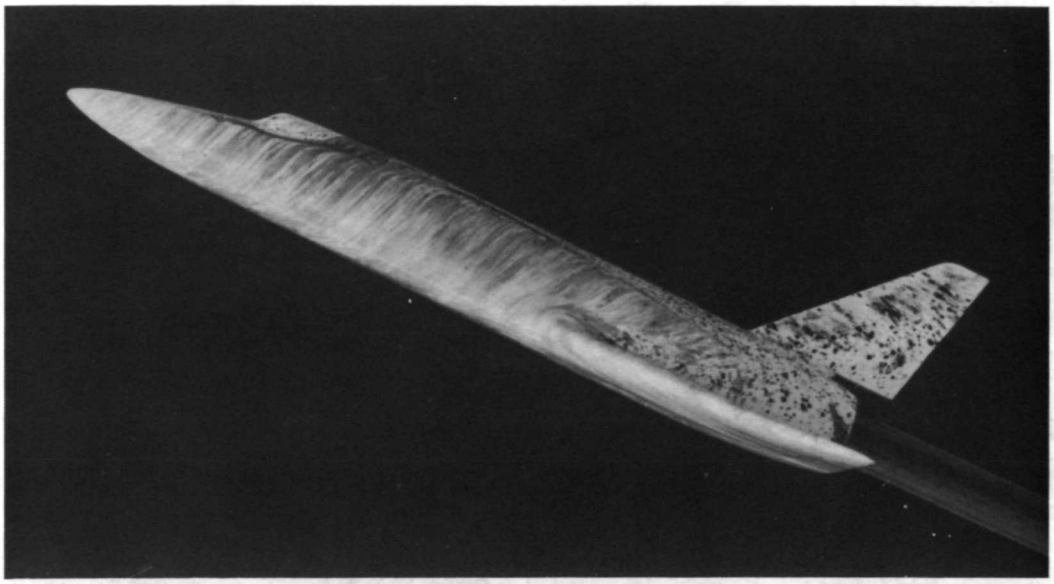

(a) Side view.

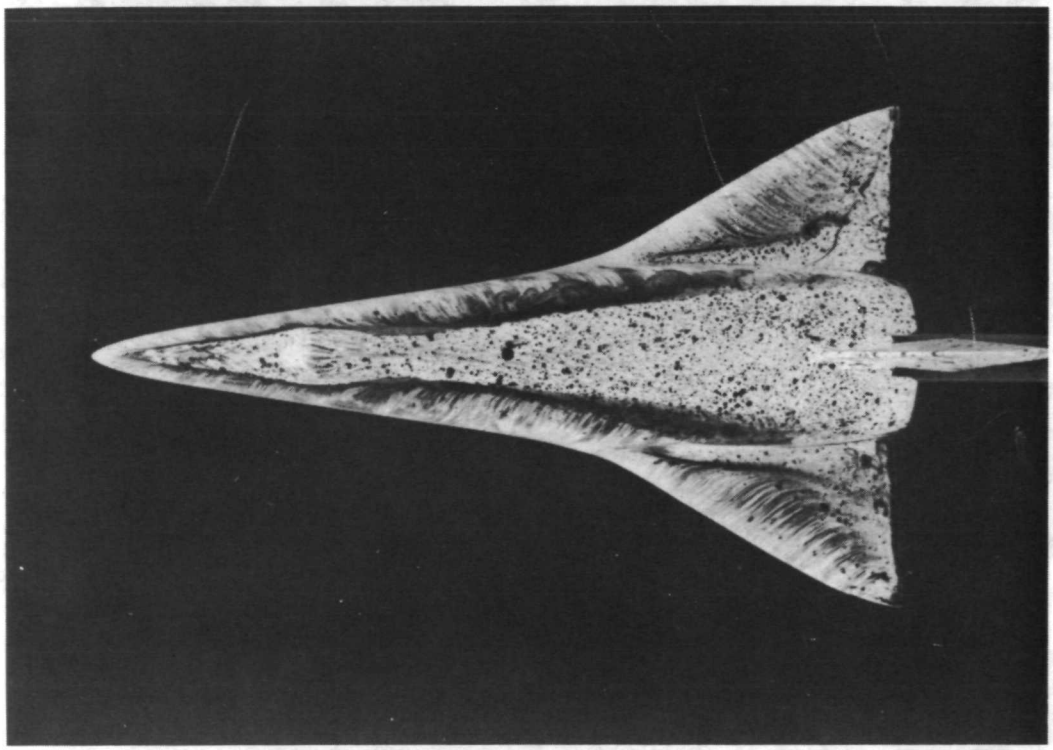

L-73-3048

(b) Top view.

Figure 5.- Postrun surface oil-flow patterns on 134D orbiter $\left(\delta_e = 0^o\right)$ for $\alpha = 30^o$.

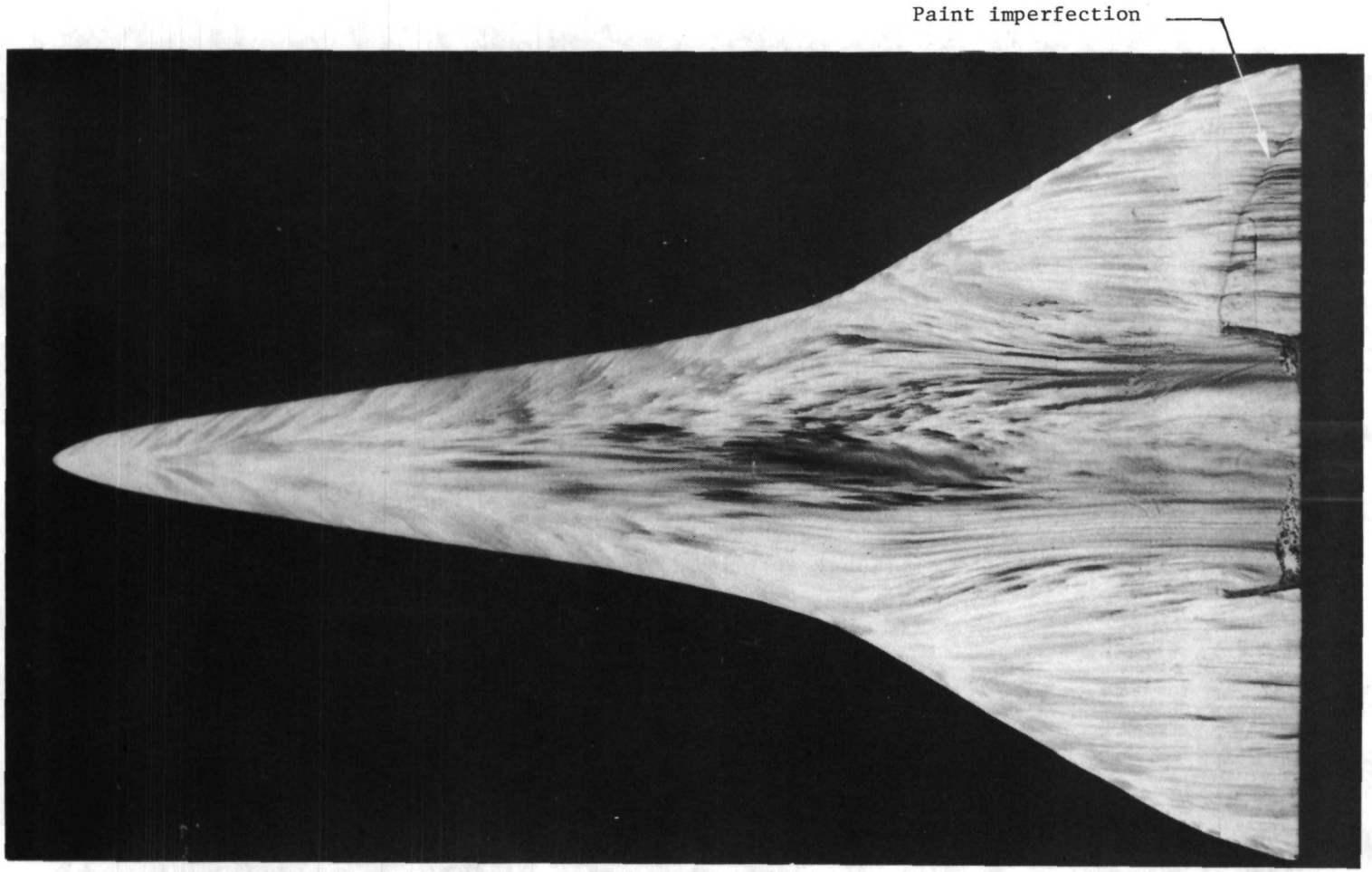

(c) Bottom view.

Figure 5.- Concluded.

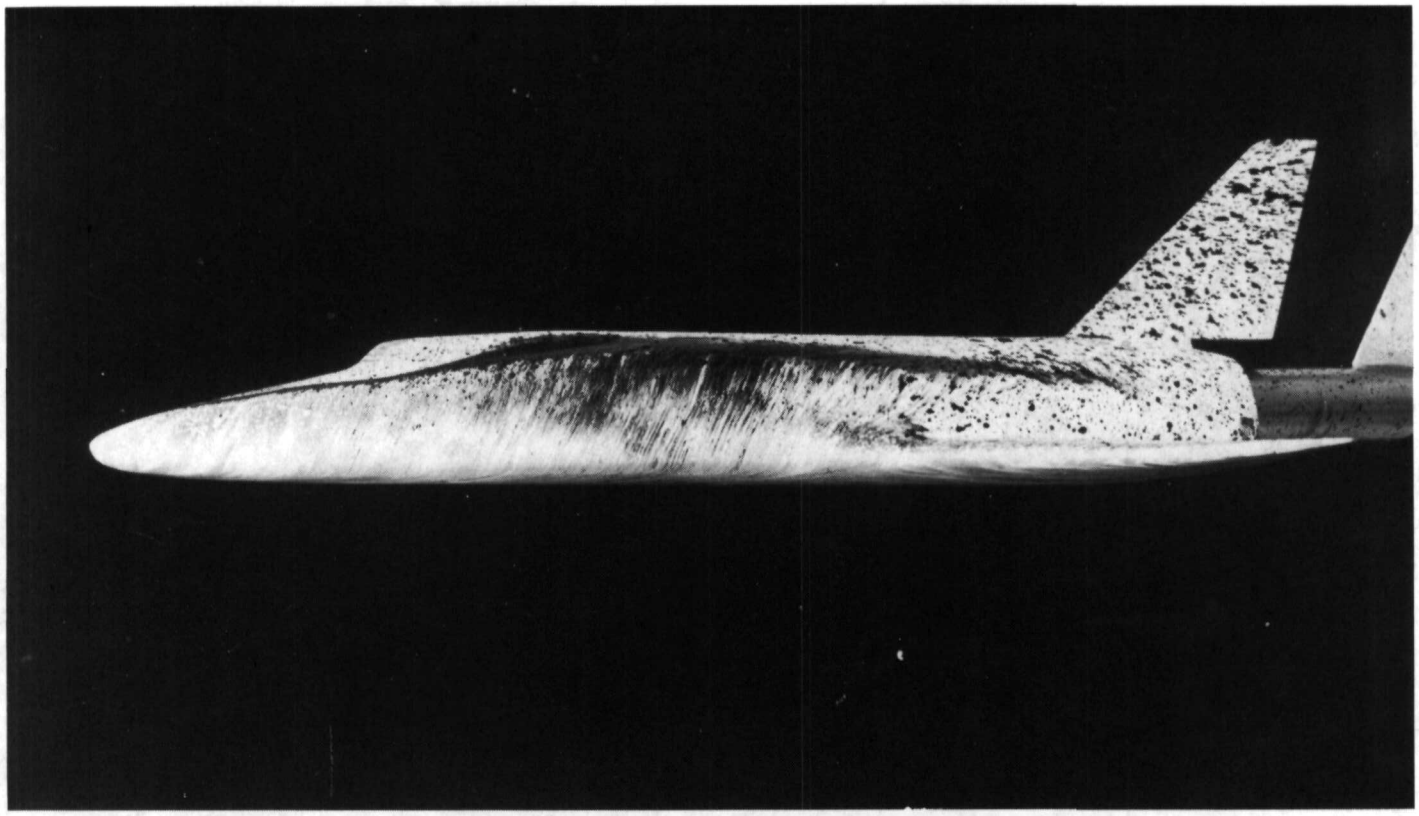

L-73-3049

(a) Side view.

Figure 6.- Postrun surface oil-flow patterns on 134D orbiter with modified forebody and $\left(\delta_e = 0^o\right)$ for $\alpha = 30^o$.

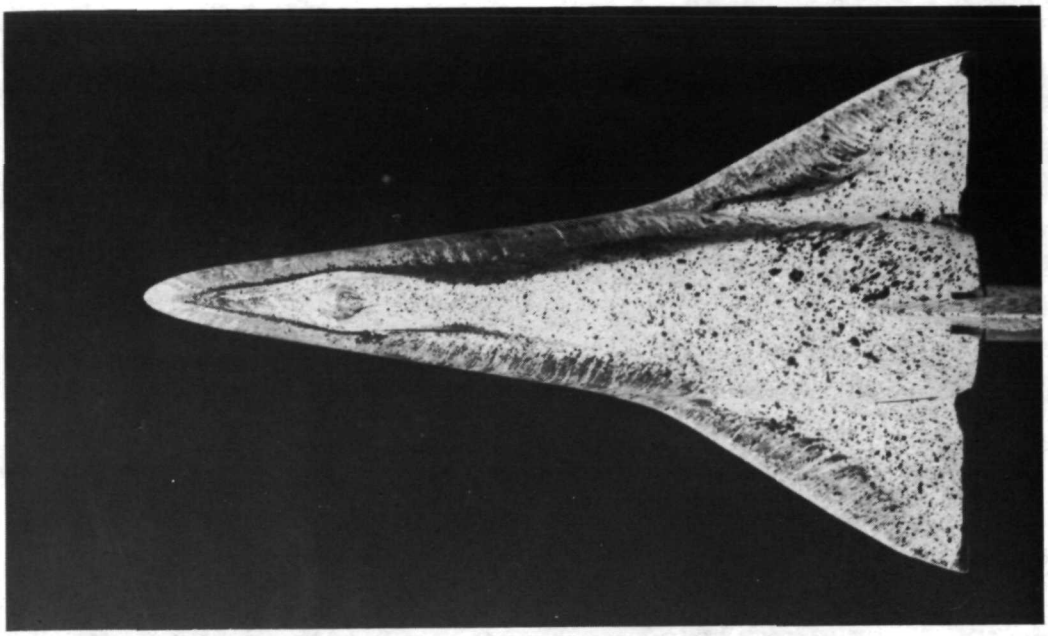

(b) Top view.

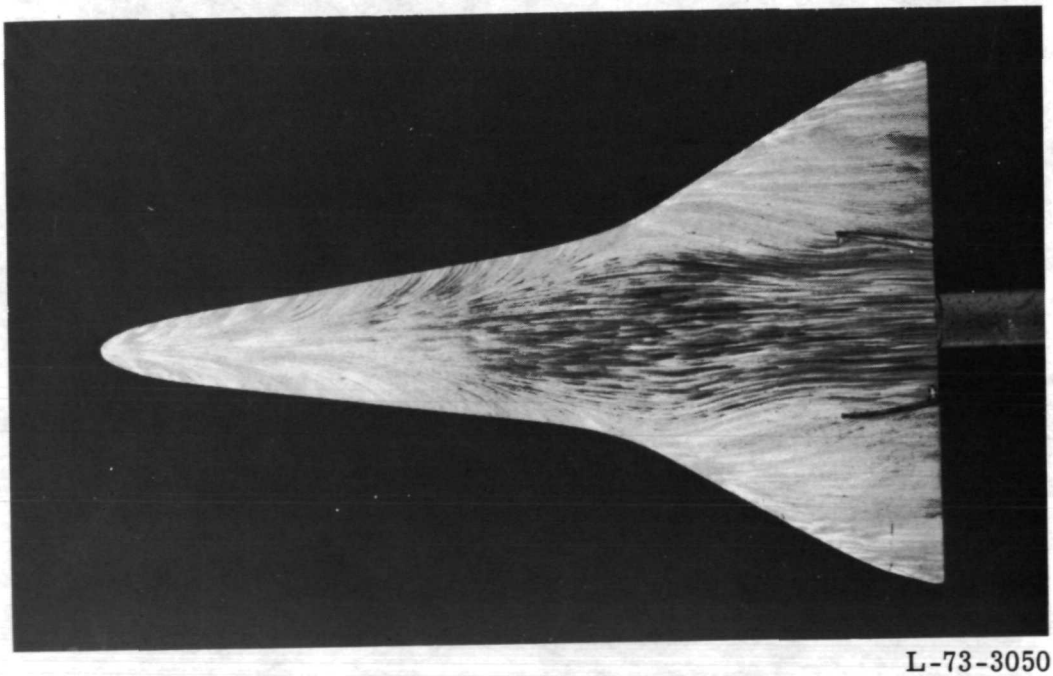

L-73-3050

(c) Bottom view.

Figure 6.- Continued.

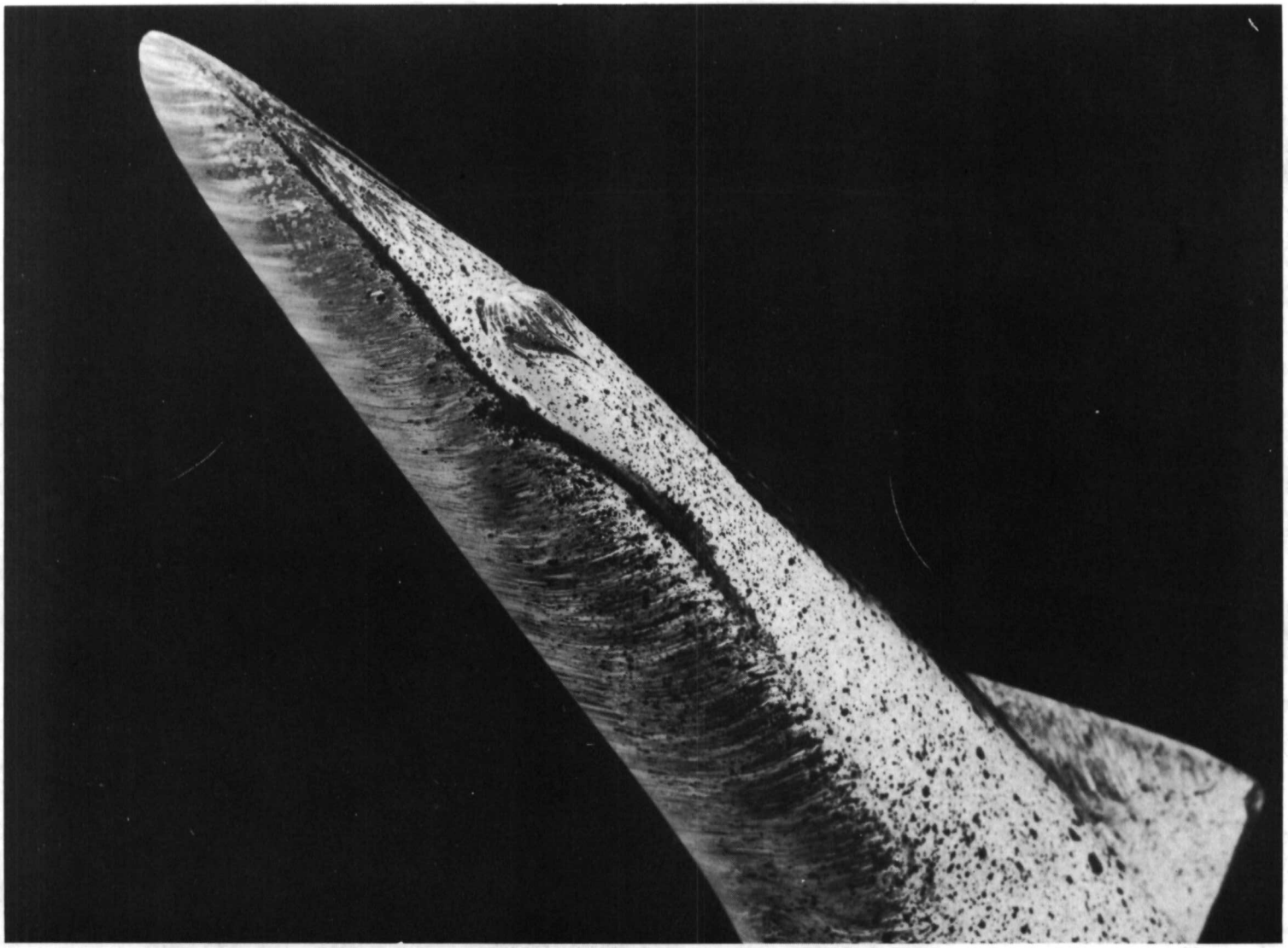

L-73-3051

(d) Oblique top view.

Figure 6.- Concluded.

L-71-2088

Figure 7.- Electron-beam-illuminated surface oil flow on 050B orbiter $\left(\delta_e = 0^o\right)$ at $\alpha = 20^o$.

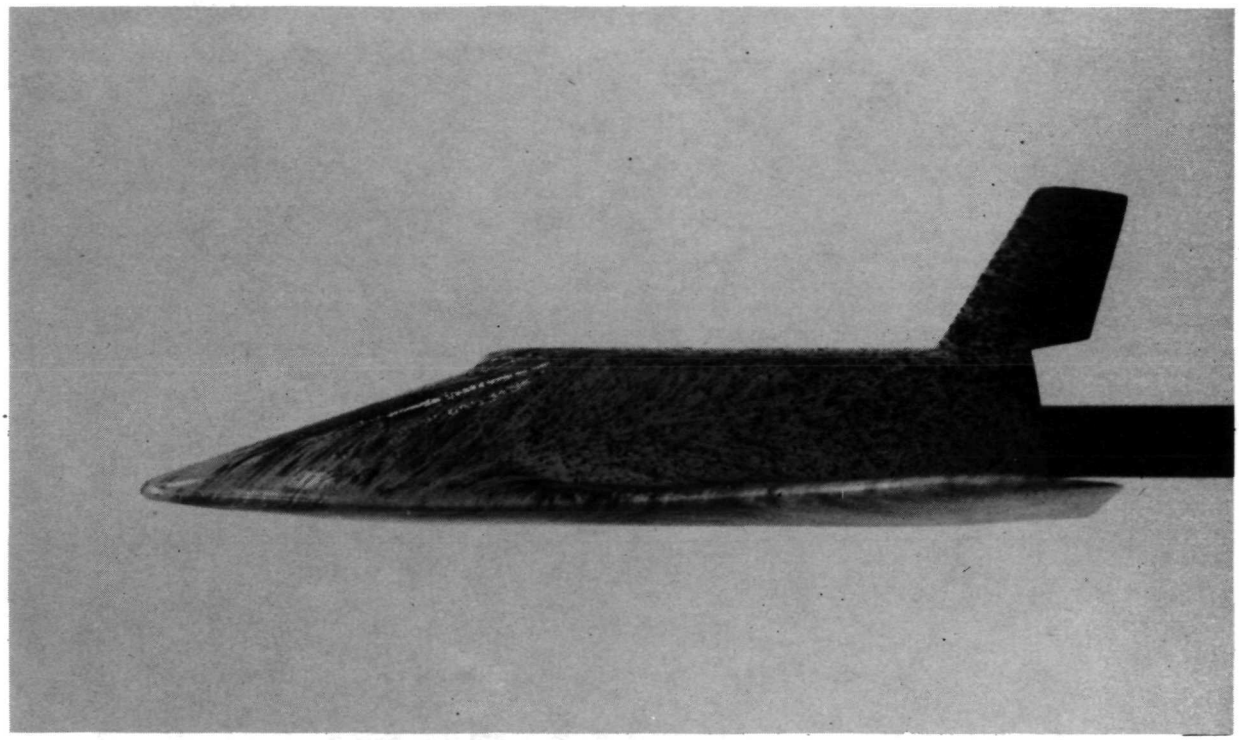

L-71-2761

(a) Side view.

Figure 8.- Postrun surface oil-flow patterns on 050B orbiter $(\delta_e = 0^o)$ for $\alpha = 20^o$.

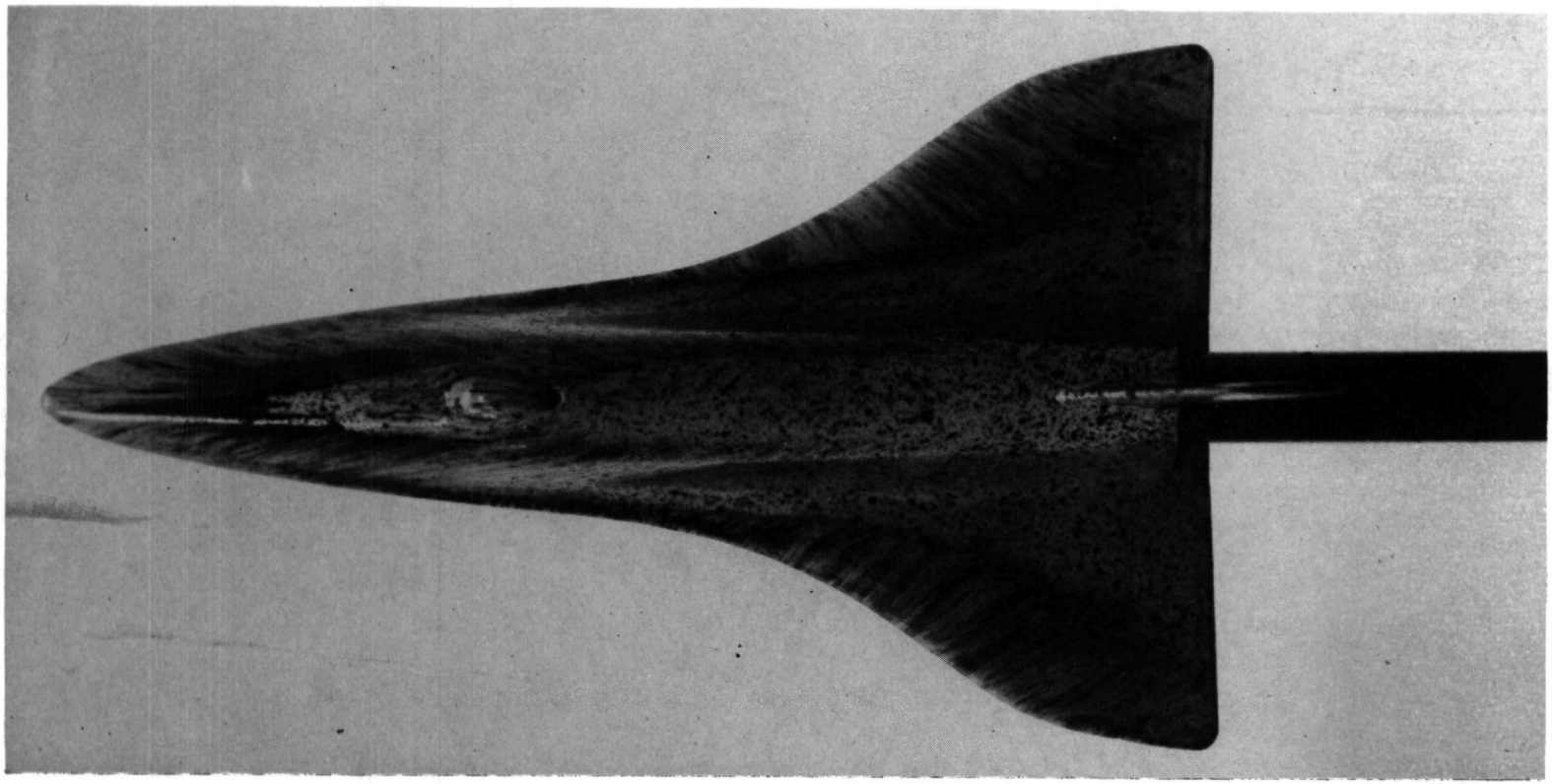

L-73-3052

(b) Top view.

Figure 8.- Continued.

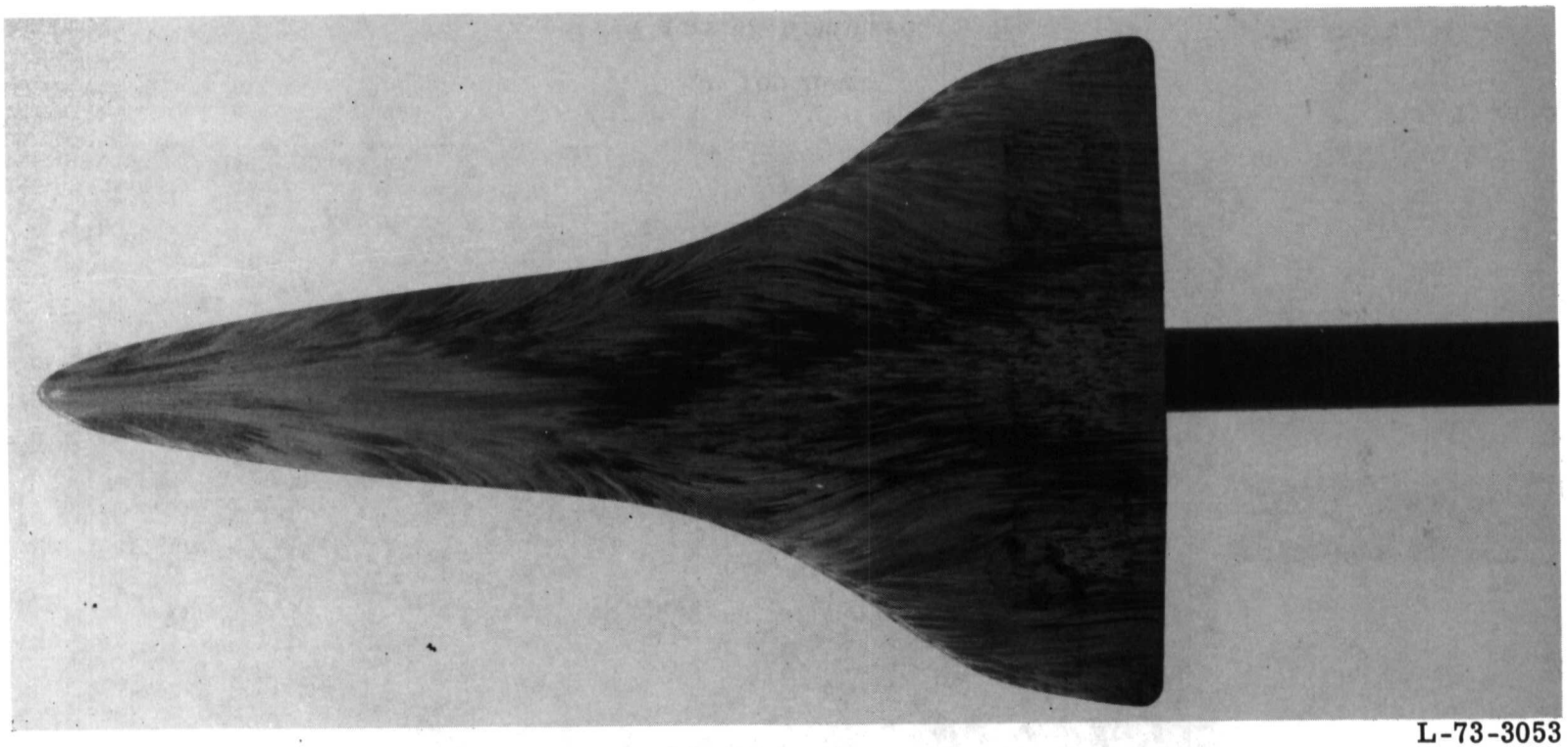

L-73-3053

(c) Bottom view.

Figure 8.- Concluded.

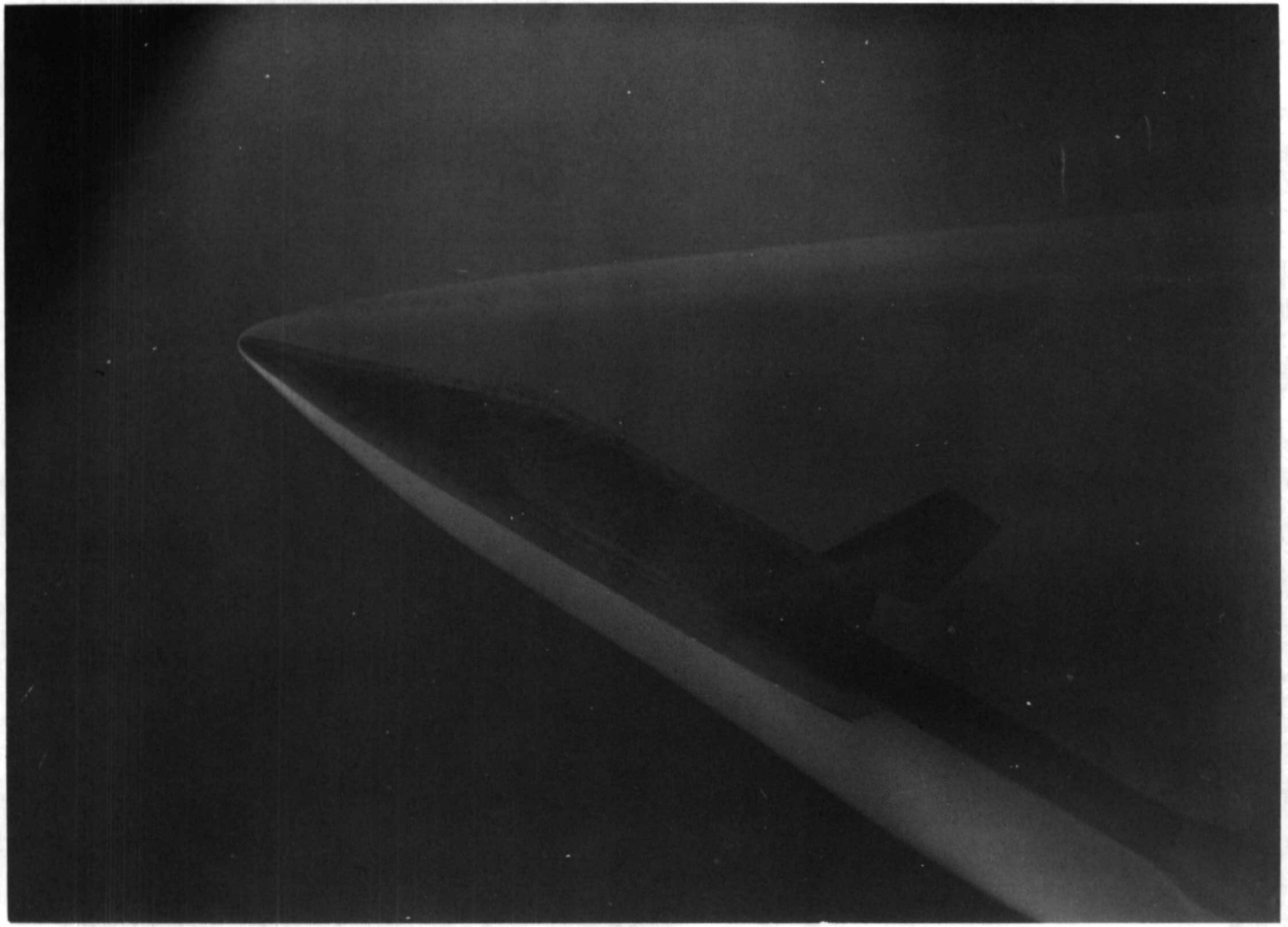

L-71-3748

(a) Side view.

Figure 9.- Electron-beam-illuminated surface oil flow on 050B orbiter $\left(\delta_e = -5^o\right)$ at $\alpha = 30^o$.

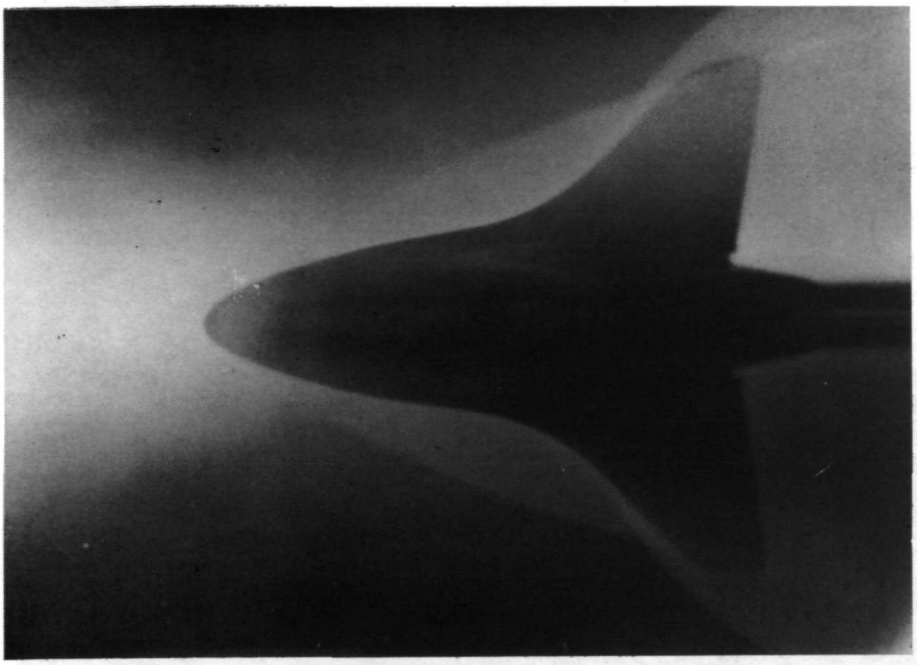

(b) Top view.

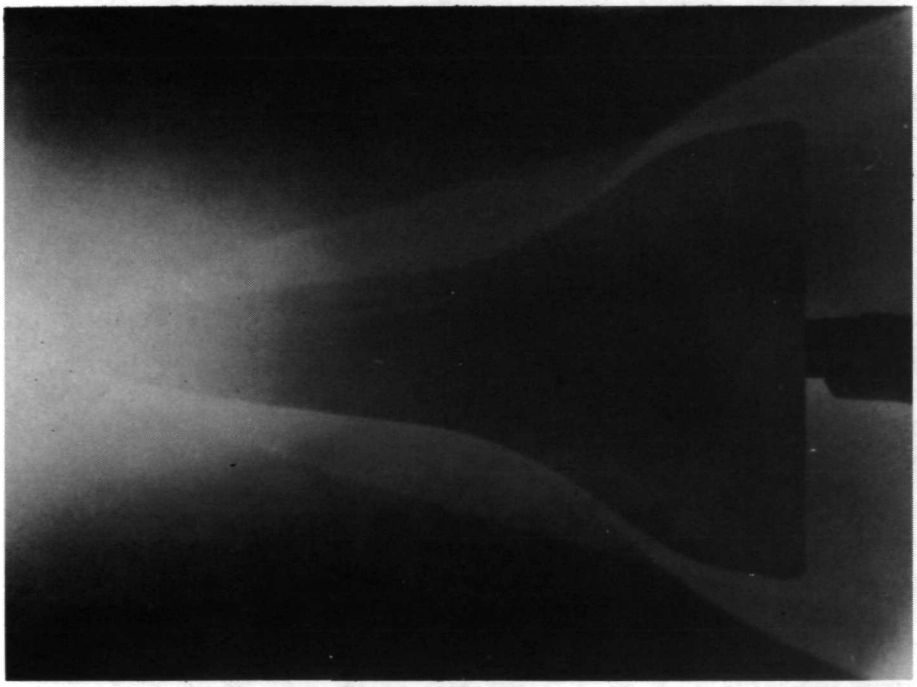

L-73-3054

(c) Bottom view.

Figure 9.- Concluded.

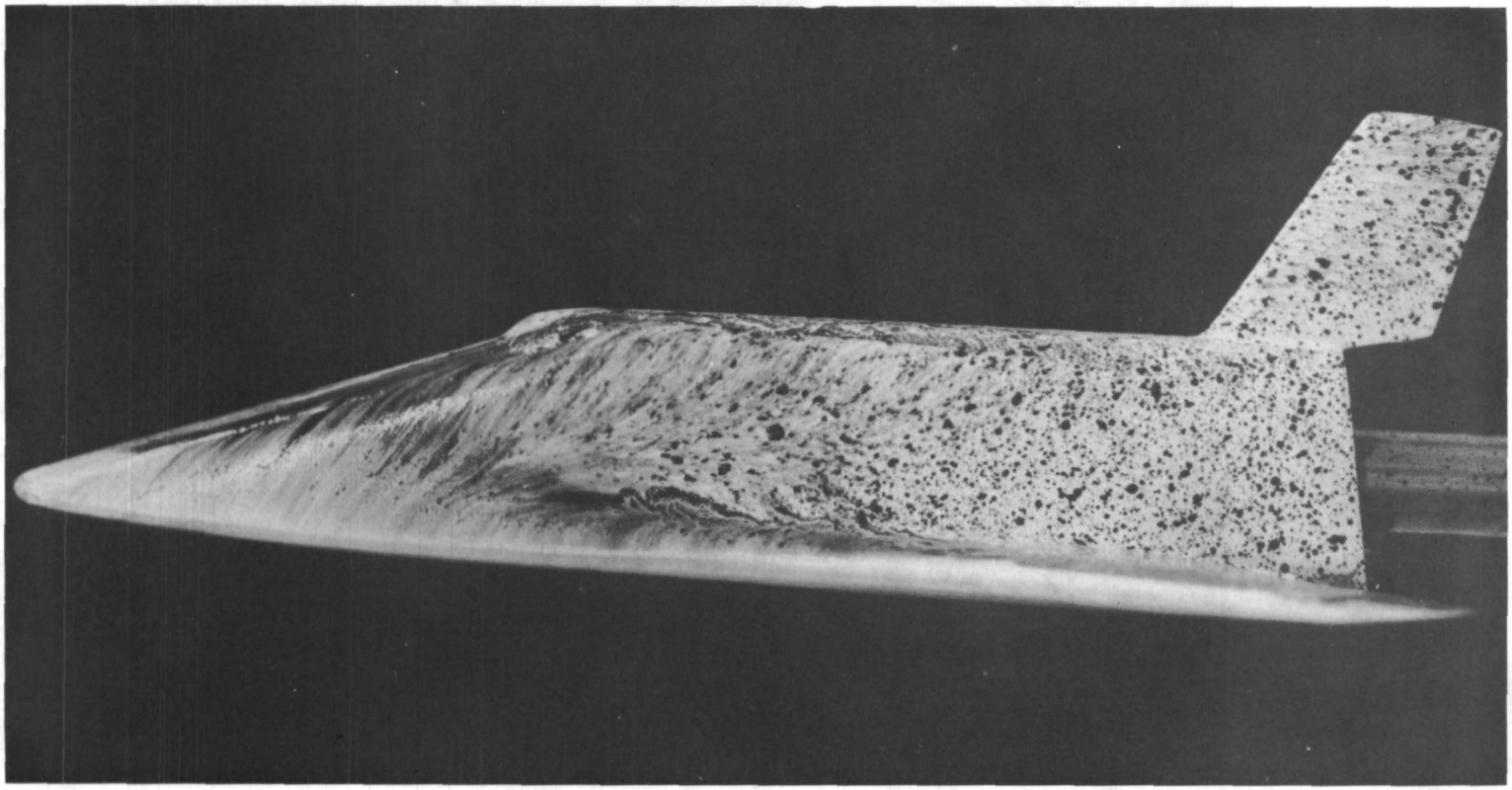

L-71-3683

(a) Side view.

Figure 10.- Postrun surface oil-flow patterns on 050B orbiter $\left(\delta_e = -5^o\right)$ for $\alpha = 30^o$.

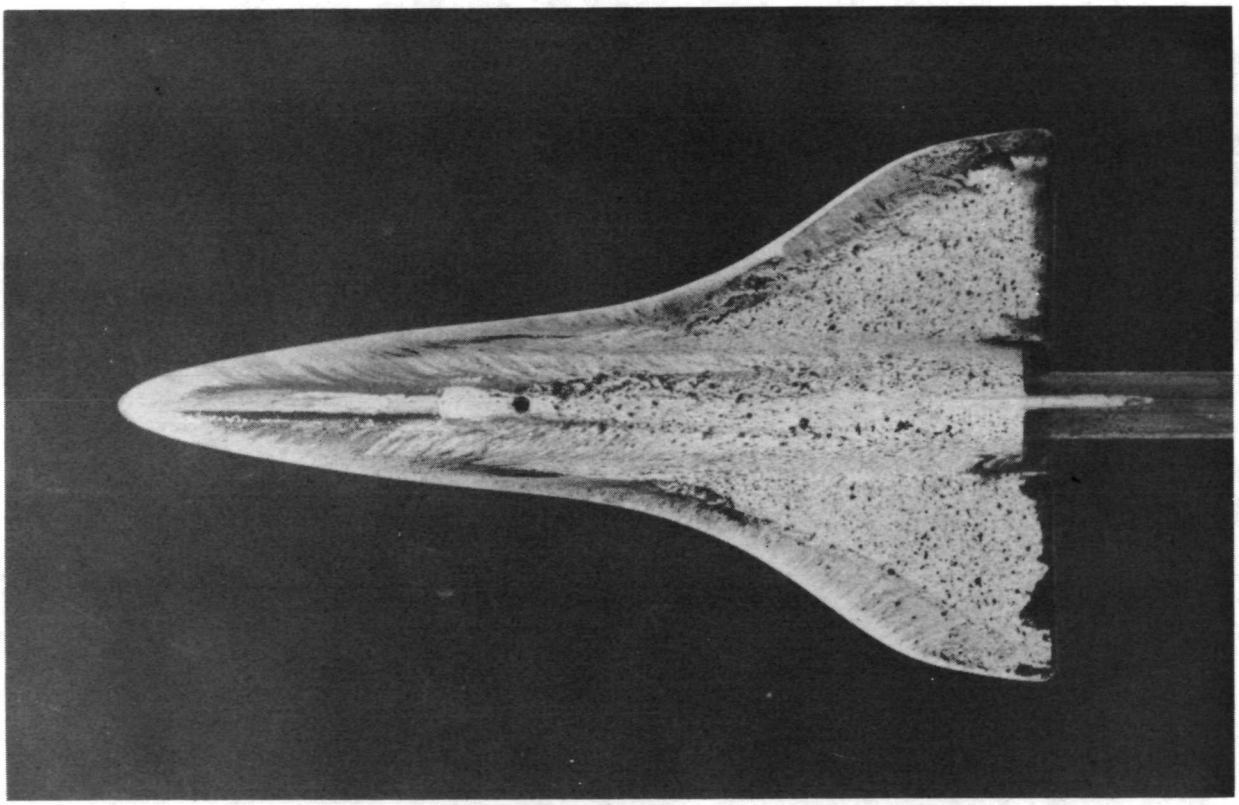

L-71-3681

(b) Top view.

Figure 10.- Continued.

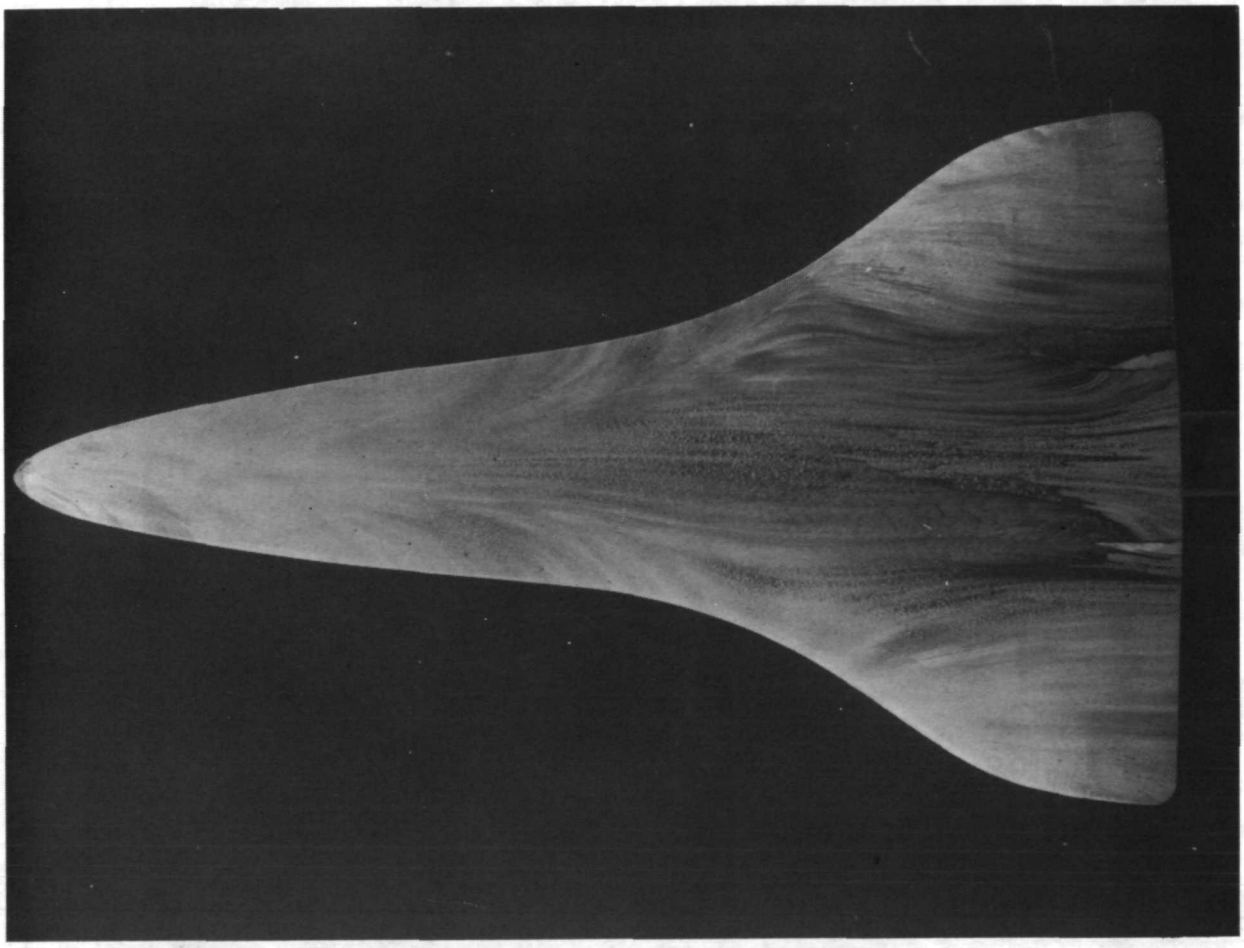

L-73-3055

(c) Bottom view.

Figure 10.- Concluded.

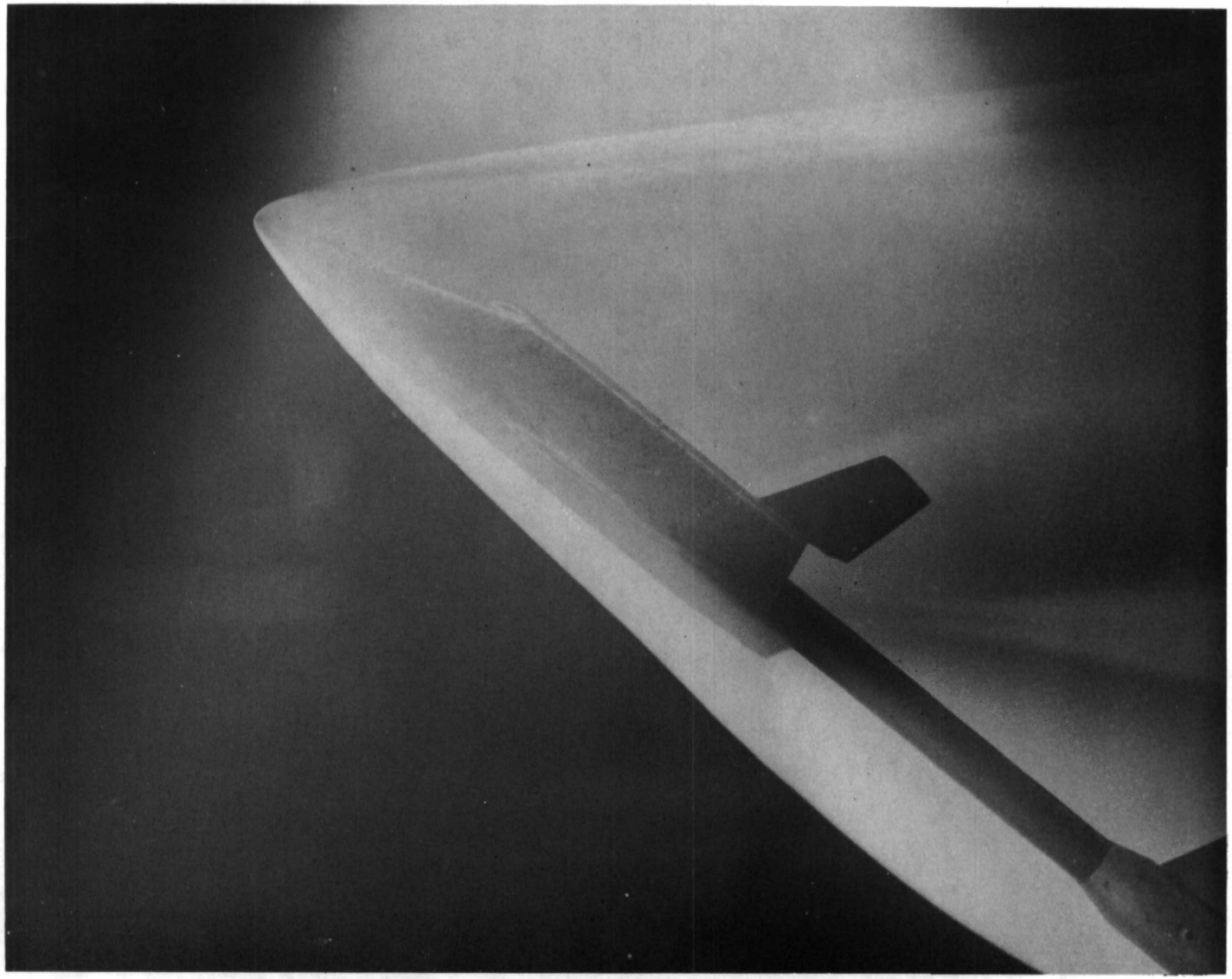

L-71-4053

(a) Side view.

Figure 11.- Electron-beam-illuminated surface oil flow on the 050B orbiter $(\delta_e = 0^o)$ at $\alpha = 40^o$.

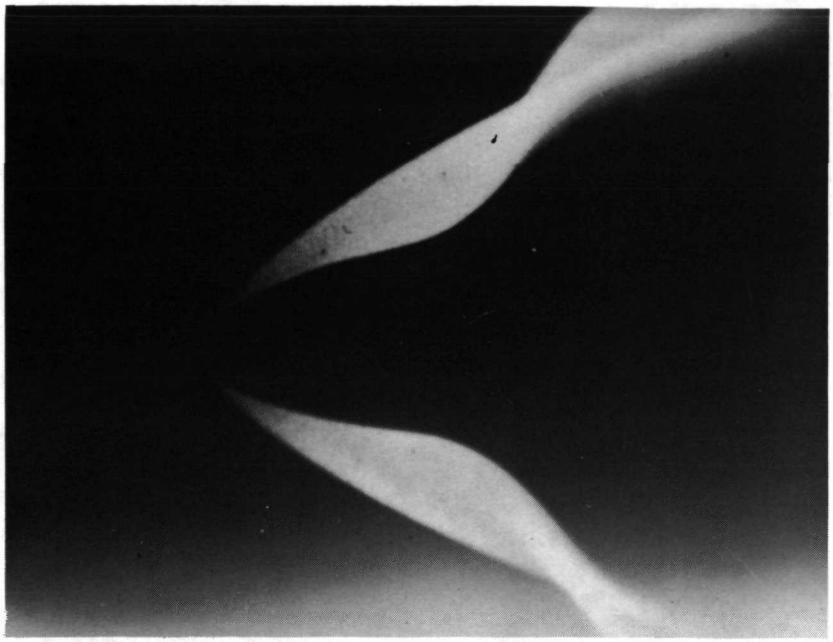

(b) Top view.

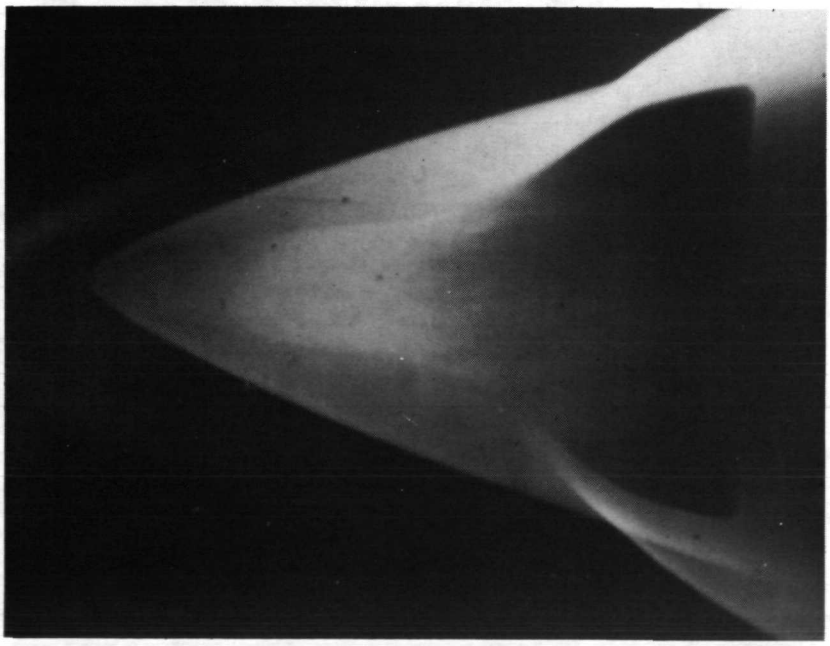

L-73-3056

(c) Bottom view.

Figure 11.- Concluded.

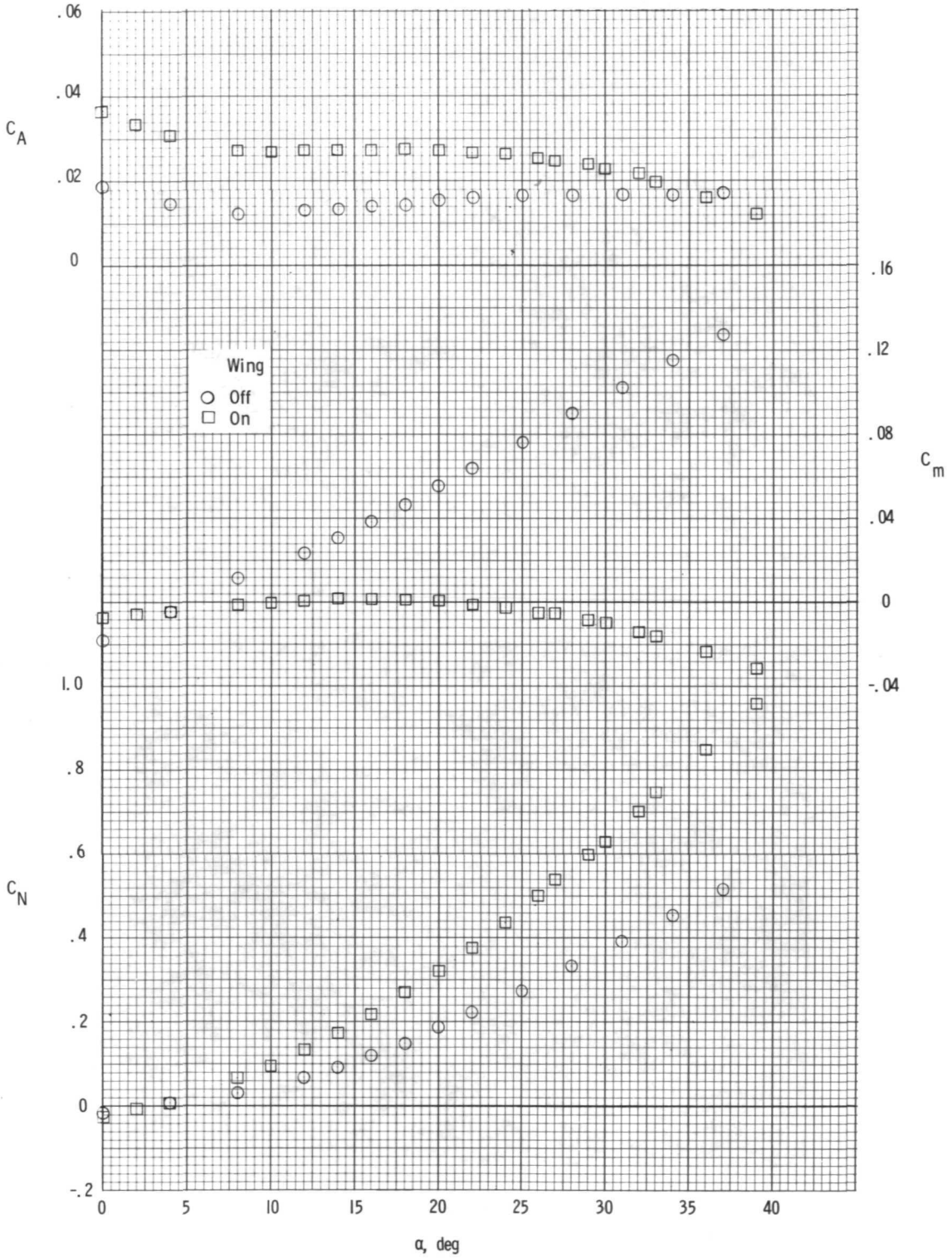

(a) Longitudinal characteristics (body axes).

Figure 12.- Effect of adding wing $\left(\delta_e = 0^o\right)$ to body of 134D orbiter.

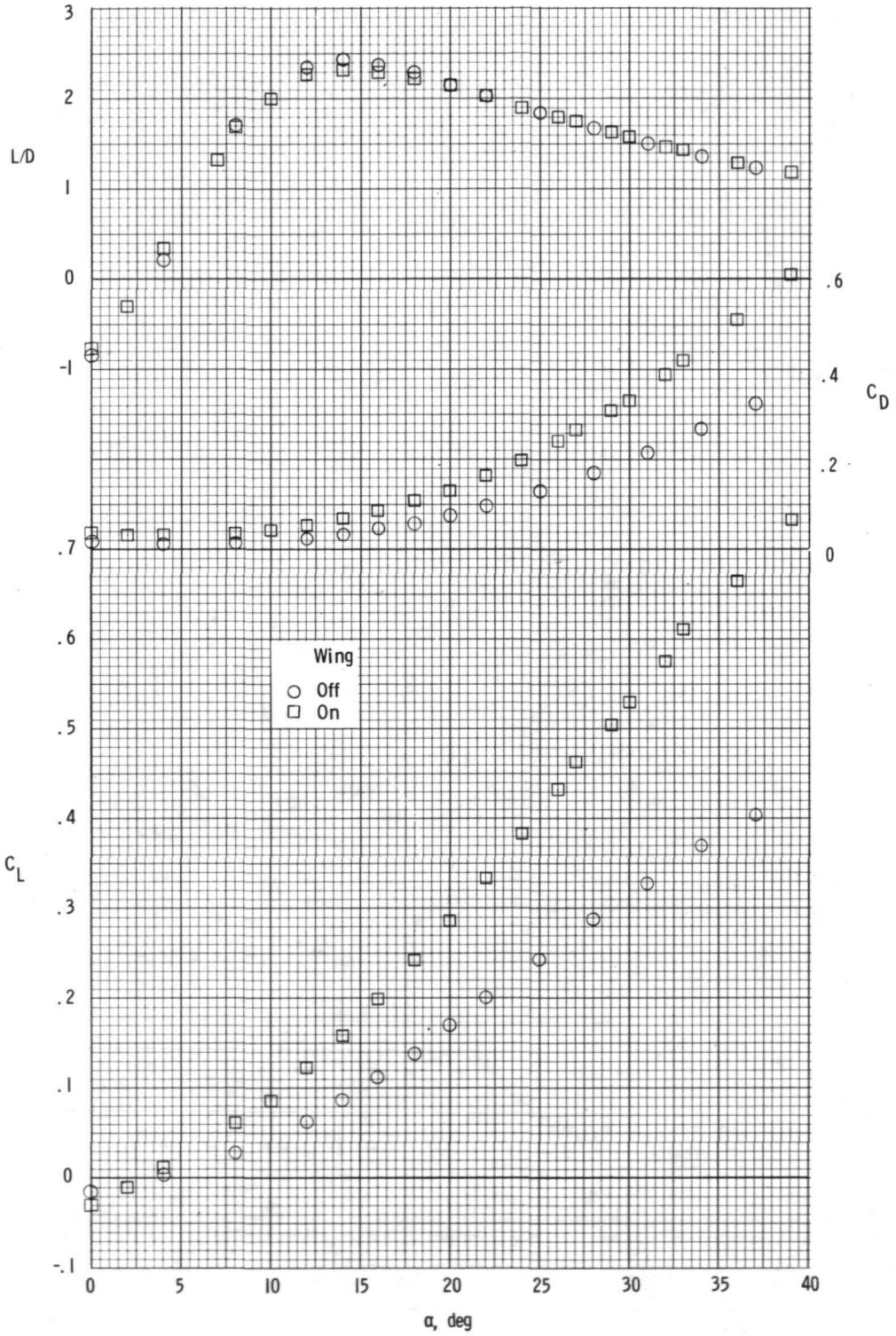

(b) Longitudinal characteristics (stability axes).

Figure 12.- Continued.

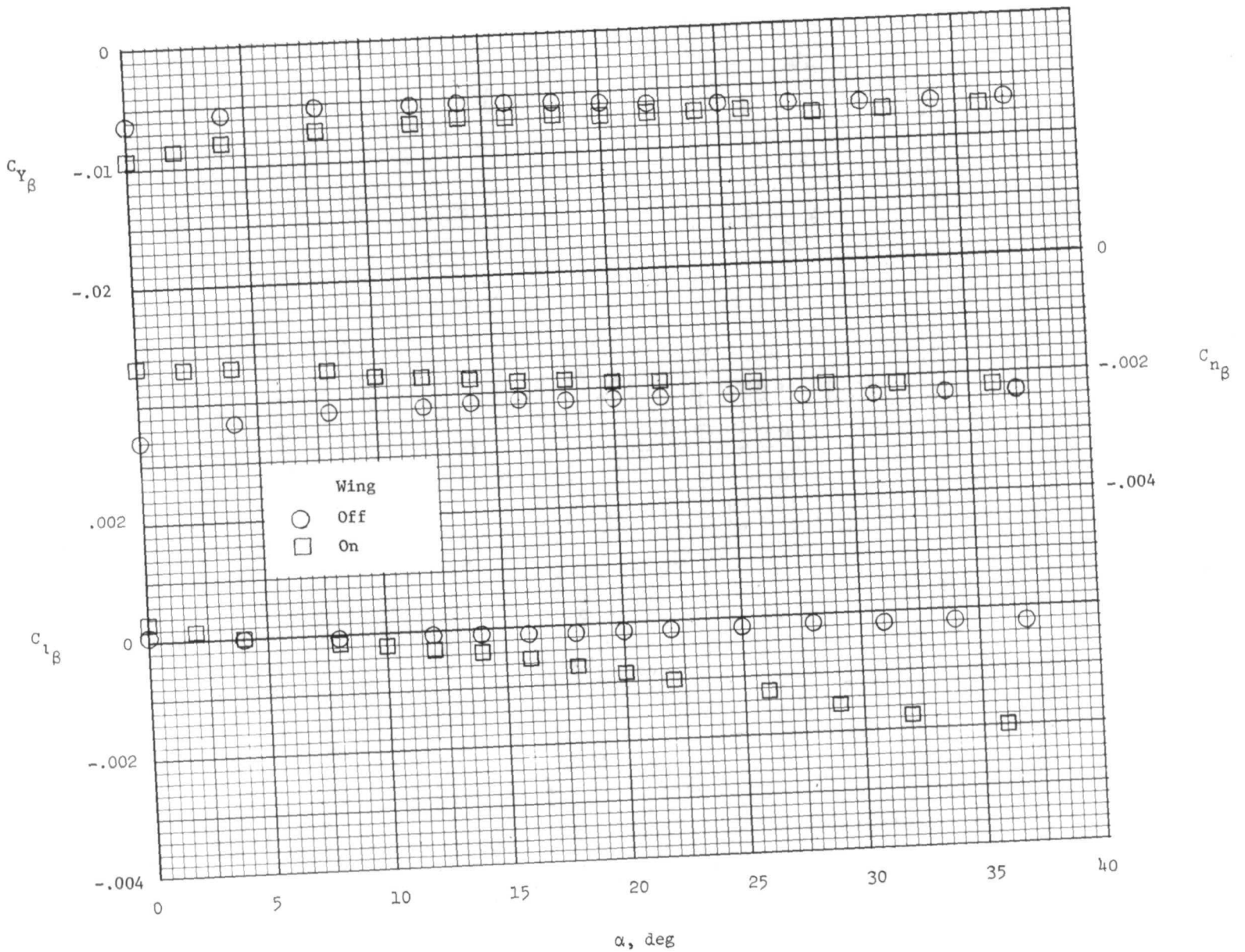

(c) Lateral and directional stability characteristics.

Figure 12.- Concluded.

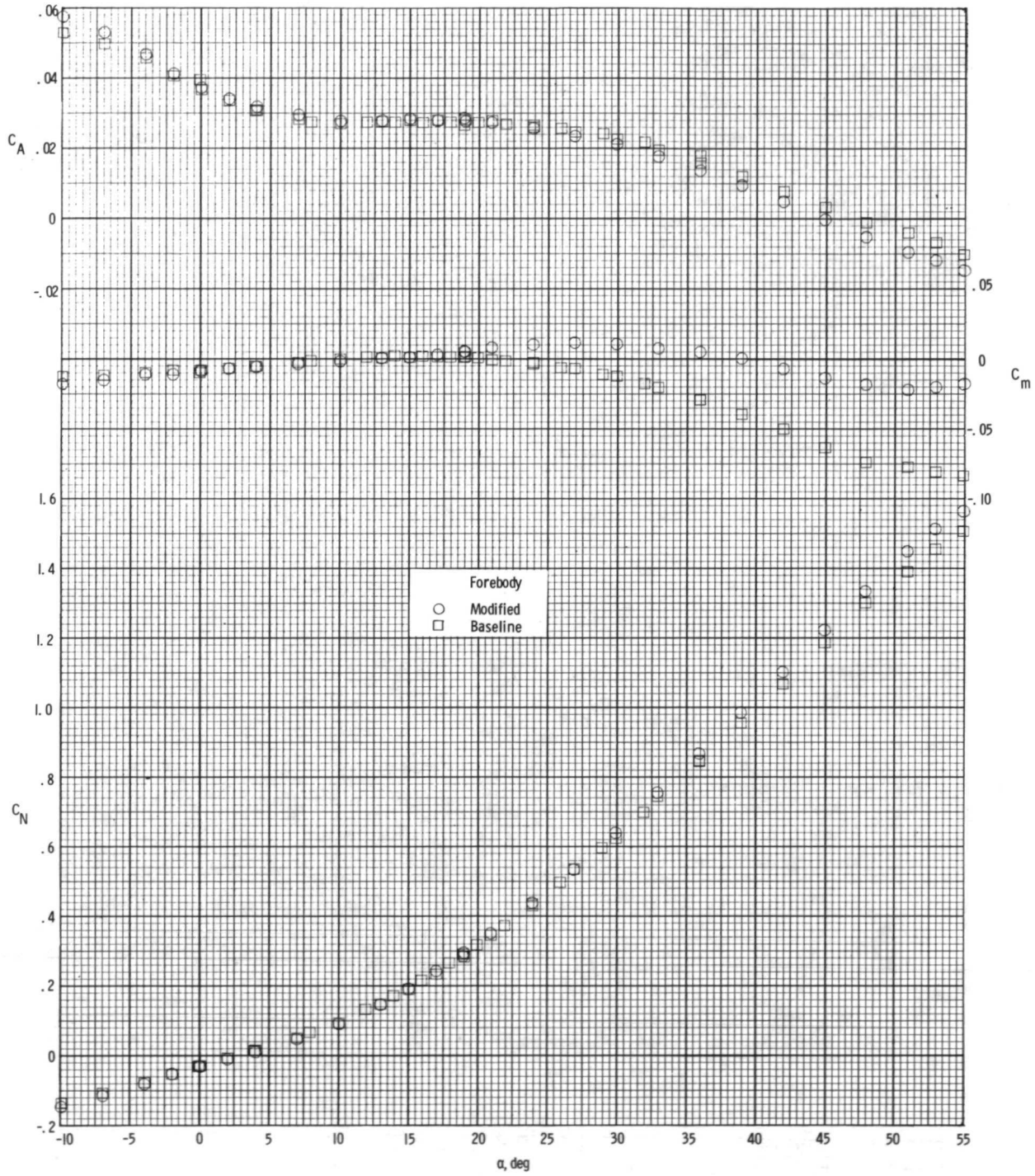

(a) Longitudinal characteristics (body axes).

Figure 13.- Effect of forebody modification on aerodynamic characteristics of 134D orbiter with $\delta_e = 0^o$.

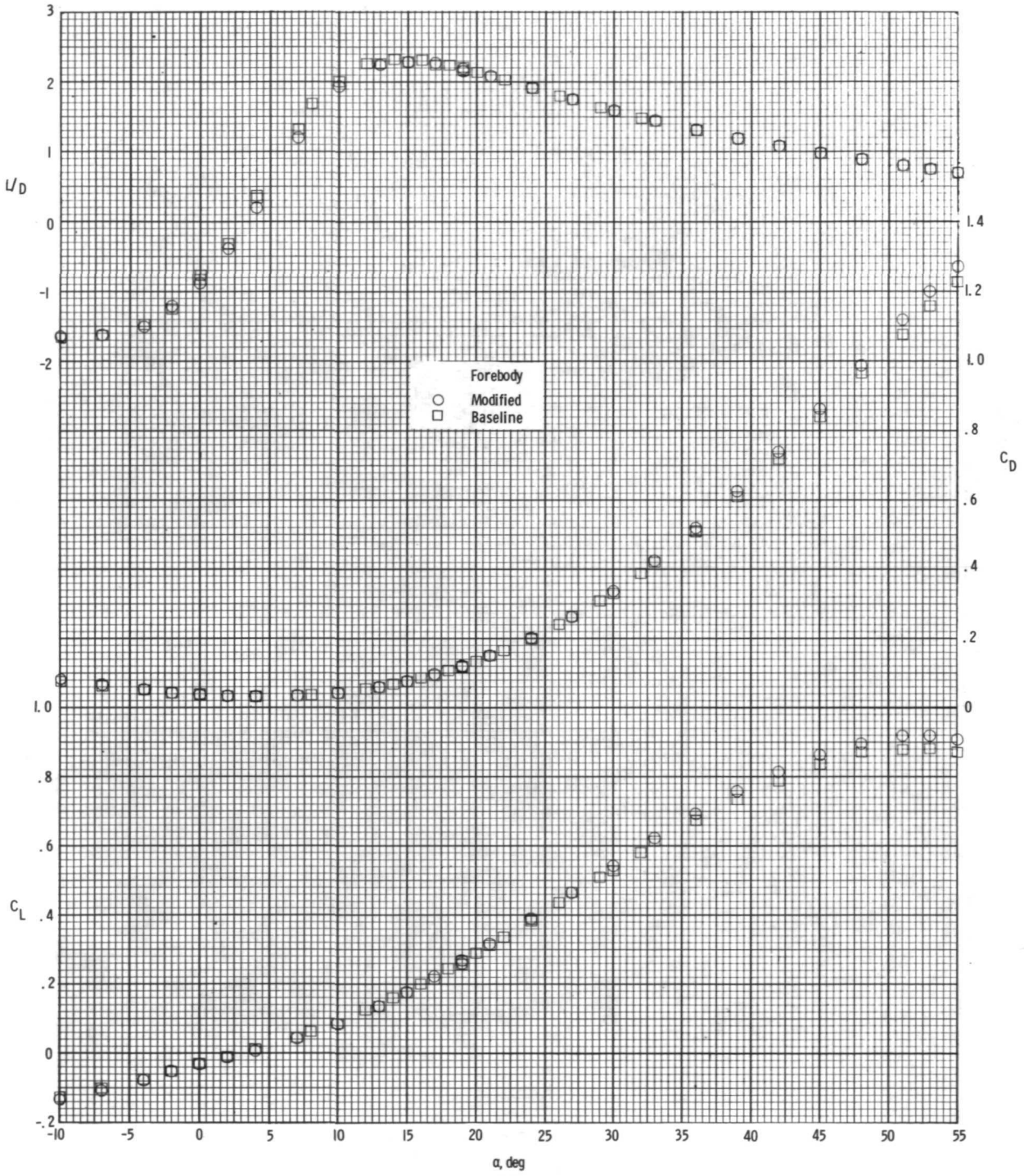

(b) Longitudinal characteristics (stability axes).

Figure 13.- Continued.

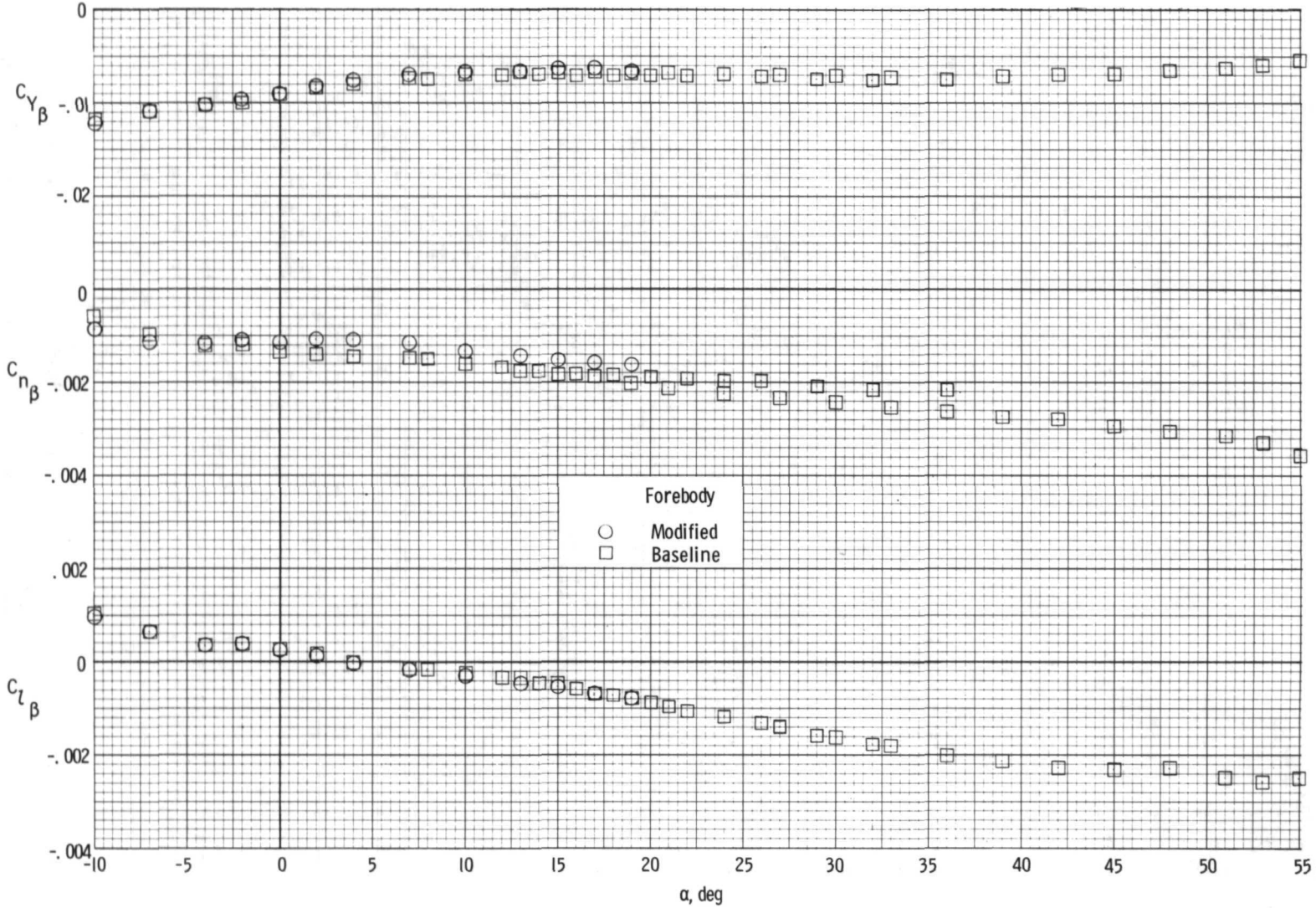

(c) Lateral and directional stability characteristics.

Figure 13.- Concluded.

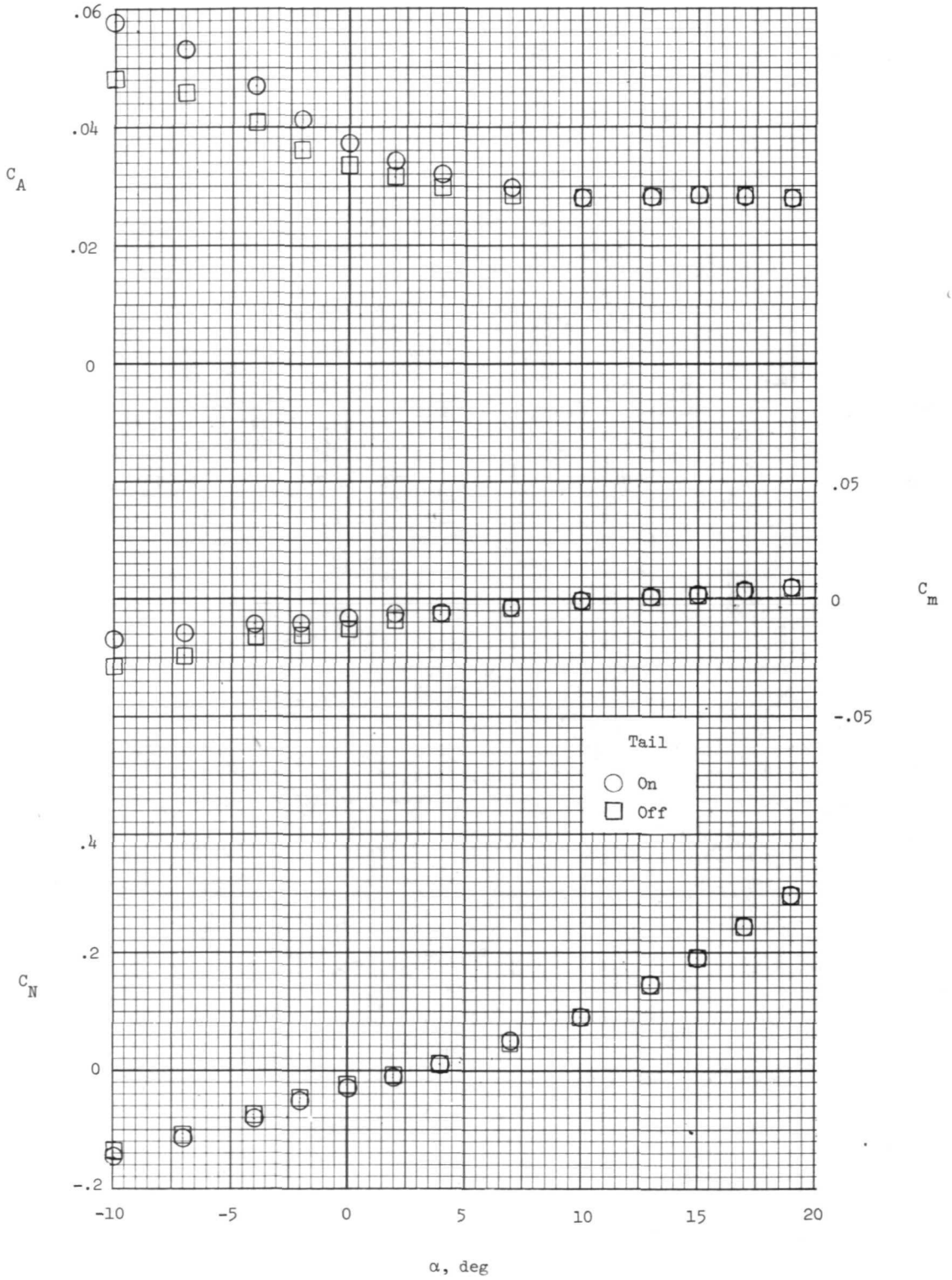

(a) Longitudinal characteristics (body axes).

Figure 14.- Effect of vertical tail on aerodynamic characteristics of 134D orbiter with modified forebody and $\delta_e = 0^o$.

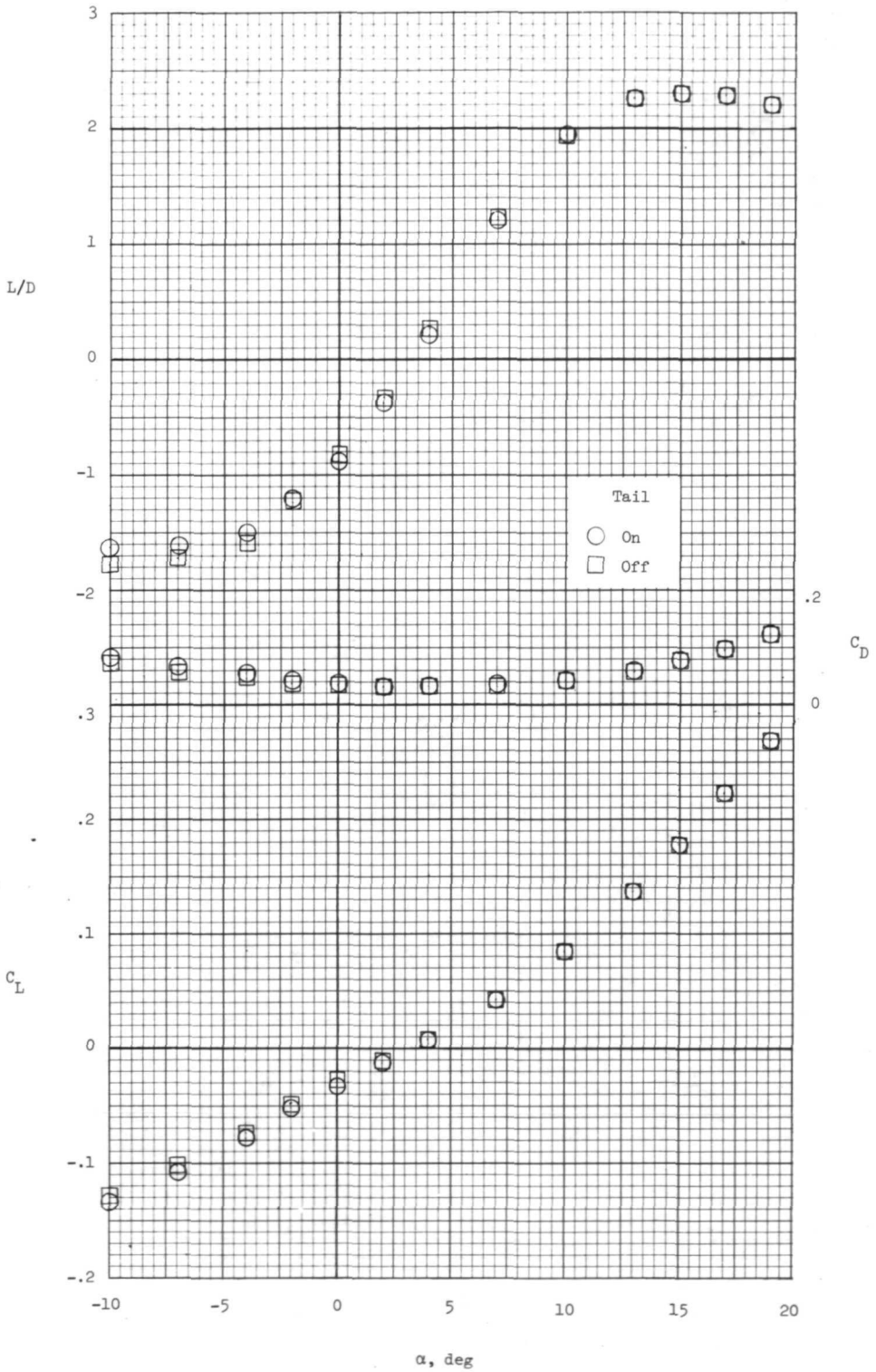

(b) Longitudinal characteristics (stability axes).

Figure 14.- Continued.

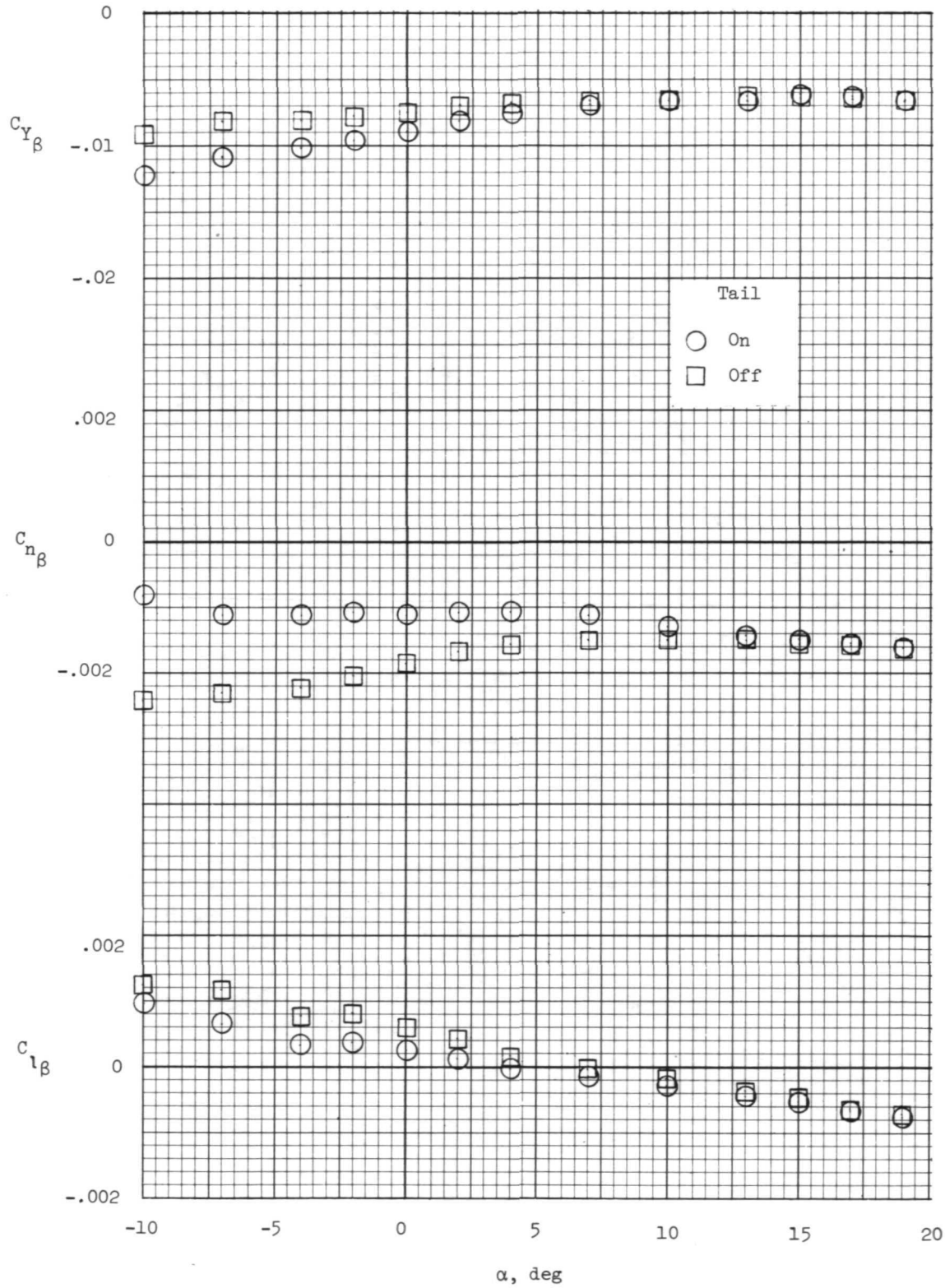

(c) Lateral and directional stability characteristics.

Figure 14.- Concluded.

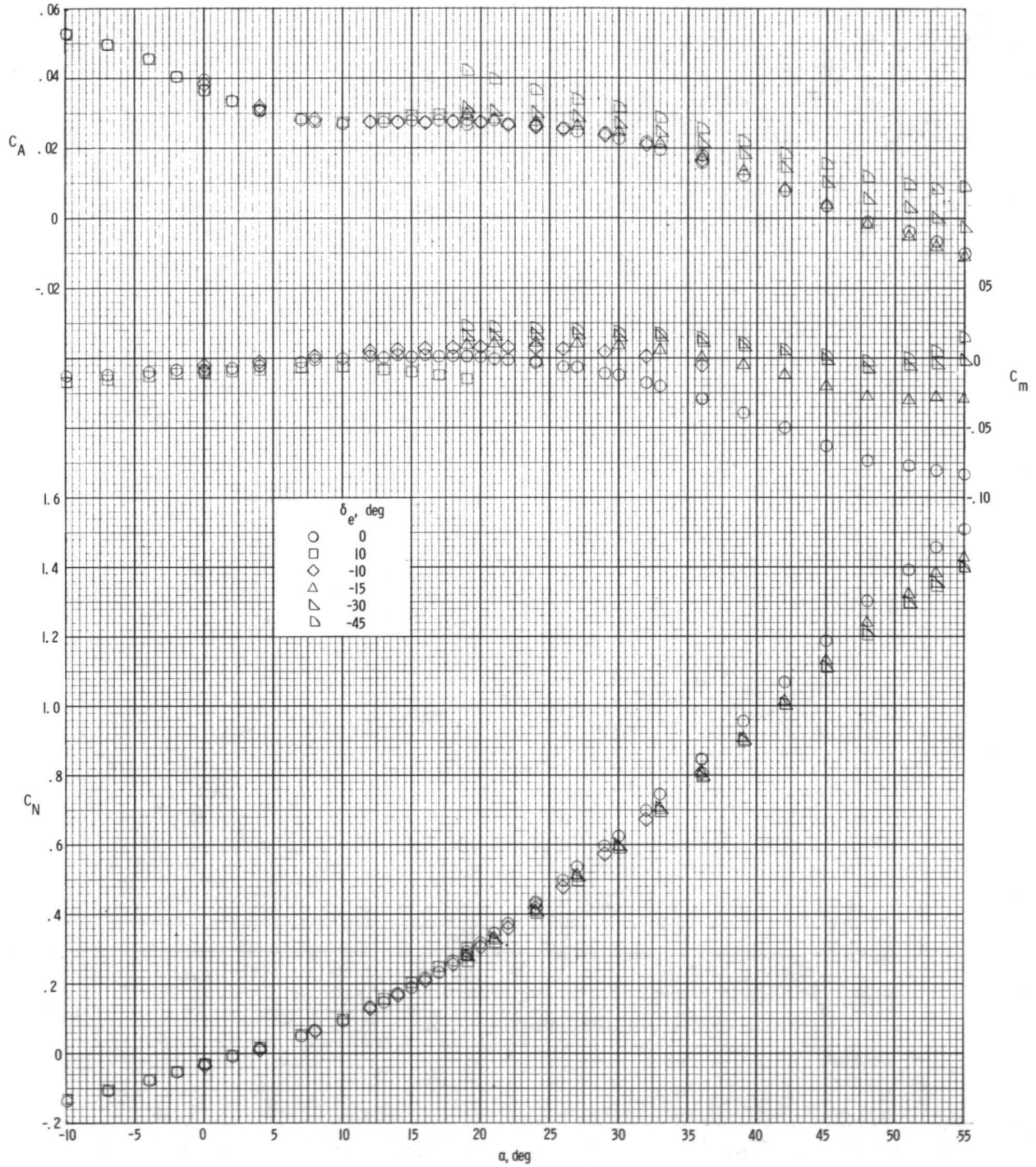

(a) Longitudinal characteristics (body axes).

Figure 15.- Effect of elevon deflections on aerodynamic characteristics of 134D orbiter.

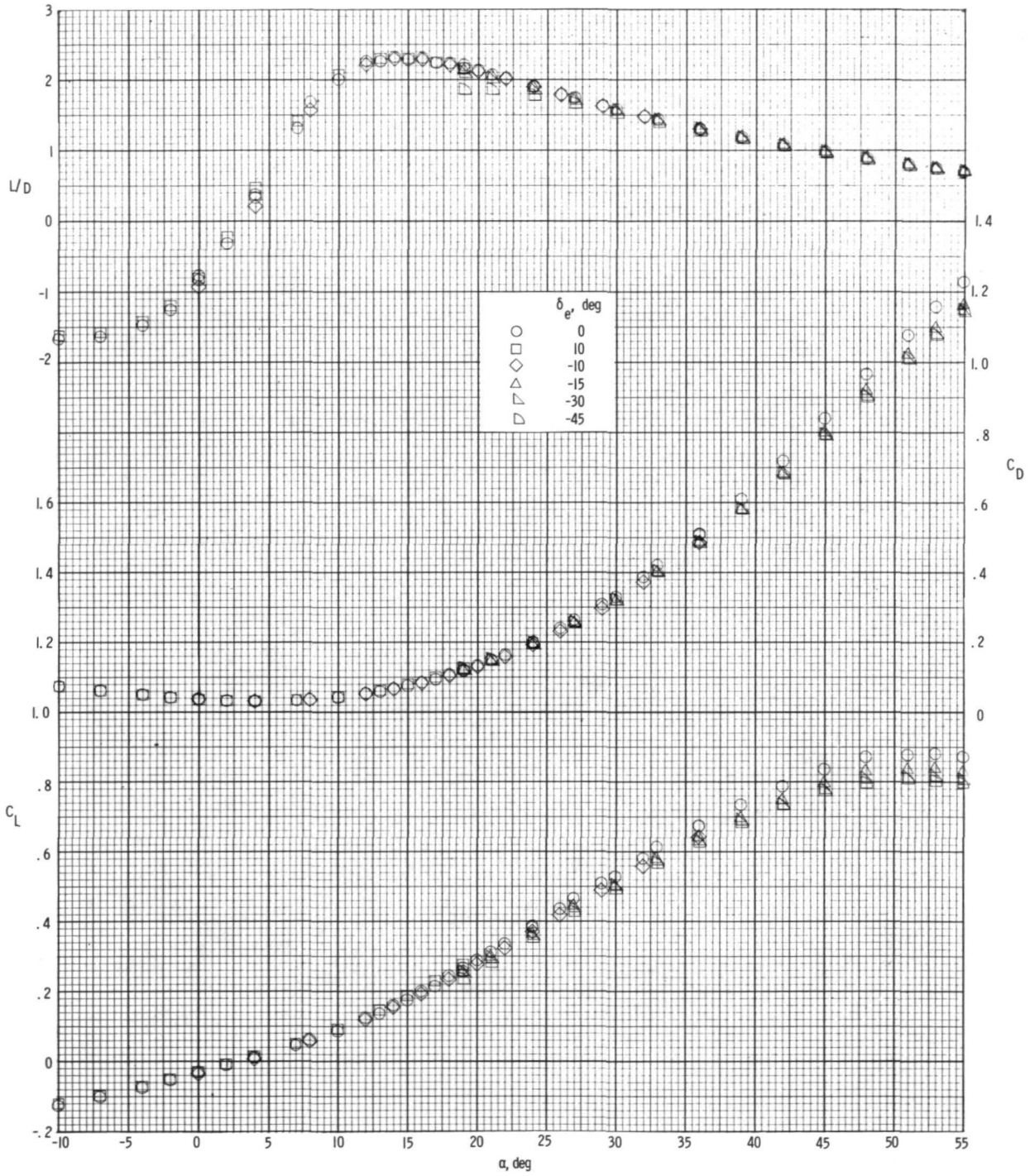

(b) Longitudinal characteristics (stability axes).

Figure 15.- Continued.

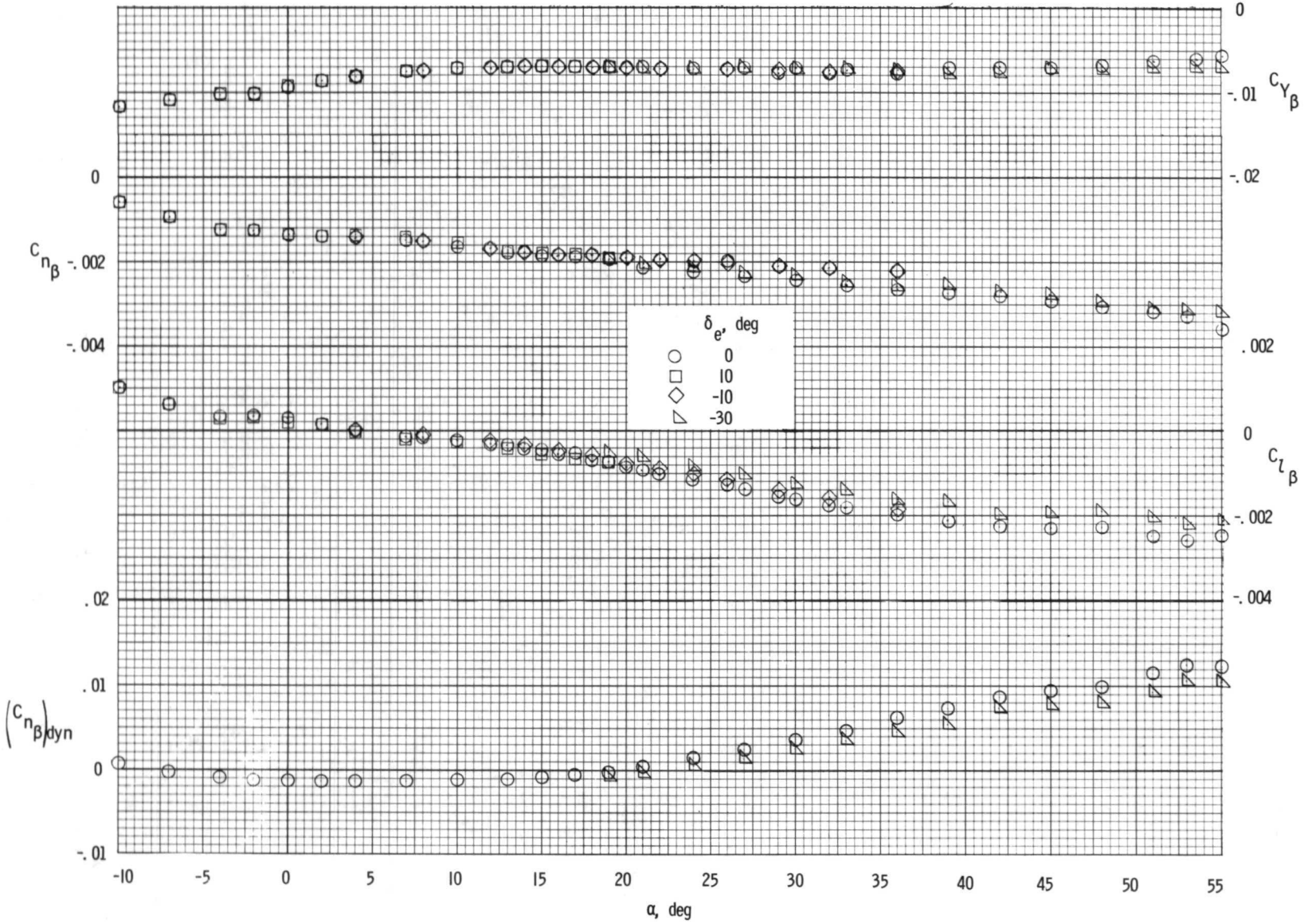

(c) Lateral and directional stability characteristics.

Figure 15.- Concluded.

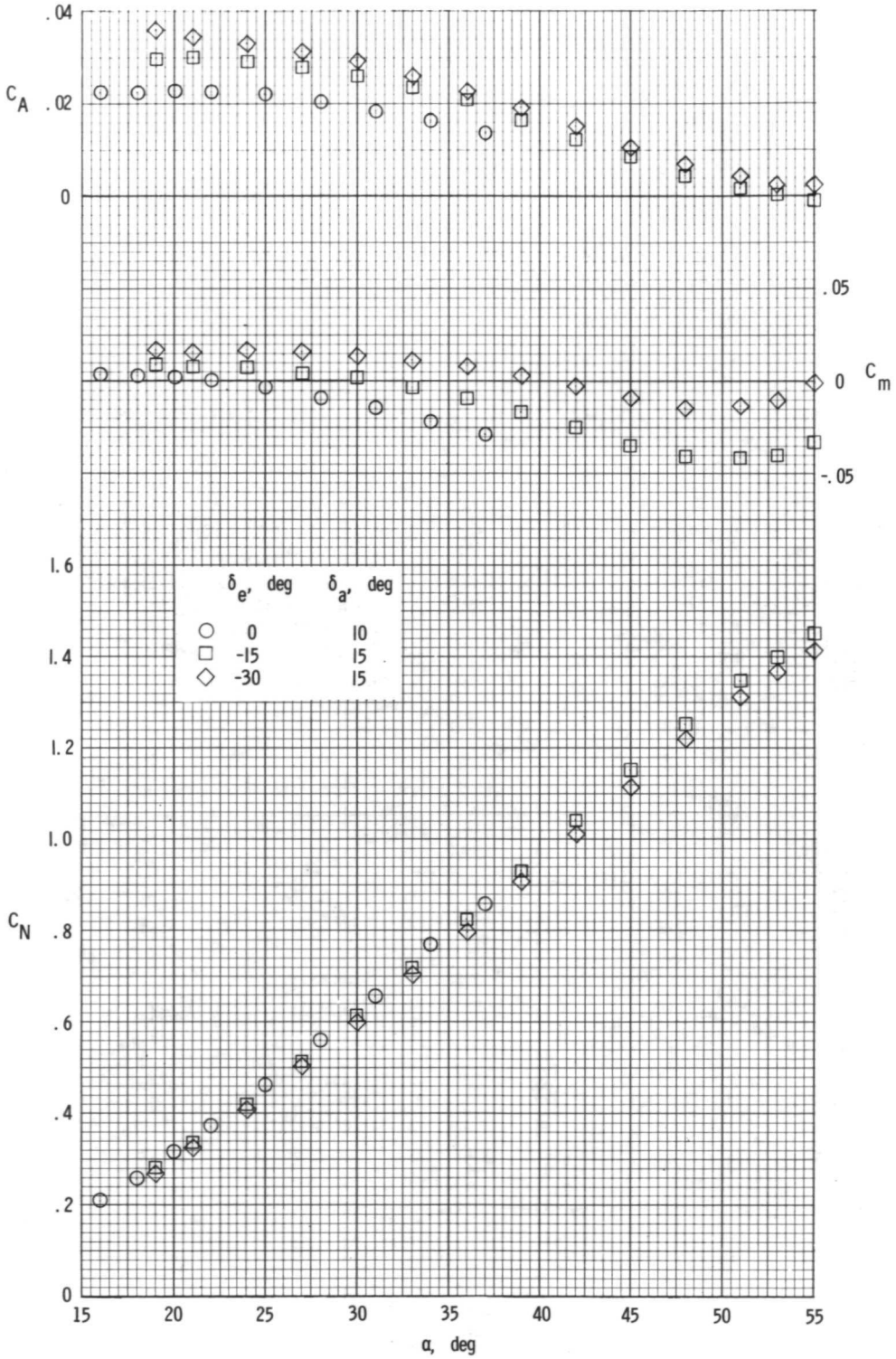

(a) Longitudinal characteristics (body axes).

Figure 16.- Effect of differential elevon deflections on aerodynamic characteristics of 134D orbiter.

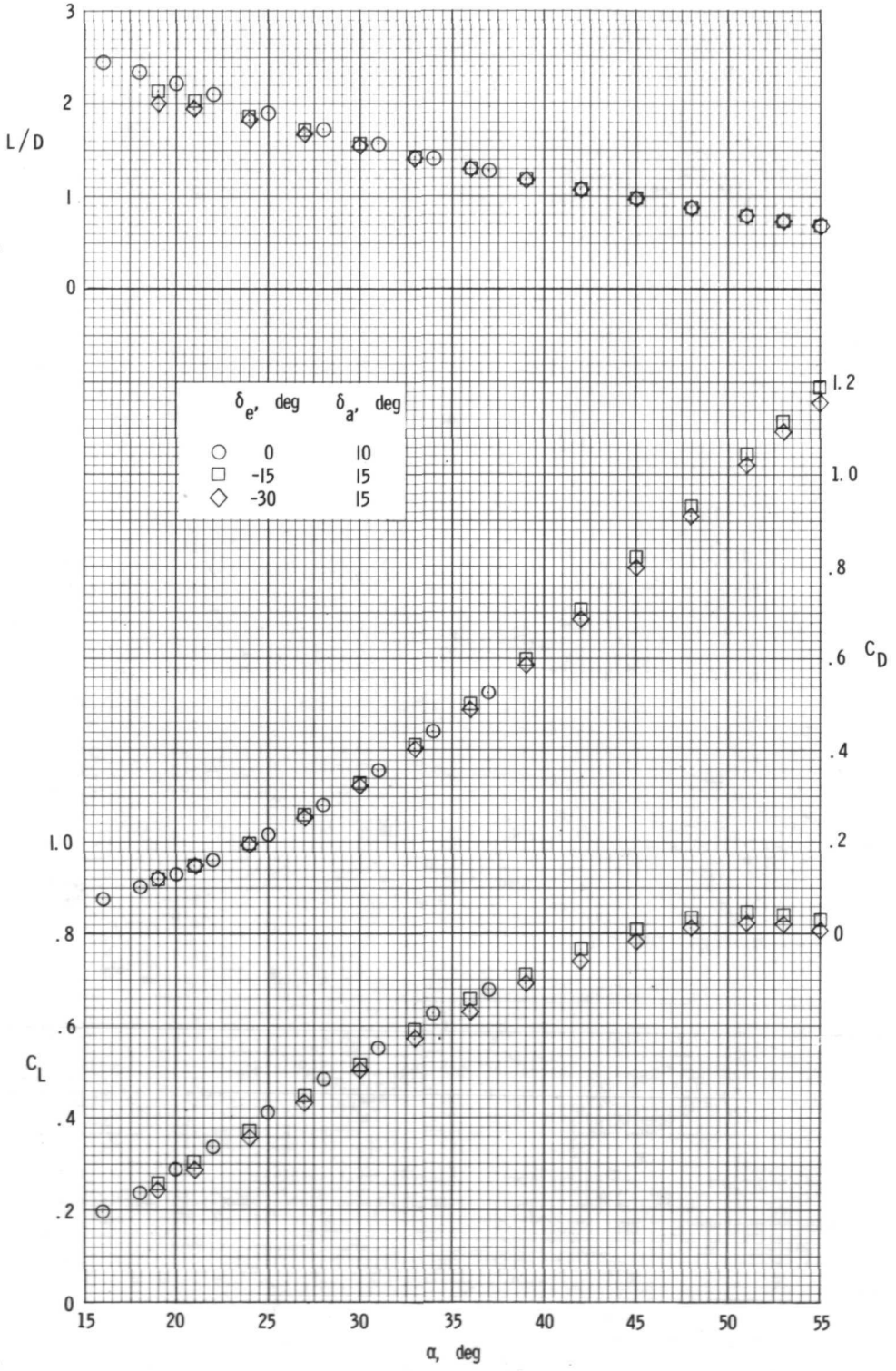

(b) Longitudinal characteristics (stability axes).

Figure 16.- Continued.

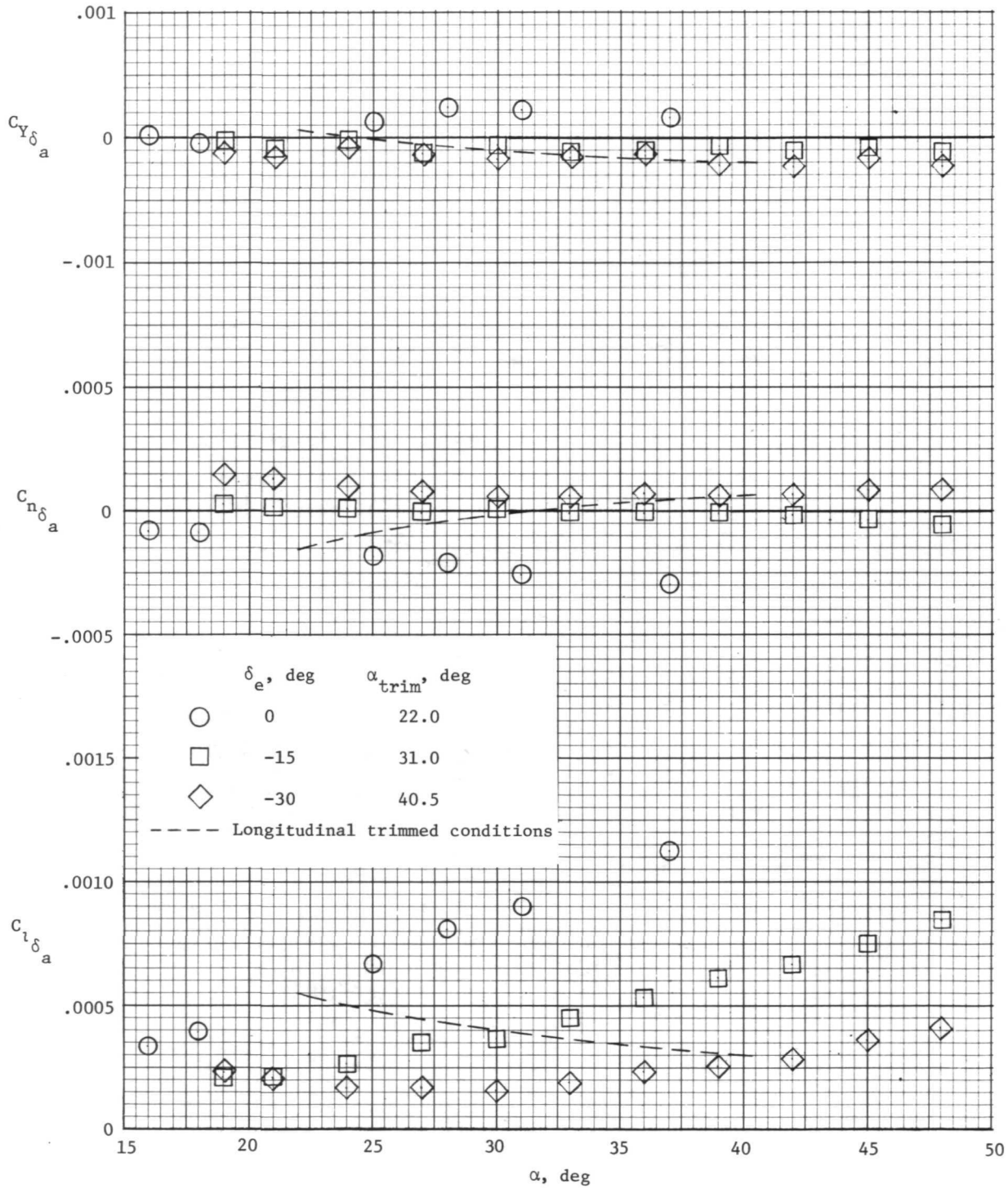

(c) Rate of change in lateral and directional characteristics.

Figure 16.- Concluded.

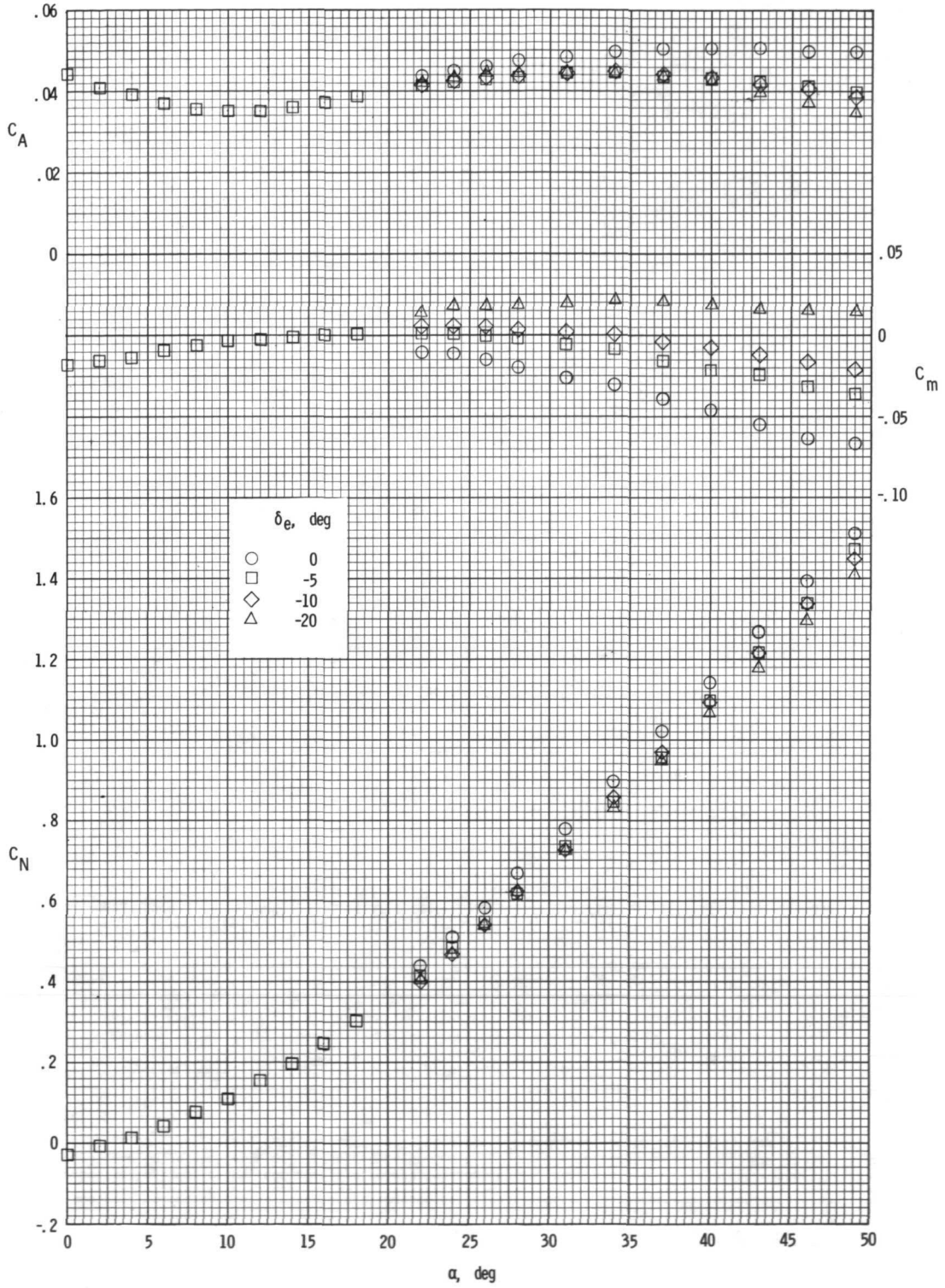

(a) Longitudinal characteristics (body axes).

Figure 17.- Longitudinal, lateral, and directional stability characteristics of 050B orbiter for various elevon deflections.

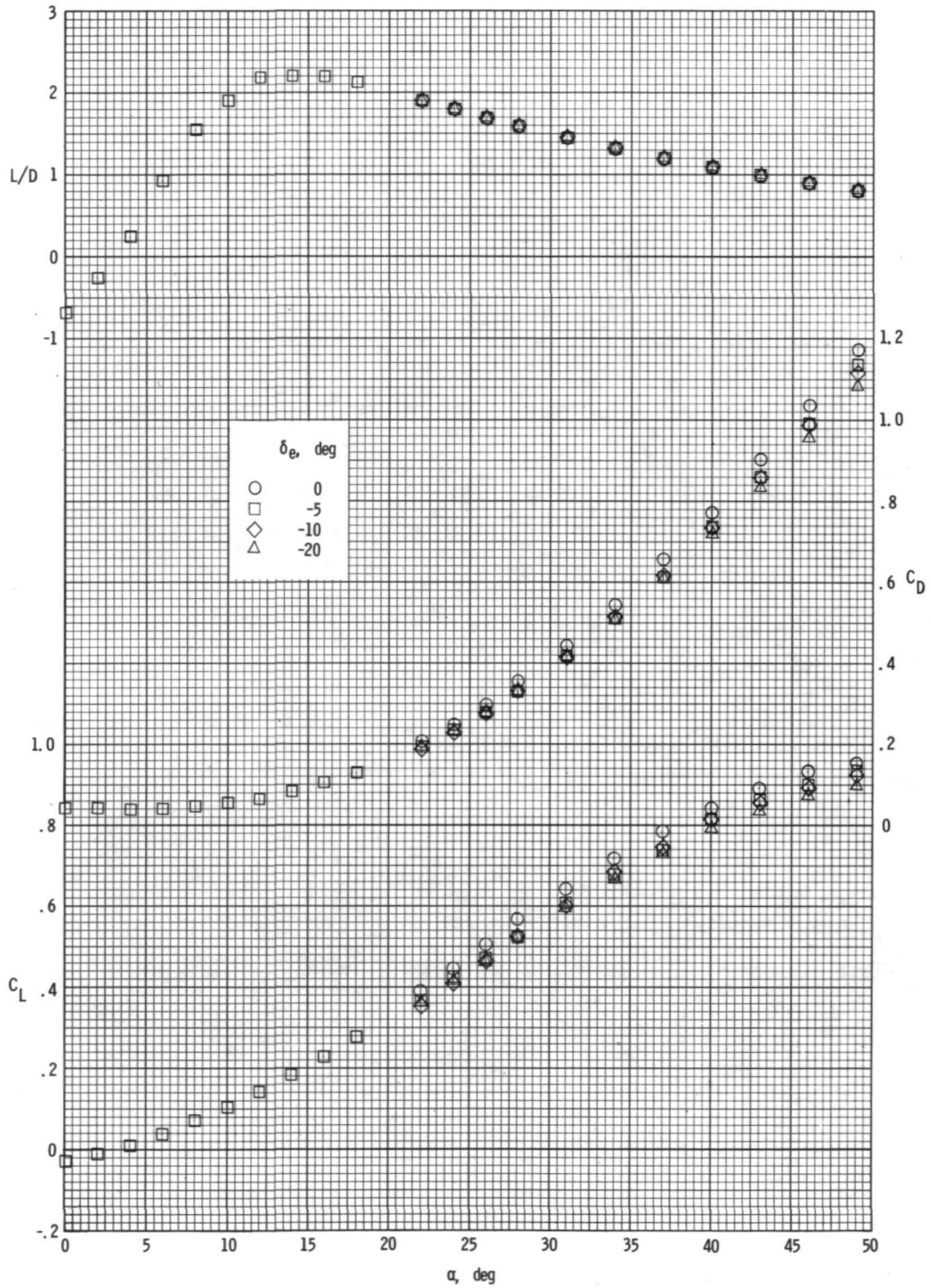

(b) Longitudinal characteristics (stability axes).

Figure 17.- Continued.

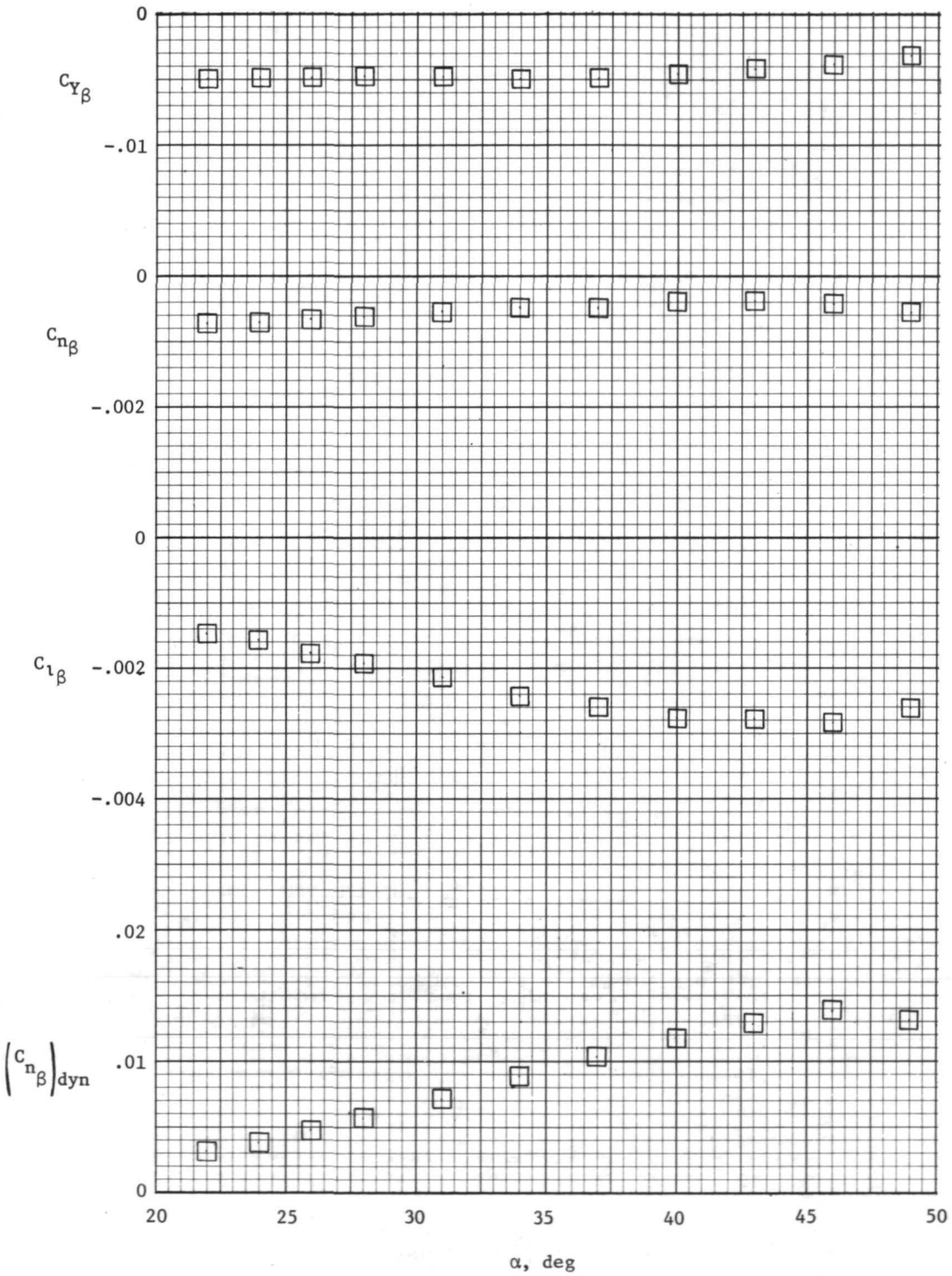

(c) Lateral and directional stability characteristics for $\delta_e = -5^o$.

Figure 17.- Concluded.

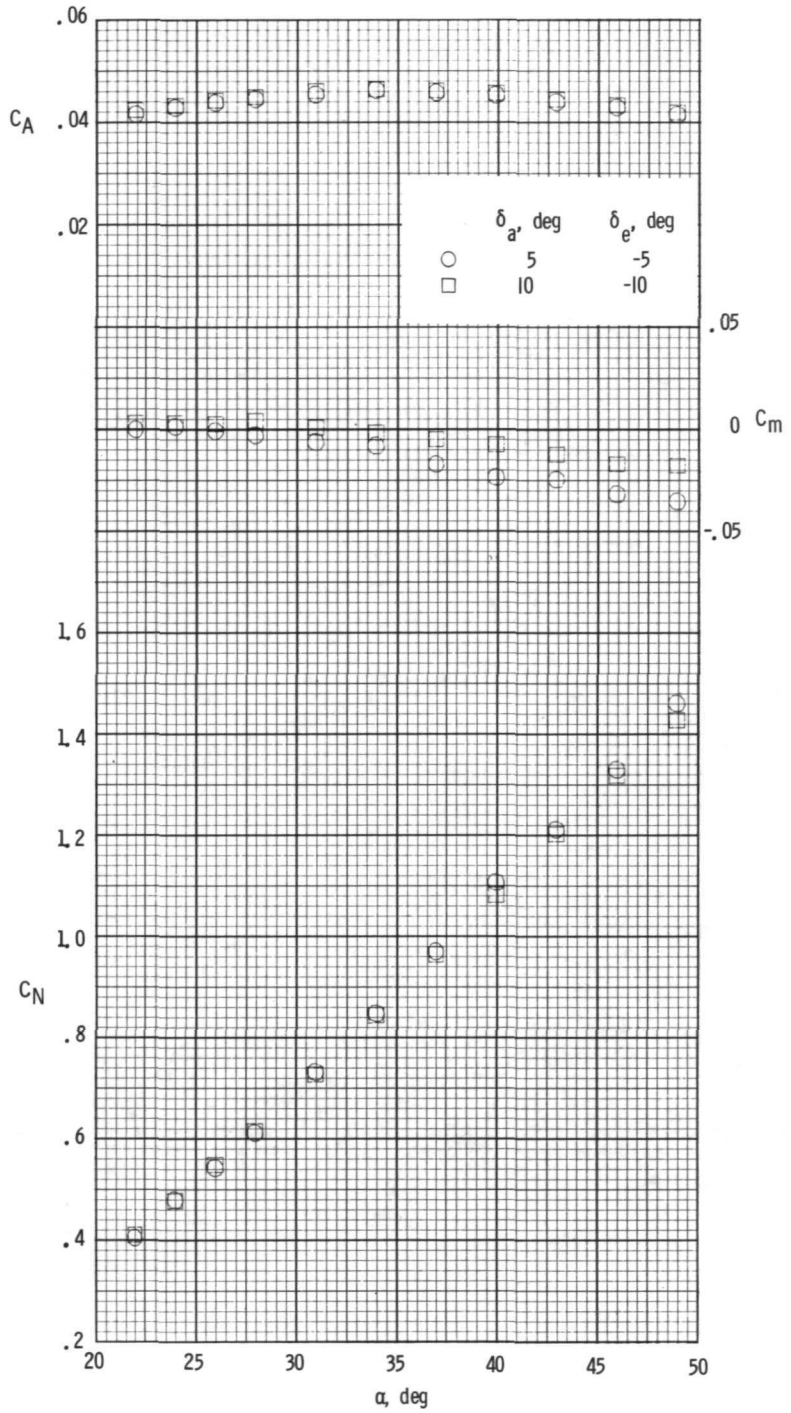

(a) Longitudinal characteristics (body axes).

Figure 18.- Effect of differential elevon deflections on aerodynamic characteristics of 050B orbiter.

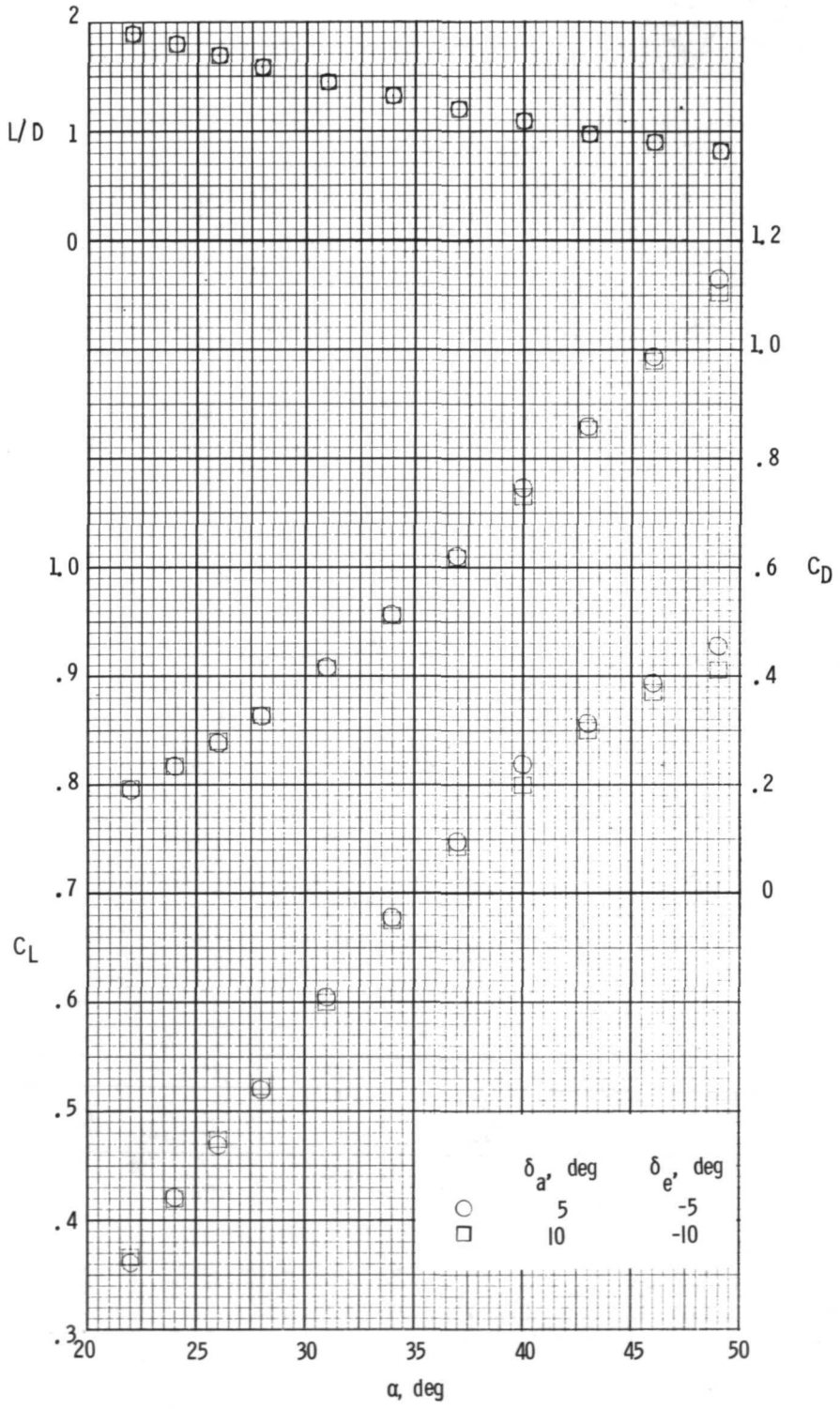

(b) Longitudinal characteristics (stability axes).

Figure 18.- Continued.

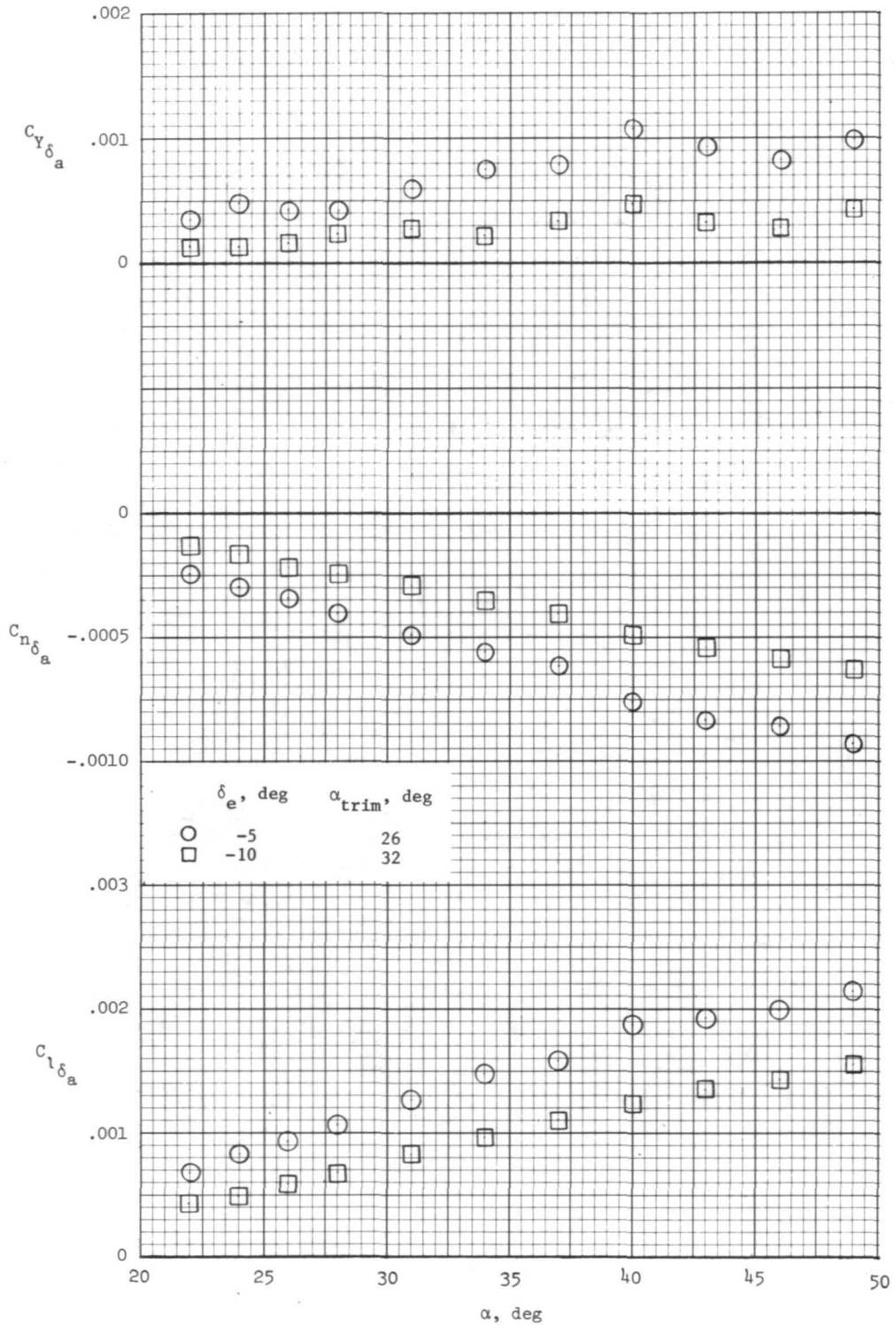

(c) Rate of change in lateral and directional characteristics.

Figure 18.- Concluded.

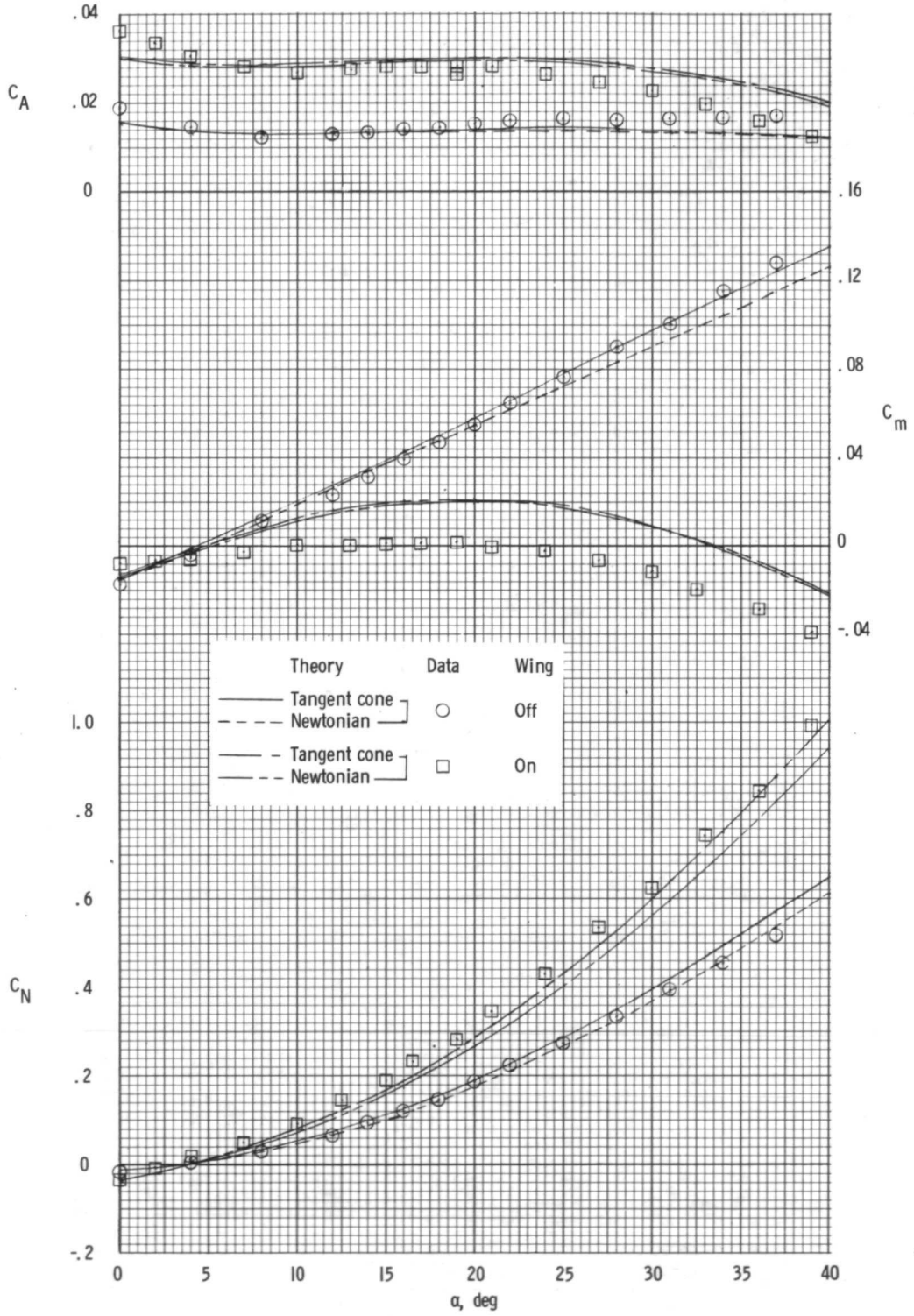

(a) Longitudinal characteristics (body axes).

Figure 19.- Comparison of experimental aerodynamic characteristics with theory for 134D orbiter with and without wing. $\delta_e = 0^o$.

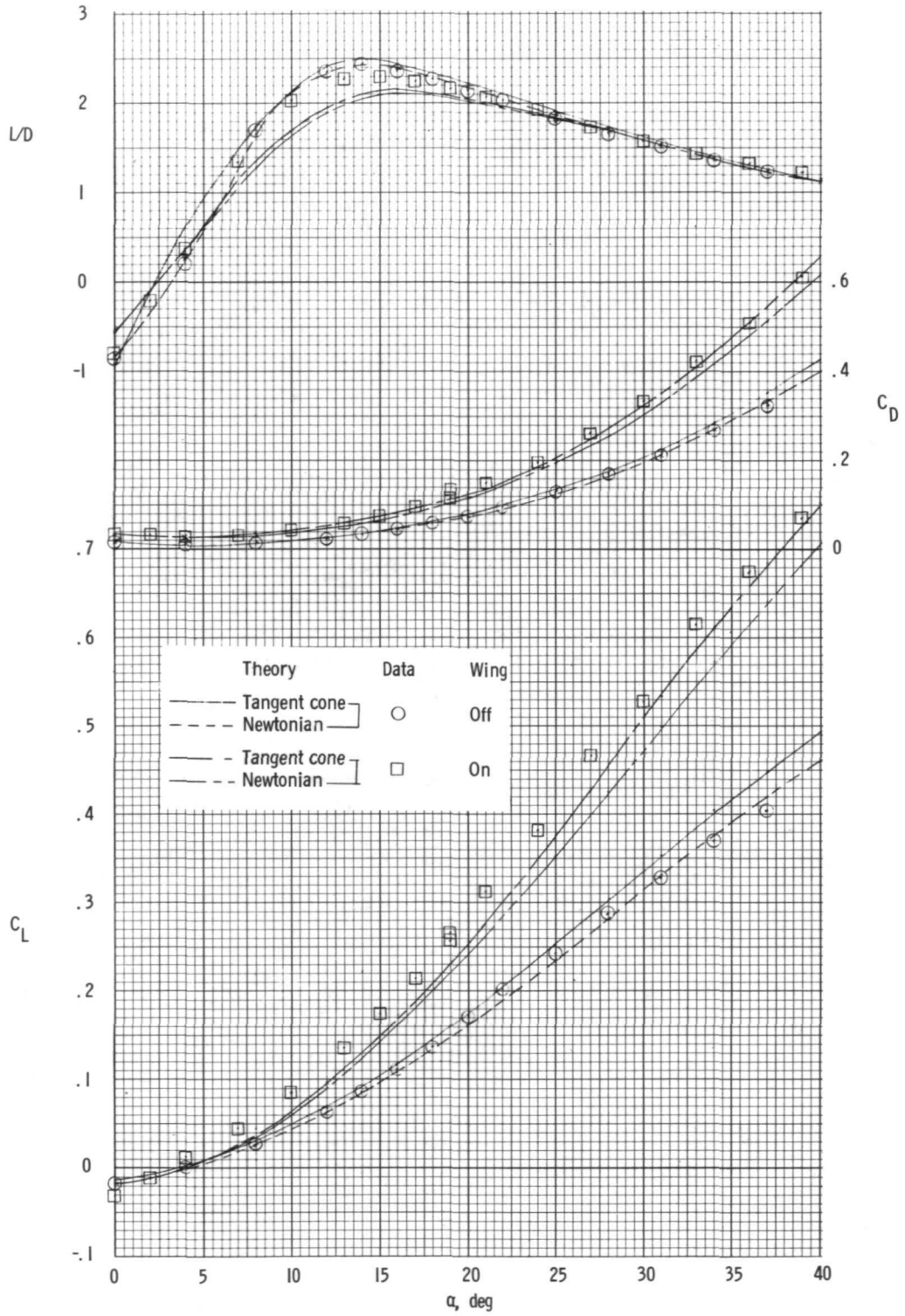

(b) Longitudinal characteristics (stability axes).

Figure 19.- Continued.

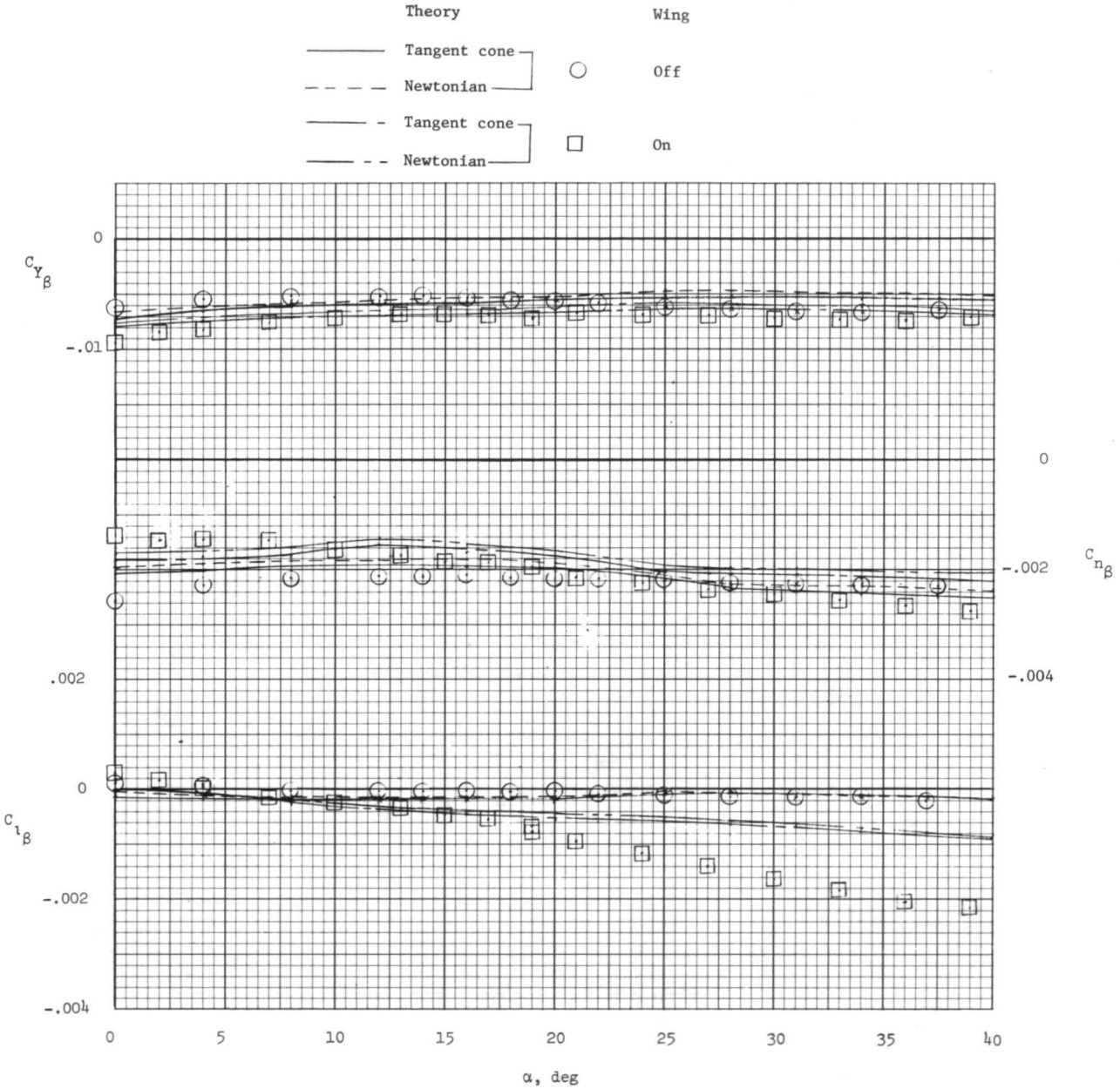

(c) Lateral and directional stability characteristics.

Figure 19.- Concluded.

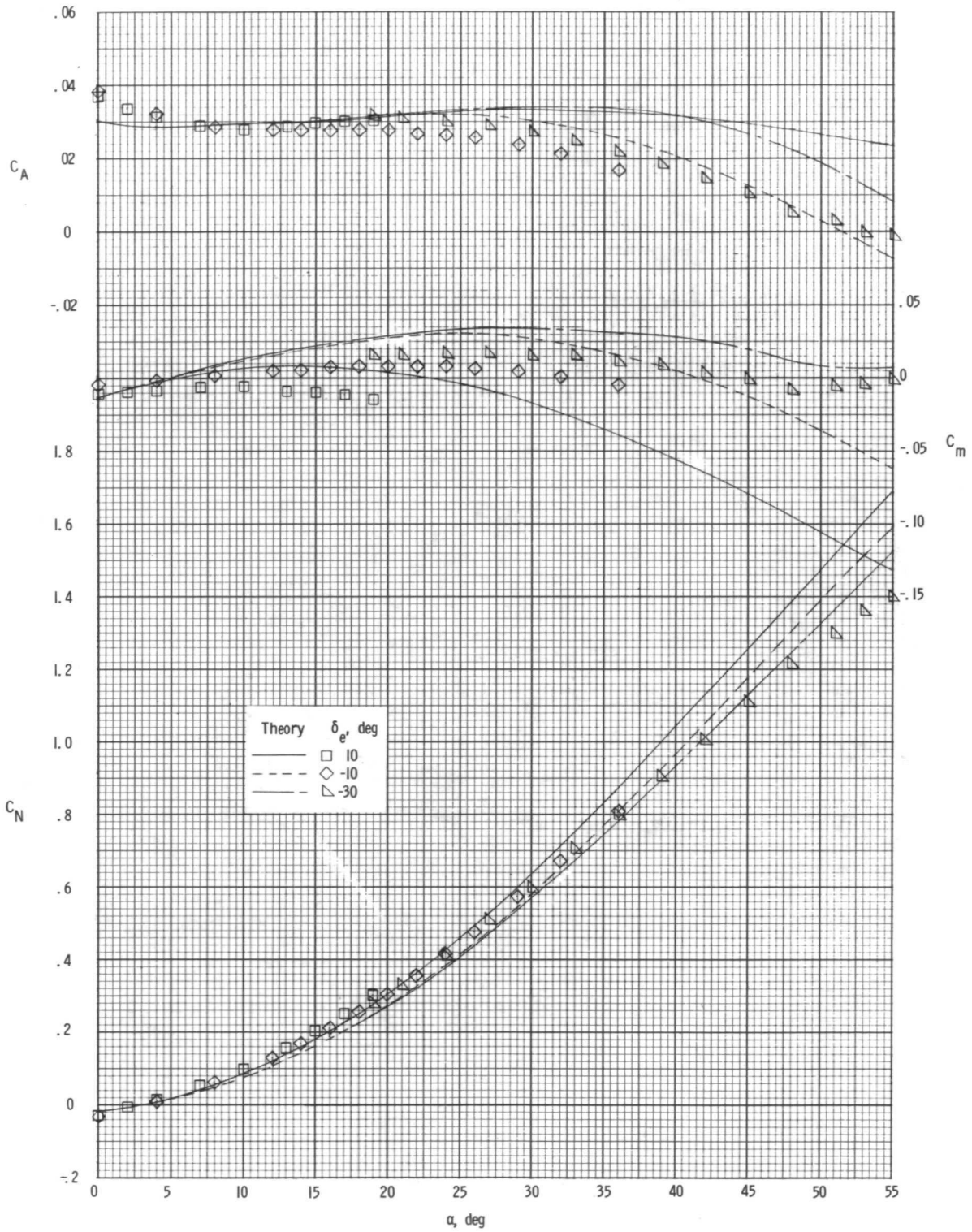

(a) Longitudinal characteristics (body axes).

Figure 20.- Comparison of experimental data with tangent-cone theory for elevon deflections on 134D orbiters.

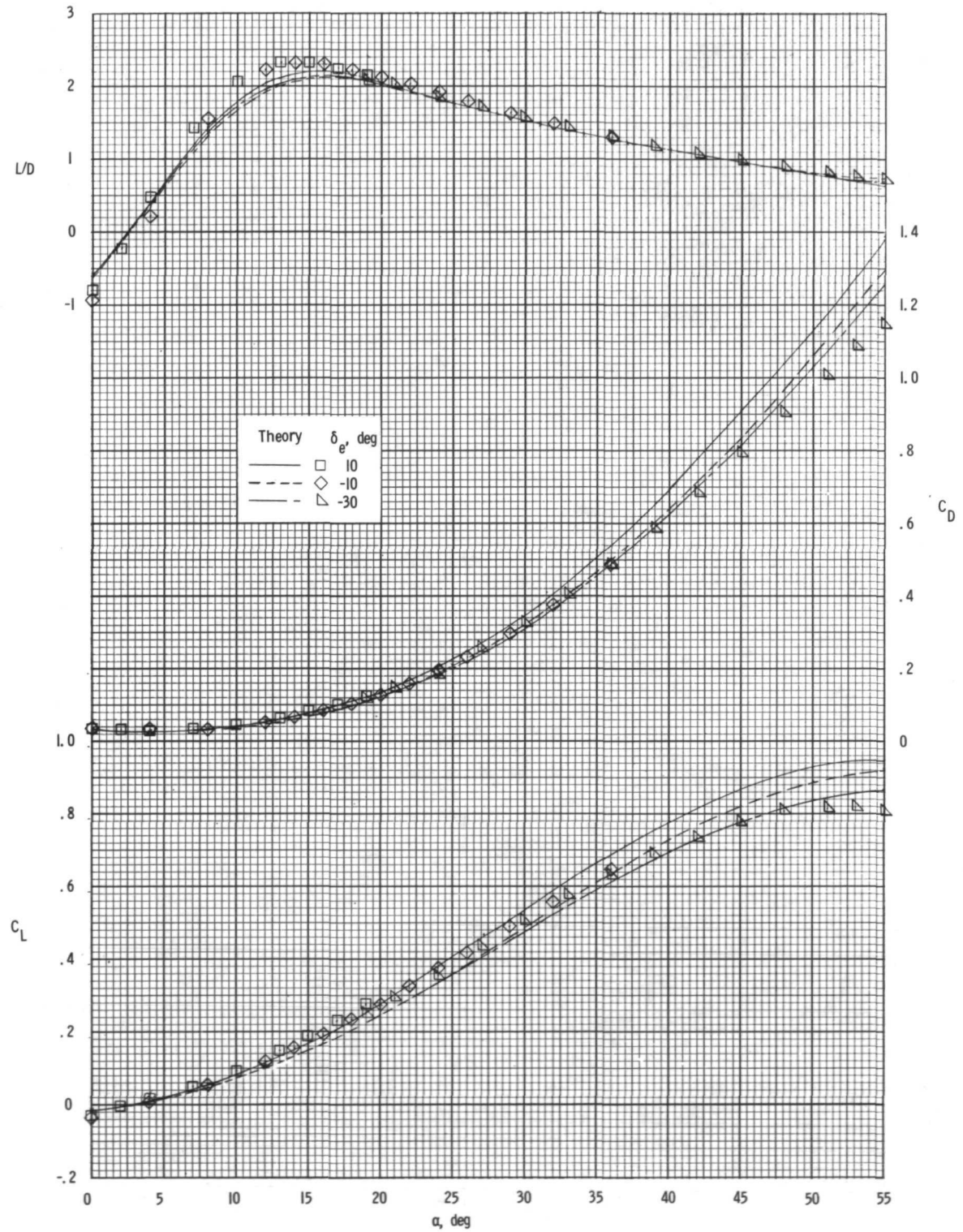

(b) Longitudinal characteristics (stability axes).

Figure 20.- Concluded.

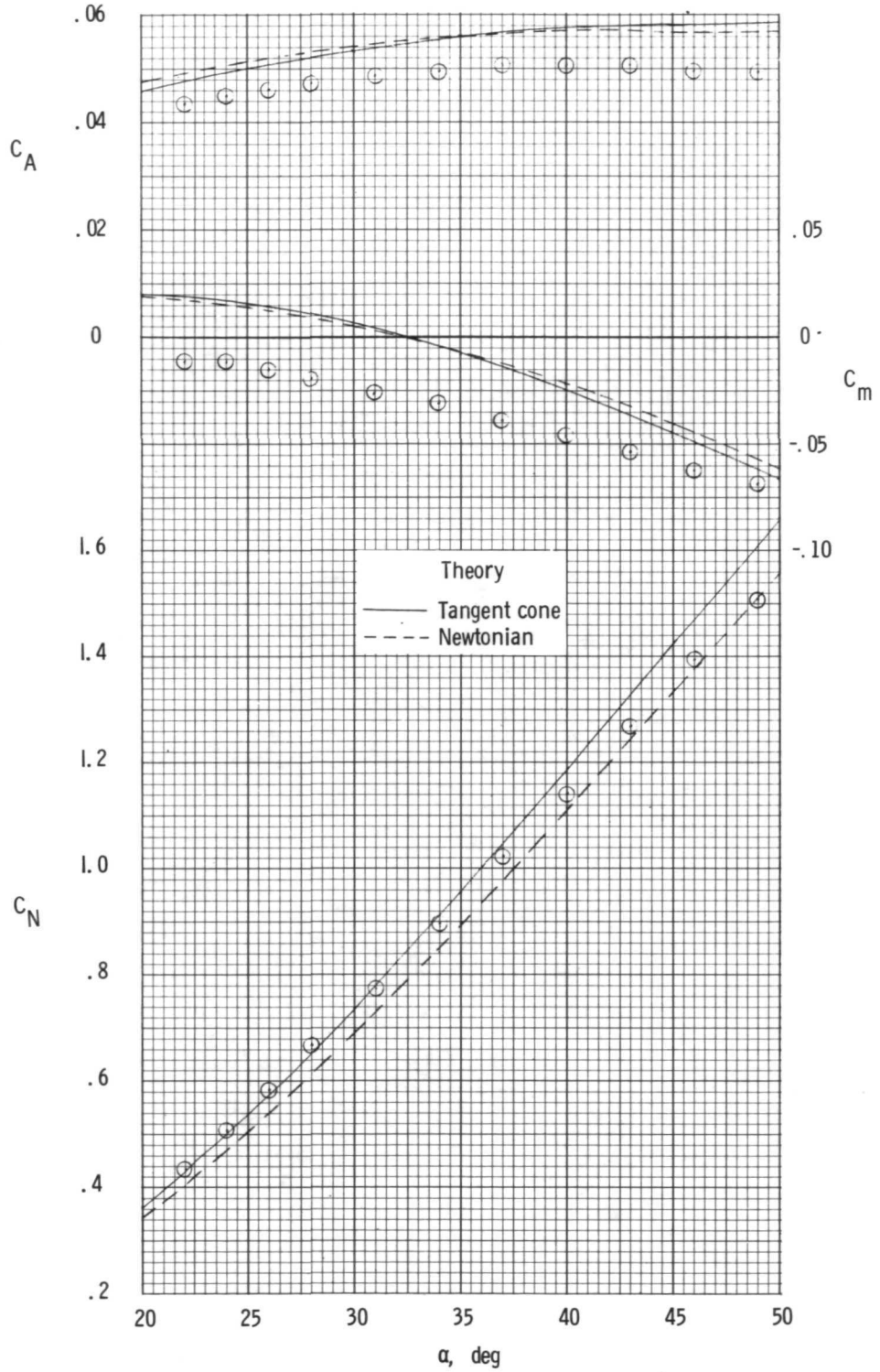

(a) Longitudinal characteristics (body axes). $\delta_e = 0^o$.

Figure 21.- Comparison of experimental aerodynamic characteristics of 050B orbiter with theory.

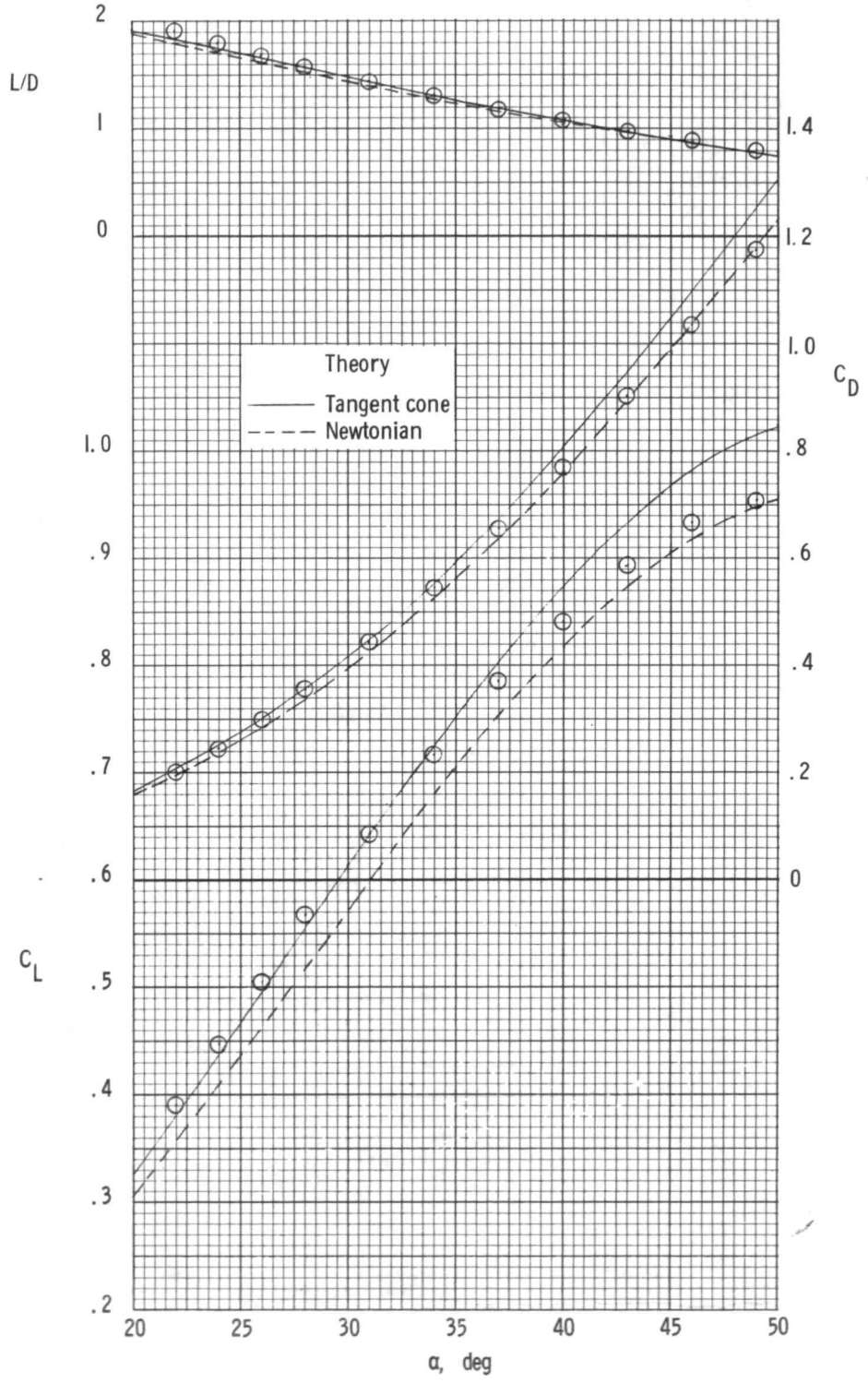

(b) Longitudinal characteristics (stability axes). $\delta_e = 0^o$.

Figure 21.- Continued.

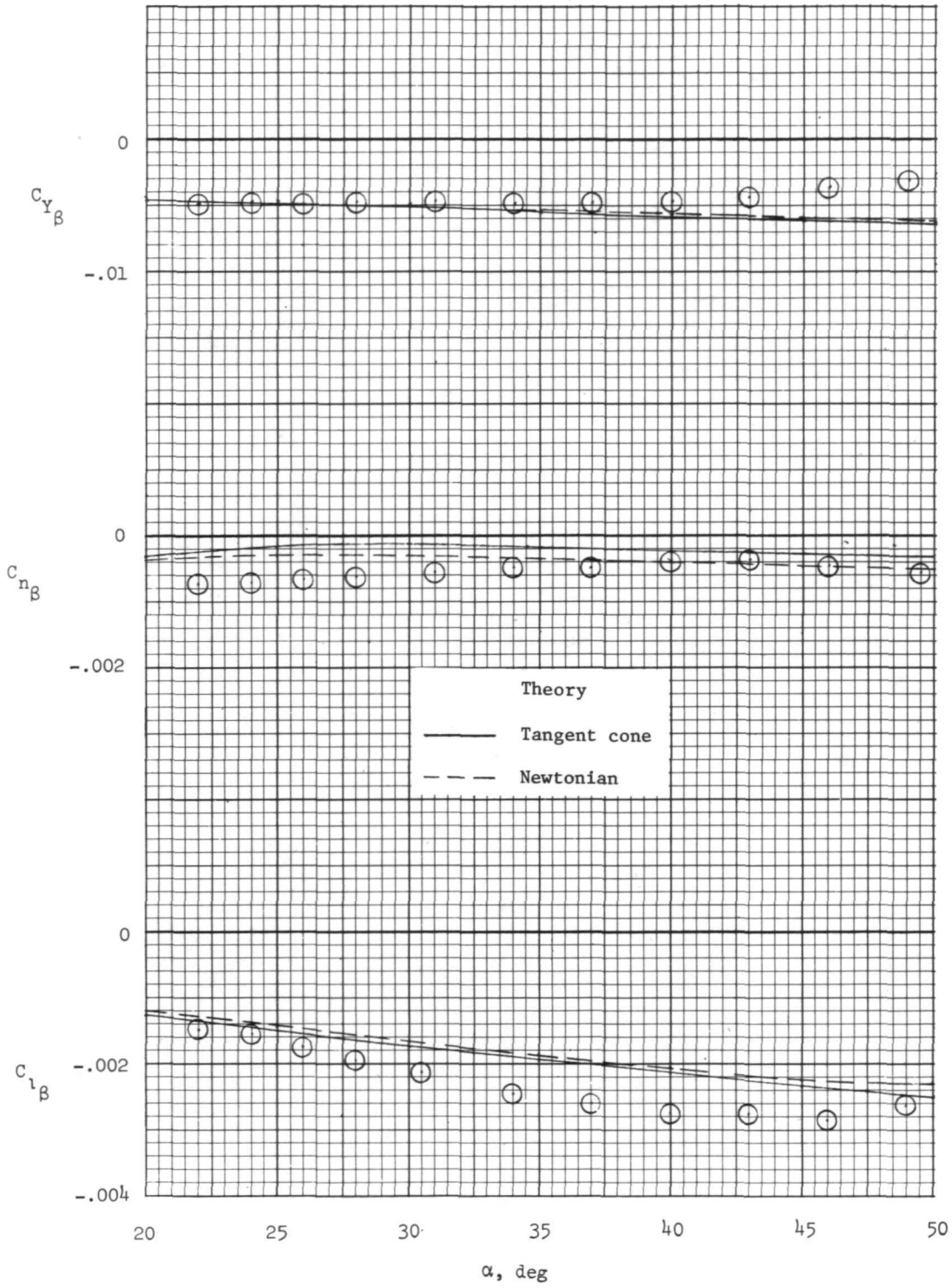

(c) Lateral and directional stability characteristics. $\delta_e = -5^o$.

Figure 21.- Concluded.

NASA-Langley, 1973 —— 1 L-8892

A motion-picture film supplement L-1137 is available on loan. Requests will be filled in the order received. You will be notified of the approximate date scheduled.

The film (16 mm, 5 min, color, silent) shows electron-beam-illuminated flow over the models at angles of attack from approximately -5° to 55° from the top, bottom, and side. Simultaneous use of the illuminated flow and surface oil-flow patterns is also included for selected angles of attack.

Film supplement L-1137 is available on request to:

NASA Langley Research Center
Att: Photographic Branch, Mail Stop 171
Hampton, Va. 23665

CUT

Date_____

Please send, on loan, copy of film supplement L-1137 to TN D-7282.

_____
Name of organization

_____
Street number

_____
City and State Zip code

Attention: Mr._____
Title_____

CUT

Place
Stamp
Here

NASA Langley Research Center
Att: Photographic Branch, Mail Stop 171
Hampton, Va. 23665

NATIONAL AERONAUTICS AND SPACE ADMINISTRATION
WASHINGTON, D.C. 20546

OFFICIAL BUSINESS
PENALTY FOR PRIVATE USE $300

SPECIAL FOURTH-CLASS RATE
BOOK

POSTAGE AND FEES PAID
NATIONAL AERONAUTICS AND
SPACE ADMINISTRATION
451

U.S.MAIL

POSTMASTER : If Undeliverable (Section 158 Postal Manual) Do Not Return

"The aeronautical and space activities of the United States shall be conducted so as to contribute . . . to the expansion of human knowledge of phenomena in the atmosphere and space. The Administration shall provide for the widest practicable and appropriate dissemination of information concerning its activities and the results thereof."

—NATIONAL AERONAUTICS AND SPACE ACT OF 1958

NASA SCIENTIFIC AND TECHNICAL PUBLICATIONS

TECHNICAL REPORTS: Scientific and technical information considered important, complete, and a lasting contribution to existing knowledge.

TECHNICAL NOTES: Information less broad in scope but nevertheless of importance as a contribution to existing knowledge.

TECHNICAL MEMORANDUMS: Information receiving limited distribution because of preliminary data, security classification, or other reasons. Also includes conference proceedings with either limited or unlimited distribution.

CONTRACTOR REPORTS: Scientific and technical information generated under a NASA contract or grant and considered an important contribution to existing knowledge.

TECHNICAL TRANSLATIONS: Information published in a foreign language considered to merit NASA distribution in English.

SPECIAL PUBLICATIONS: Information derived from or of value to NASA activities. Publications include final reports of major projects, monographs, data compilations, handbooks, sourcebooks, and special bibliographies.

TECHNOLOGY UTILIZATION PUBLICATIONS: Information on technology used by NASA that may be of particular interest in commercial and other non-aerospace applications. Publications include Tech Briefs, Technology Utilization Reports and Technology Surveys.

Details on the availability of these publications may be obtained from:

SCIENTIFIC AND TECHNICAL INFORMATION OFFICE

NATIONAL AERONAUTICS AND SPACE ADMINISTRATION

Washington, D.C. 20546